AFWAL-TR-88-3017

DISPLAY SYSTEMS DYNAMICS REQUIREMENTS FOR FLYING QUALITIES

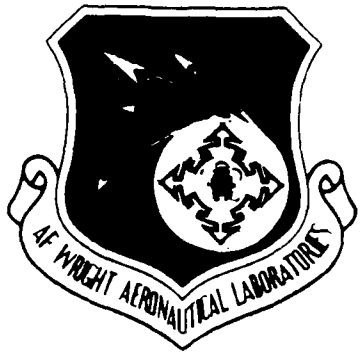

Honeywell Inc.
Systems and Research Center
3660 Technology Drive
Minneapolis, Minnesota 55418

May 1988

Final Report for Period October 1986 to December 1987

Approved for public release;
distribution is unlimited.

FLIGHT DYNAMICS LABORATORY
AIR FORCE WRIGHT AERONAUTICAL LABORATORIES
AIR FORCE SYSTEMS COMMAND
WRIGHT-PATTERSON AIR FORCE BASE, OHIO 45433-6553

UNCLASSIFIED

SECURITY CLASSIFICATION OF THIS PAGE

REPORT DOCUMENTATION PAGE

Form Approved
OMB No. 0704-0188
Exp. Date: Jun 30, 1986

1a. REPORT SECURITY CLASSIFICATION Unclassified	1B. RESTRICTIVE MARKINGS –
2a. SECURITY CLASSIFICATION AUTHORITY –	3. DISTRIBUTION/AVAILABILITY OF REPORT Approved for public release; distribution is unlimited
2b. DECLASSIFICATION/DOWNGRADING SCHEDULE –	
4. PERFORMING ORGANIZATION REPORT NUMBER(S) 88SRC19	5. MONITORING ORGANIZATION REPORT NUMBER(S) AFWAL-TR-88-3017
6a. NAME OF PERFORMING ORGANIZATION Honeywell Systems and Research Center 6b. OFFICE SYMBOL (If applicable)	7a. NAME OF MONITORING ORGANIZATION Flight Dynamics Laboratory; (AFWAL/FIGCB) Air Force Wright Aeronautical Laboratories; Air Force Systems Command
6c. ADDRESS (City, State, and ZIP Code) 3660 Technology Drive, P.O. Box 1361 Minneapolis, MN 55440	7b. ADDRESS (City, State, and ZIP Code) Wright Patterson AFB, Ohio 45433-6553
8a. NAME OF FUNDING/SPONSORING ORGANIZATION Flight Dynamics Laboratory; (AFWAL/FIGCB) Air Force Wright Aeronautical Laboratories; Air Force Systems Command 8b. OFFICE SYMBOL (If applicable) AFWAL/FIGC	9. PROCUREMENT INSTRUMENT IDENTIFICATION NUMBER F33615-86-C-3615
8c. ADDRESS (City, State, and ZIP Code) Wright-Patterson AFB, Ohio 45433-6553	10. SOURCE OF FUNDING NUMBERS PROGRAM ELEMENT NO.: 62201F PROJECT NO.: 2403 TASK NO.: 05 WORK UNIT ACCESSION NO.: 65
11. TITLE (Include Security Classification) Display Systems Dynamics Requirements for Flying Qualities	
12. PERSONAL AUTHOR(S) Kevin Boettcher, David K. Schmidt, Lori Case	
13a. TYPE OF REPORT Final Report	13b. TIME COVERED FROM Oct. 86 TO Dec. 87
14. DATE OF REPORT (Year, Month, Day) 1988 May 9	15. PAGE COUNT 178
16. SUPPLEMENTARY NOTATION	

17. Cosati codes		
FIELD	GROUP	SUB-GROUP
01	04	
05	08	

18. SUBJECT TERMS (Continue on reverse if necessary and identify by block number)
Flying qualities; Multivariable control; Display dynamics; Pilot Modeling

19. ABSTRACT (Continue on reverse if necessary and identify by block number)

This report summarizes research performed to develop a methodology for deciding requirements for display dynamics that ensure good flying qualities. To this end, a model-based approach was pursued that uses the optimal control model (OCM) of human operator behavior. One aspect of the investigation was to further establish the utility of the OCM in this context by correlating model-based quantities with flying qualities data from existing data bases. Another aspect was to consider how various factors at the pilot/display interface map into usual OCM perceptual parameters.

A third element of the investigation was to examine the specific case of an STOL vehicle in an approach and landing configuration, with an explicitly modeled processing delay in the HUD. This case study showed the negative impact of the delay and demonstrated how the introduction of additional display dynamics can compensate for its effect.

Finally, a methodology for deciding display dynamics requirements has been suggested that is based on multivariable control theory, specifically the structured singular value. The methodology provides a means for assessing robustness of system performance and pilot workload to variations in pilot behavior and with respect to variable aircraft dynamics. It also incorporates a synthesis procedure that selects display dynamics so that a balance is achieved between optimal performance and adequate robustness. From such synthesis results, display dynamics requirements can be abstracted. A detailed example that illustrates this approach is provided.

20. DISTRIBUTION/AVAILABILITY OF ABSTRACT [X] UNCLASSIFIED/UNLIMITED [ ] SAME AS RPT [ ] DTIC USERS	21. ABSTRACT SECURITY CLASSIFICATION Unclassified	
22A. NAME OF RESPONSIBLE INDIVIDUAL Lt. Mark Detroit	22b. TELEPHONE (Include Area Code) (513) 255-8494	22c. OFFICE SYMBOL AFWAL/FIGC

DD FORM 1473. 84 MAR

83 APR edition may be used until exhausted.
All other editions are obsolete.

SECURITY CLASSIFICATION OF THIS PAGE

UNCLASSIFIED

FOREWORD

This report summarizes the work performed by Honeywell Inc. for the Air Force under Contract Number F33615-86-C-3615. The period of performance was from October 1986 to December 1987. The study was sponsored by the Flying Qualities Group within the Flight Dynamics Laboratory (FIGC), which at the time of contract origination was under the direction of Mr. Frank George. Lt. L. McCormack was the original Technical Monitor. Lt. M. Detroit assumed this role midway during the contract.

At Honeywell, the original Principal Investigator was Dr. Dale Enns, with Dr. Kevin Boettcher serving in this role for the latter part of the effort. Dr. David Schmidt of the School of Aeronautics and Astronautics at Purdue University consulted on the project. Ms. Lori Case, Ms. Kathryn Lenz, Mr. David Lowry, Dr. Blaise Morton, and Mr. Douglas Weed, all of Honeywell, assisted on the project, as did Dr. Sanjay Garg of Purdue University.

TABLE OF CONTENTS

TABLE OF CONTENTS (concluded)

LIST OF ILLUSTRATIONS

LIST OF ILLUSTRATIONS (continued)

LIST OF ILLUSTRATIONS (concluded)

LIST OF TABLES

SECTION I

INTRODUCTION

1. MOTIVATION AND OBJECTIVES

Current and emerging military aircraft present a number of challenges with respect to ensuring good flying qualities. One of these is depicted in Figure 1, which shows major elements in a pilot-in-the-loop manual control system. Flying qualities, as rated subjectively by the pilot, are influenced by the dynamic characteristics of the other two elements in the loop. Improvement of flying qualities through augmentation of the aircraft dynamics by a control system has been studied extensively, with current and evolving standards in existence. Consideration of the dynamic characteristics of displays has not been subject to similar study, however, even though their potential impact on flying qualities is no less significant. Figure 2 shows the typical signal path

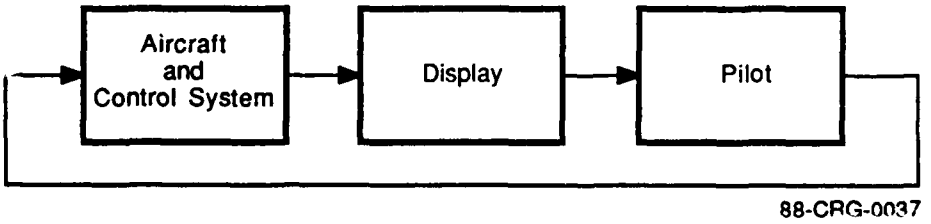

Figure 1. Major Elements in Manual Control Loop.

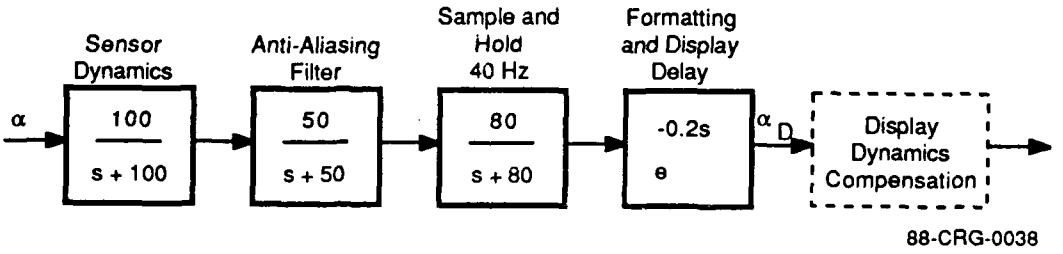

Figure 2. Typical Measurement and Display Dynamics.

for the measurement and display of pitch attitude in a modern tactical aircraft. Though perhaps negligible individually, the cumulative effects of these dynamic elements can be significant, particularly with respect to phase loss and in view of the pilot's effective control bandwidth. The last two elements in the figure are peculiar to digital display technology and can introduce nontrivial dynamic complexities into the manual control task.

Thus the information displayed has not only its inherent dynamic properties but also reflects the impact of additional dynamics in the measurement and display path. Besides providing the compensation needed for the underlying control task, these are additional effects that the pilot must also overcome or in some way compensate for.

With the advent of digital-based display technology, it is especially attractive to consider the possibility of introducing an additional dynamic element in the measurement and display path. As indicated in Figure 2, this element would serve in some way to compensate for the dynamics introduced by measurement and display hardware. It might also provide additional augmentation that would ease the pilot's workload, improve task performance, and/or improve flying qualities. This type of compensation does, of course, occur in many systems in the form of a flight director, a flight path predictor, or some other element such as a "tunnel in the sky." Though each of these choices is well-grounded in considerations of human behavior and system performance, there is still a need for a set of guidelines for specifying display system dynamics requirements that ensure good flying qualities.

Given the complex nature of current and emerging military aircraft and the often costly consequences of poor design with respect to flying qualities, such guidelines should be applicable at an early stage in the design process. They should also include adequate consideration of the interface between pilot and display, especially of how motion and visual cues are perceived and with what fidelity. Such guidelines should result in display compensation dynamics that take into account uncertainties inherent in vehicle dynamics, and the fact that actual pilot compensation varies with respect to individual differences and environmental factors.

This project's objective has been to investigate and develop methodology for deciding display dynamics requirements that ensure good flying qualities. A driving factor in the development has been that the methodology be applicable at an early stage of the design process. This implies that it be predictive and virtually dictates that it be model-based as well. Furthermore, given the multivariable nature of modern aircraft systems, the methodology must be able to address this aspect of the problem and take advantage of the potential benefits of using a multivariable compensation scheme within the display. Finally, the model-based analysis methodology must be tied to the qualitative assessment of flying qualities (i.e., pilot ratings and comments).

2. OVERVIEW

The characteristics sketched above for a methodology for display dynamics requirements specification have been used as guidelines in pursuing the research reported here. The so-called optimal control model (OCM) was selected as a basis for developing the methodology. Because of the emphasis on the pilot display interface and the potential impact a given set of display formats might have on the perception of information that has been modified by display dynamics, the enumeration and representation of factors that impact this interface have been considered. The report includes an extensive discussion of psychophysical and display-related factors that are relevant in this context, and furthermore, how these factors merge into OCM-related model elements and parameters. In addition, the representation in OCM-compatible terms of how motion and visual cues are perceived has been revisited, with a new model included that is appropriate for the approach-to-landing task situation. Using this model, an OCM-based analysis has been performed in conjunction with the Cooperative Synthesis technique. Results of this investigation demonstrate how the systematic selection of display dynamics can potentially improve flying qualities.

A substantial amount of program effort has been devoted to developing a methodological framework for abstracting display dynamics that combines the basic OCM with recent advances in multivariable control theory, specifically the so-called structured singular value. The progress made on developing this framework is presented, including an

extensive example. Among the key features of the framework are its inherent multivariable nature and the ability to consider explicitly deviations in system elements from their nominal models, including variations in pilot behavior and unmodeled or unknown plant dynamics. The framework also has the potential for synthesizing sets of display dynamics that strike a balance between maintaining good flying qualities across a range of pilot behaviors and aircraft uncertainties on the one hand, and optimizing a performance criterion on the other.

3. REPORT ORGANIZATION

This report is organized as follows. The next section reviews the basic OCM framework and presents a calibration of model-based results to actual rated flying qualities in order to establish a connection between the two that will be useful in subsequent considerations. Section III contains the review and discussion of factors that impact the modeling of the perceptual interface. Section IV considers the approach-to-landing situation and presents analysis using the so-called Cooperative Synthesis technique that demonstrates the potential for improvement through the systematic selection of display dynamics. In Section V, the structured-singular value-based methodological framework is described and an example problem is treated in order to demonstrate its features. Also included in this section is a discussion on experimentally testing the hypotheses that have been generated using the various model-based techniques considered. Section VI summarizes the report. Finally, an appendix has been included that contains a detailed discussion on the relationship of psychophysical factors to OCM-parameters.

SECTION II

MODEL-BASED ANALYSIS FRAMEWORK

The optimal control model was the basic framework used in the research toward developing a methodology to decide display dynamics requirements. This section briefly reviews the features of this model to establish notation. It also presents the results of a model-based analysis using the OCM in which performance and workload measures have been calibrated with respect to rated flying qualities. This forms the basis for subsequent consideration of display dynamics using the OCM.

1. OPTIMAL CONTROL MODEL STRUCTURE

Figure 3 shows the structure of the OCM as introduced by Kleinman et al. (Reference 1). In a typical OCM formulation, the control task is modeled as a linear, time-variant system in state space format. The operator exercises control through the variables, u. The disturbances, w_C, are the fundamental modeling construct that is used to represent the actual control task, e.g., a signal to be tracked or an error to be minimized. The

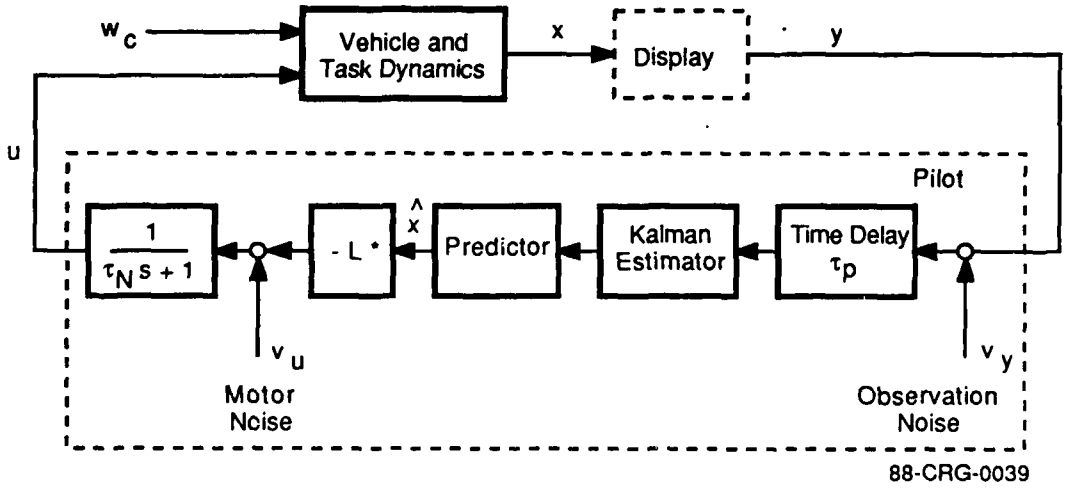

Figure 3. Optimal Control Model of Human Behavior.

operator typically has available a limited set of observations (y) derived from the system's state (x). In Figure 3, a display element is indicated, although in previous uses of the model this element has been restricted to a constant observation matrix.

The underlying premise of the OCM is that the performance of a well-trained, well-motivated human operator at a manual control task is that of an optimal controller, modified to reflect human limitations. One of the limitations made explicit is that the signals observed by the operator are subject to error. This is modeled by the introduction of an additive observation noise, which is taken to be white, with intensity related to the mean square of the observed signal. Specifically, the intensity, V_{yi}, of the observation noise, v_{yi}, for the i^{th} observed variable, y_i, is defined as:

$$V_{yi} = \frac{\rho_i \pi}{f_i \; N^2\left(\sigma_{yi}, \alpha_{yi}\right)} \; E\left\{y_i^2\right\} \qquad (1)$$

In Equation 1, ρ_i is a noise-to-signal ratio, which is typically set equal to 0.01 (-20 dB) based on limited laboratory data (Reference 2).

The factor $\rho_i\pi$ represents a minimum observation error and is essentially a characterization of remnant in the OCM framework. The other factors in Equation 1 modify this nominal noise-to-signal ratio to include the fraction of attention allocated to y_i (f_i) and to include a factor that represents the potential indifference that an operator may have to the change in value of a given signal. The former is determined either arbitrarily or as part of an optimization process that determines the best attention allocation policy for the observed variables. A common modeling assumption in the OCM is to assume that if a variable is displayed directly in analog format (e.g., a needle indication), then the rate of change of that variable is also observed. In this situation, the fraction of attention given to each variable in the position-rate pair is equal, but, because both are observed simultaneously, they contribute in the total attention allocated as though they were one variable.

Operator indifference to small changes in a variable is modeled using a describing function, N, where

$$N(\sigma_y, \alpha_y) = \sqrt{\frac{2}{\pi}} \int_{-\infty}^{\frac{-\alpha_y}{\sigma_y}} e^{\frac{-x^2}{2}} dx \qquad (2)$$

In Equation 2, α_y is the smallest change in the signal, y, that the operator will not be indifferent to, expressed in the units of the displayed variable. This quantity is influenced by human physiological considerations, as well as the physical distance between the operator and the display. The quantity σ_y is the standard deviation of y.

Other human limitations contained in the OCM include a perceptual/cognitive delay (τ_p) and a motor noise (v_u). The former is a lumped representation of a number of human processes and is typically taken to be 200 ms. The latter is assumed to be of the same form as the nominal observation noise, with the noise-to-signal ratio typically set at -25 dB.

With these limitations represented explicitly, an optimal control problem is formulated to complete the OCM characterization. Using the well-trained, well-motivated assumption, a cost function is formulated to reflect the operator's presumed control objectives. Typically, it is of the form

$$J(u) = \lim_{T \to \infty} E \left\{ \frac{1}{T} \int_0^T \left(y^T Q y + \dot{u}^T R \dot{u} \right) dt \right\} \qquad (3)$$

In Equation 3, the first term reflects a usual control objective expressed in quadratic terms, which is to minimize the (weighted) mean square of some combination of observed variables y (Reference 1). In the present case, these variables might include flight path error, for example. The second term in Equation 3 reflects a desire to minimize the (weighted) mean square of the rate of control action required. Besides being desirable from an optimal control point of view, it also reflects human neuromuscular limitations. The inclusion of a control rate weighting in the cost function gives rise to the first-order *neuromuscular lag* shown in Figure 3. Indeed, for the case

where the control is one-dimensional, there is an inverse relationship between τ_N, the neuromuscular time constraint, and R. In the sequel, only single dimensional control will be considered and the value of R will always be chosen to yield a value of τ_N equal to 0.1, unless otherwise indicated. A value of $\tau_N = 0.1$ yields an effective bandwidth in the pilot model that is near human limitations, which qualitatively reflects a more aggressive piloting behavior.

Solution of a minimizing u in Equation 3 results in the control gains, L^*. Mechanically, this involves the solution of an algebraic matrix Riccati equation (Reference 1). Since this solution assumes full state feedback, an estimator must be constructed to complete the model. This is done using a standard Kalman estimator. Because of the perceptual delay, however, a prediction is required as well, and a linear predictor is used for this purpose. These estimation and prediction elements are selected to satisfy the noise-to-signal constraints specified in the definition of observation and motor noises. To reach this equilibrium, an iteration process is required, which at the same time can be used to optimize the attention allocation fractions (f_i). Details of this process are given in Reference 3.

This, then, is the basic optimal control model. Since it was introduced in the 1970s, it has been validated in a number of laboratory task situations and has been used widely to analyze a number of complex problems, including the formatting of displays. Previous applications of this latter type will be considered in Section III, where the perceptual interface from operator to display is discussed.

2. OCM-BASED CHARACTERIZATION OF FLYING QUALITIES

a. Introduction

To use the OCM as a vehicle to decide display dynamics that give good flying qualities, it is necessary to link the quantitative analysis results obtainable using the OCM with the more qualitative concept of flying qualities. This subsection presents evidence for one

such link. Though not conclusive, the indications provided will be used subsequently for purposes of developing a methodology for abstracting display dynamics requirements.

The basic approach taken here is to use existing flying qualities data bases, where specific flight task and aircraft dynamics are known, model these dynamics using the OCM, and then attempt to correlate model-based quantities with observed flying qualities. Taking such an approach is not new. Schmidt and his students have correlated rated flying qualities on pitch-tracking and approach-to-landing tasks with OCM-based quantities (References 4 and 5). Specifically, RMS tracking error has been used as a performance indication and "equivalent phase lead" as a workload indication. For the tasks considered, a reasonable grouping of rated flying qualities according to Levels 1, 2, and 3 has been obtained from these performance and workload quantities, and this work serves as a point of departure for the present effort.

Because of the desire to have a methodology for display dynamics analysis that treats multivariable situations, the mapping of flying qualities to the model-based quantities used in References 4 and 5 is not directly applicable in the present context. In particular, the *concept of phase margin does not translate readily into multivariable settings.* Thus, an alternative indication of workload has been sought. The quantity selected is that of RMS control rate, denoted $\sigma_{\dot{u}}$. (Since the use of RMS is restricted to zero-mean quantities in the sequel, the terms RMS and standard deviation are interchangeable for these quantities.) As with the performance indication of RMS tracking error, control rate extends readily (in principle) to multivariable situations. Moreover, it is also an established measure of workload (Reference 6), although care must be taken in using this metric, particularly with respect to its sensitivity to the interaction of pilot gain and the actual spectral shape of the stick input. Nevertheless, because of its potential application to multivariable settings, its use has been pursued in the present study. In the discussion below, the pitch tracking and approach-to-landing data bases are revisited, and a correlation of model-based values of σ_{err} and $\sigma_{\dot{u}}$ with rated flying qualities is presented. A set of guidelines based on these results is then discussed, along with a number of issues relevant to their use.

b. Pitch-Tracking Task

The Neal-Smith investigation (Reference 7) produced a data base that includes flying qualities ratings at a pitch-tracking task for a number of aircraft/flight control system sets

of dynamics. Following on the approach used in Reference 4, an OCM-based analysis of this data base has been conducted as follows. First, since the basic control task is one that involves pitch attitude, the aircraft and flight control system transfer function of interest is $\theta(s)/F(s)$, where $\theta(s)$ is pitch angle and $F(s)$ is stick displacement. The form of this transfer function is given as

$$\frac{\theta(s)}{F(s)} = \frac{K_\theta (\tau_1 s + 1)(\tau_{\theta 2} s + 1)}{s(\tau_2 s + 1)\left(\frac{s^2}{\omega_3^2} + \frac{2\zeta_3 s}{\omega_3} + 1\right)\left(\frac{s^2}{\omega_{sp}^2} + \frac{2\zeta_{sp}}{\omega_{sp}} S + 1\right)} \quad (4)$$

The expression in Equation 4 forms the *vehicle dynamics* element in Figure 3, with specific values of the parameters determining the flight configuration.

The *task dynamics* element in the OCM model was developed as follows. The pilot's objective was to maintain the error between desired and actual pitch angles small. This is considered to be the *critical task* that must be represented adequately in order to perform model-based analysis using the OCM. The model adopted to accomplish this is to generate a pitch command signal, θ_c, by shaping a white noise disturbance using a second order filter. Specifically, the model for θ_c is given as

$$\ddot{\theta}_c + 0.5\,\dot{\theta}_c + 0.25\,\theta_c = .25\,w_c \quad (5)$$

where w_c is a white Gaussian noise with intensity equal to 64. This model for θ_c approximates the frequency content of the IFR tracking task used in the Neal-Smith experiments. The value for noise intensity has been selected to yield a reasonable RMS for pitch attitude variation of 4 deg. This commanded signal is differenced with θ to obtain a pitch tracking error, θ_e.

To complete the OCM formulation for this task, definition of variables observed and various human parameters must be made (Table 1). Note that where appropriate, parameters are set to typical values. The indifference thresholds are set at optimistic values; the effect is that they do not contribute significantly to the results.

TABLE 1. OCM FORMULATION FOR NEAL-SMITH DATA BASE ANALYSIS

OCM Parameter	Value
Observed variables (y)	θ_e, $\dot{\theta}_e$, θ, $\dot{\theta}$
Cost function weights (Q)	Diag (1, 0, 0, 0)
Observation noise-to-signal ratio (ρ)	-20 dB
Perceptual delay (τ_p)	200 ms
Indifference thresholds: (α_y)	
• Position	0.05 deg
• Rate	0.20 deg/sec
Attention fractions (f_i)	equal at 0.5
Neuromuscular time constant (τ_N)	0.1 sec
Motor noise-to-signal ratio	-25 dB

The key modeling assumptions evident in Table 1 are the selections of observed variables, cost function weights, and attention fractions. It is assumed that the pilot observes a position/rate pair of pitch error θ_e, as well as the actual pitch angle and rate. Furthermore, it is assumed that only the value of θ_e is significant with respect to the control task. Finally, it is assumed that equal attention is given to each of the two position/rate pairs observed. These assumptions are believed to reflect the actual task under consideration. Modifying them, in particular optimizing the attention fractions, does change the results presented below somewhat in absolute terms. The qualitative characteristics remain the same, however.

Using this OCM formulation, selected configurations from the Neal-Smith data base were examined. These are listed in Table 2, along with the flying qualities level obtained experimentally. In all cases $\tau_{\theta 2}$ was set to 1.25. For some configurations, multiple experiments were completed, which resulted in a variation in pilot ratings. Where this variation spans two flying qualities levels, both levels are indicated in the table, with the dominant level underscored. For each configuration in Table 2, RMS values of θ_e and $\dot{u}$ were calculated as the performance and workload indicators. These

TABLE 2. NEAL-SMITH DATA BASE CONFIGURATIONS CONSIDERED

Configuration	$1/\tau_1$	$1/\tau_2$	ω_{sp}/ζ_{sp}	ω_3/ζ_3	K_θ	Flying Qualities Level
1A	0.5	2.0	2.2/0.69		7.2	2
1B	2.0	5.0		--	6.0	1-2
1C	2.0	5.0		16/0.75	8.0	1-2
1D	∞	∞		--	5.0	1-2
1E	∞	5.0		--	9.0	2
1F	∞	2.0		--	6.0	3
1G	∞	0.5		--	6.0	3
2A	2.0	5.0	4.9/0.70	--	5.5	2
2B	2.0	5.0		16/0.75	6.0	2
2C	5.0	12.0		--	4.6	1-2
2D	∞	∞		--	6.0	1
2E	∞	12.0		--	3.6	1-2
2F	∞	5.0		--	5.5	1-2
2G	∞	5.0		16/0.75	5.5	2-3
2H	∞	2.0		--	5.5	2
2I	∞	2.0		16/0.75	4.6	3
2J	∞	0.5		--	5.0	2-3
3A	∞	∞	9.7/0.63	--	5.5	2
4A	∞	∞	5.0/0.28	--	6.0	2
5A	∞	∞	5.1/0.18	--	10.0	2-3

values are plotted in Figure 4. Each point in the $\alpha_{\theta e}$ and $\sigma_{\dot{u}}$ plane is labeled with its configuration designator and is also encoded with its actual flying qualities level.

Of particular interest in Figure 4 is whether the experimentally derived flying qualities levels are grouped in identifiable regions of the ($\sigma_{\theta e}$, $\sigma_{\dot{u}}$) plane. There is modest evidence that this is the case. A region of Level 1 flying qualities is apparent within a narrow interval of $\sigma_{\dot{u}}$ (around 10) and for $\sigma_{\theta e}$ less than 0.9. A Level 2 region surrounds the Level 1 region, and a Level 3 region is evident for high $\sigma_{\theta e}$, high $\sigma_{\dot{u}}$ values. The qualitative features of these regions will be discussed subsequently, after performing a similar analysis with a different data base.

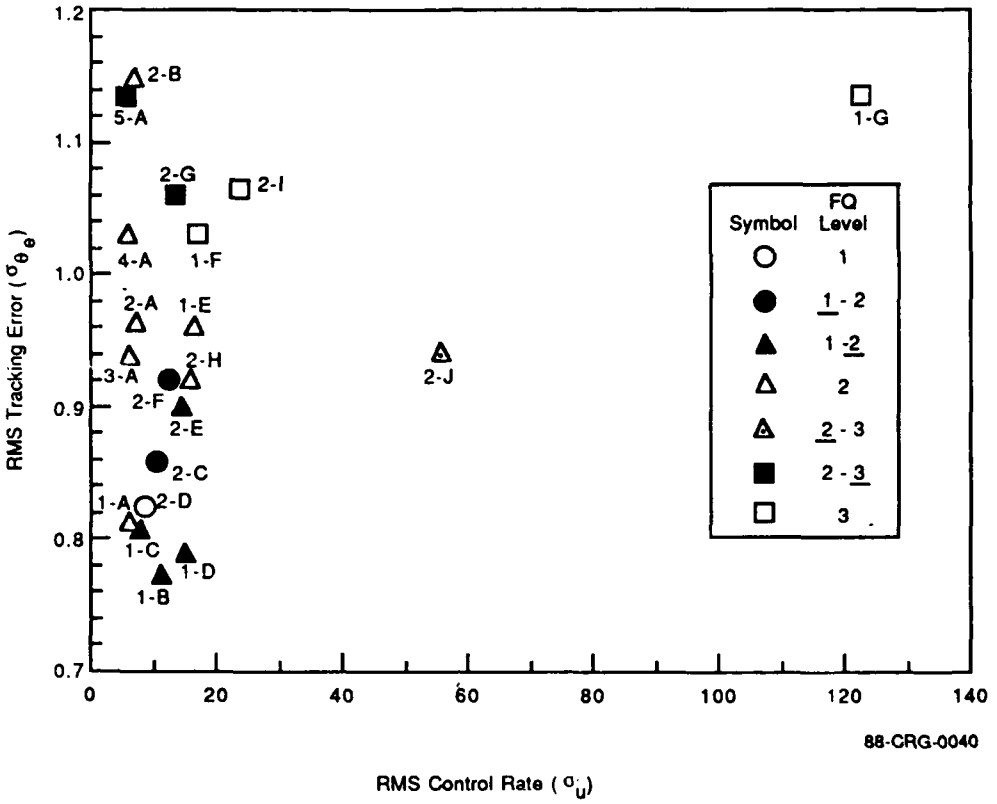

Figure 4. Performance/Workload Plot for Neal-Smith Configurations.

c. Approach-and-Landing Task

An investigation similar to that of Neal and Smith has been performed for the approach and landing task. Termed the LAHOS study (Reference 8), its objective was to study highly augmented fighter aircraft in the landing flight phases under visual flight rules (VFR) conditions. As with the Neal-Smith pitch tracking task, model-based analysis of the LAHOS data requires a representation in OCM format of the critical task in approach and landing. Following on the analysis in Reference 5, this task is defined as the precision control of flight path γ.

A model for this task is readily derived from the pitch tracking model using the γ/θ response relationship:

$$\frac{\gamma\ (s)}{\theta\ (s)} = \frac{1}{\tau_{\theta_2} s + 1} \tag{6}$$

Equations 6 and 4 together yield a model for the stick to γ aircraft and flight control system dynamics. Equation 6 is also used to generate a flight path command signal, γ_c, from the signal θ_c defined in Equation 5. As with the previous analysis, an error signal γ_e is formed as the difference of γ_c and γ. To complete the formulation, OCM parameters are set to those used for the pitch tracking task analysis, with the exception that the observed quantities are changed to reflect the current task. Specifically, the vector of observed variables is taken as:

$$y^T = \left[\gamma_e, \dot{\gamma}_e, \gamma, \dot{\gamma}, \theta, \dot{\theta}\right] \tag{7}$$

In addition, it is assumed that attention is shared equally among all elements of y ($f_i = 1/3$). Finally, the pilot's control objective is assumed to be that of minimizing flight path error, γ_e, and the matrix Q is selected as diag (1, 0, 0, 0, 0,0) accordingly. Even though only flight path error is included in the OCM cost function, the model that results for the pilot is one that effectively closes three loops: pitch attitude control, flight path control, and response to flight path command. This is illustrated in Figure 5, where the shaded regions indicate the pilot's compensation and designate the transfer functions for each loop.

Twenty-eight configurations from the LAHOS data base were considered in the present analysis. The parameter values for Equation 4 for each configuration are summarized in Table 3. In addition, the values of $\tau_{\theta 2}$ and ζ_3 were fixed at 2 and 0.7, respectively. Furthermore, K_θ was (arbitrarily) fixed at 0.3 for the purposes of analysis. For each configuration listed in Table 3, RMS values of σ_{γ_e} and $\sigma_{\dot{u}}$ were calculated as the indicators of performance and workload. These values are plotted in Figure 6, where the configuration and its experimentally obtained flying qualities levels are also indicated.

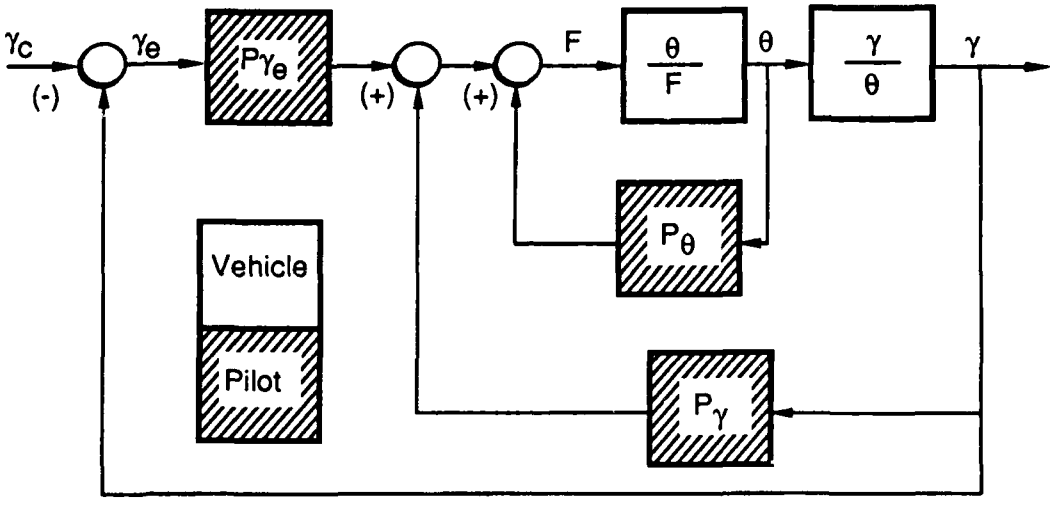

Figure 5. Multiloop Structure of Flight Path Tracking Task

As with the pitch tracking task, the data in Figure 6 is of interest with respect to the grouping of similar flying qualities levels. From the figure, it is evident that regions exist in the (σ_{γ_e}, $\sigma_{\dot{u}}$) plane that correspond to Level 1, 2, and 3 flying qualities, even though the specific boundaries of such regions are perhaps less clear. For present purposes, however, the qualitative observation that RMS values of γ_e and $\dot{u}$ can be used to indicate flying qualities in an approach to landing task is sufficient.

d. Summary

The foregoing analysis suggests that RMS values of model-based quantities can be used as indicators of flying qualities. Though the results presented in this section are not conclusive in general, they will be taken as indicative of general trends for purposes of subsequent methodology development. Specifically, it would appear that a Level 1

TABLE 3. LAHOS CONFIGURATIONS EXAMINED

Configuration	ω_{sp}/ζ_{sp}	τ_1	τ_2	ω_3	Flying Qualities Level
1-C	1.0/0.74	0.2	0.1	--	1-2
1-1		--	--	--	1-2
1-3		--	0.25	--	3
1-6		--	--	16	2
2-A	2.3/0.57	0.4	0.1	--	2
2-C		0.2	0.1	--	1
2-1		--	--	--	1
2-2		--	0.1	--	2
2-3		--	0.25	--	2
2-6		--	--	16	2
2-7		--	--	12	2-3
2-9		--	--	6	3
3-C	2.2/0.25	0.2	0.1	--	1-2
3-1		--	--	--	2
3-2		--	0.1	--	2
3-3		--	0.25	--	3
3-6		--	--	16	2
4-C	2.0/1.06	0.2	0.1	--	1-2
4-1		--	--	--	1
4-4		--	0.5	--	2-3
4-6		--	--	16	1-2
4-7		--	--	12	1-2
4-10		--	--	4	3
5-1	3.9/0.54	--	--	--	2-3
5-3		--	0.25	--	2-3
5-4		--	0.50	--	2-3
5-5		--	1.0	--	2-3
5-6		--	--	16	2-3

flying qualities region is characterized by having a maximum acceptable performance RMS value and an interval of acceptable RMS workload values. For the former, this is easily understood to be an expression of the fact that in order for a system to be Level 1, good performance must be achievable.

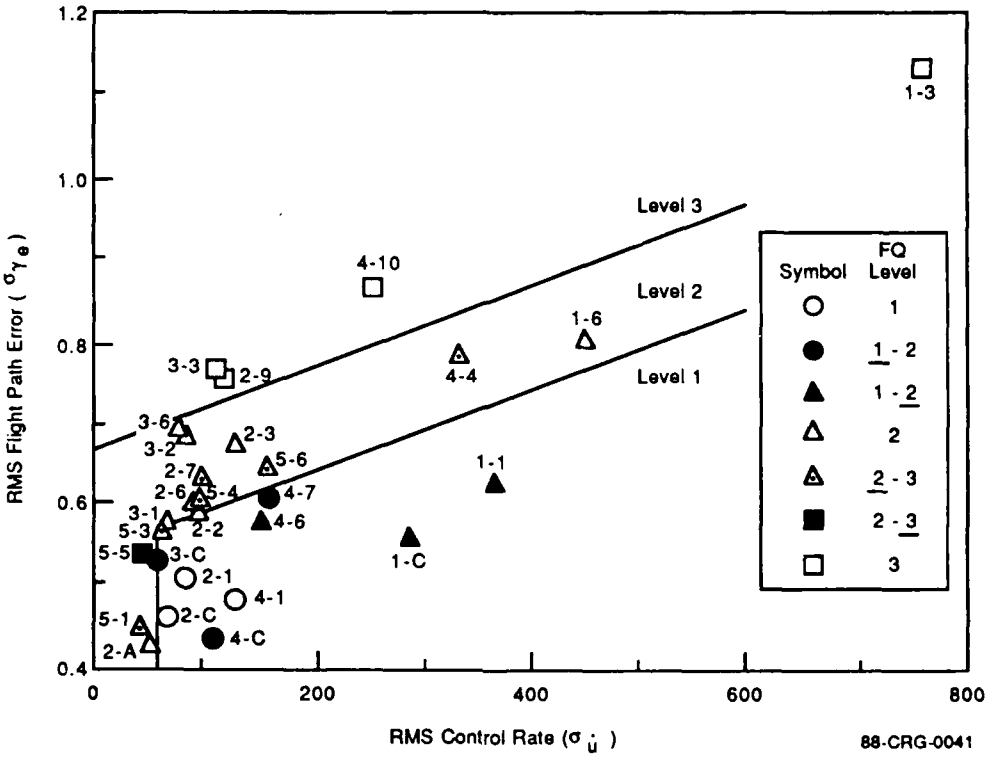

Figure 6. Performance/Workload Plot for LAHOS Configurations.

Performance is achieved at some expense to workload, however, and the upper limit to workload for a Level 1 rating states that even though good performance can be achieved, the workload required to do so might be unacceptably high. The lower limit on workload for Level 1 flying qualities is related to a different phenomenon, however. Even though good performance could be achieved with low workload, as is evidenced by the results in Figures 4 and 6 for a number of configurations, such a configuration is not given a Level 1 rating because the aircraft is too sensitive to pilot control inputs. This forces the pilot to use an extra degree of restraint with respect to taking control action, which is itself an addition to workload. Thus there appears to be a workload interval, centered about some

value, which corresponds to a Level 1 rating. From the data presented, a rough characterization of this interval might be that of ±50% of some central value.

From a methodological viewpoint, then, the results of this section point to the existence of a link between flying qualities ratings and OCM-based quantities. This link is through the use of RMS values that characterize performance and workload. Indeed, a qualitative characterization of the Level 1 region in RMS performance/workload space has suggested itself as a result of the analysis performed on the Neal-Smith and LAHOS data bases. The generality of this characterization is an open question, however, since the analysis performed is limited in scope.

In addition to the limited amount of evidence that has been presented, there are several significant issues that must be explored further before this characterization can be considered solid enough. First, even though RMS values were selected because their use can be generalized to multivariable situations, this in fact remains to be established. One possible generalization is to return to the cost function in Equation 3. Consider that the first term corresponds to performance, and the second term corresponds to workload. This places the issue directly in terms of selecting the Q and R matrices, which is reasonable, since they are themselves critical to the validity of the analysis performed.

A second issue with respect to the characterization of Level 1 flying quantities in an RMS performance/workload space is the definition of a central value for RMS σ_u. As was evident from the two cases studied, differences in scale can be encountered in OCM-based analysis, as well as potential task-dependent differences with respect to what constitutes an acceptable level of workload. (The latter is also an issue when using pilot phase compensation as a workload indicator.) Deciding a central value for $\sigma_{\dot{u}}$, especially when performing analysis in a predictive (e.g., design) context, is a key question that warrants additional investigation.

SECTION III

MODELING THE PERCEPTUAL INTERFACE

Even though the focus of the effort reported here is on display dynamics, the interaction between the dynamics of how information is presented with the format with which it is displayed can be significant and hence affect how a pilot perceives the information itself. For this reason, some consideration has been given to the perceptual interface, in particular to the representation of perceptual factors in OCM terms. The following subsections briefly review previous display-related applications of the OCM, present two specific observation representations, and survey a variety of psychophysical factors, considering their relationship to lumped OCM parameters.

1. REPRESENTING DISPLAY-RELATED EFFECTS IN OCM TERMS

a. Deciding Display Formats

After the introduction of the basic OCM in the 1970s, much of its subsequent development and enhancement has been in an effort to represent more accurately a number of perceptual effects. The original model, for example, did not include attention fractions or perceptual thresholds. Both of these factors were incorporated into the model to enable the study of display-related issues. Baron and Levison (Reference 9) introduced attention fractions and the notion of position-rate pairs to model the observation of more than one variable (or variable pairs) in a complex manual control task. They also used this model to compare the alternative of having multiple indicators on a display with that of combining variables into a single indicator, e.g., a flight director. Kleinman and Baron (Reference 10) introduced observation thresholds in order to capture significant elements of an approach-to-landing task. The representation of threshold effects was refined in Reference 11 to include the describing function given in Equation 2. A comparative analysis of two display format alternatives was considered in this study as well, where the alternatives again corresponded to a baseline display of

indicators and an integrated display that included pictorial aids. Depending on the alternative considered, the thresholds, the fractions of attention, and the complement of variables actually observed were different.

Several researchers have used the OCM as a basis for the systematic development of display formats. Curry et al. (Reference 12) describe a three-level analysis procedure based on the OCM. At the first level, an information level, the complement of observed variables is not restricted, and optimization over attention fractions is used to determine those variables that are critical to the control task. At the second level, which is the display element level, the display variables selected are grouped in position/rate pairs, nominal observation thresholds are chosen, and a preliminary evaluation that incorporates these display elements is made. The third level, the display format level, is similar to the second, except that a specific display layout is represented. This means that all OCM parameters are then chosen to match this situation and to evaluate performance.

Another display design approach based on the OCM has been articulated by Hess (Reference 13). In addition to suggesting (limited) guidelines for display layout based on OCM results, the approach outlines a method for flight director design that is derived from OCM-generated pilot transfer functions. Finally, a number of display configurations are evaluated in Reference 14 using the OCM, including a specific predictor display and a flight director.

Although display dynamics are not addressed directly in the work described above (except for the consideration of flight directors), previous enhancements to the OCM and their use in evaluating alternative display concepts point to the applicability of the model in the present context. This previous work serves as a starting point for the representation of effects that are critical with respect to the development of a systematic methodology for defining display dynamics.

b. Modeling Scene Perception

Recent consideration of the notion of a "virtual cockpit", i.e., a cockpit in which no direct out-the-window observation is possible, makes it essential to understand which features in a visual scene are the critical information cues for piloting and how best to represent them in a (possibly) pictorial display. An analytical framework that is capable of deciding whether pictorial or indicator display formats are best, especially in conjunction with considering the addition of any compensating display dynamics, would be an important tool for design. Viewing this capability as something that will eventually be important for display dynamics considerations, the following briefly discusses previous work in scene perception that is believed to be relevant in the present context, particularly with respect to incorporation into an OCM-based methodology.

Much of what is currently understood about scene perception is based on the work of Gibson (Reference 15), who introduced the concept of streamers associated with textual points in the visual field. That is, except for the point in the horizon toward which a (piloted) vehicle is moving, all textural points in the visual field have a relative motion with velocity vectors called streamers. These streamers seem to expand from the single stationary point. It is from them that the various cues necessary for manual control of the vehicle's path are derived. From this premise, those cues that are actually used by the operator must be identified and then an analytic description must be constructed using their respective geometries in the visual field.

In addressing the modeling of scene perception for understanding manual control in such situations, Baron and Berliner (Reference 16) cite a taxonomy of visual cues developed by Matheny et al. (Reference 17) that is useful in structuring the problem. Relevant cues are those that are directly useful for controlling the vehicle or for making decisions. Nonrelevant cues (with respect to control) are those that are not essential to successful operation of the vehicle; they may, however, add realism to the control task. Relevant cues are further divided into primary, secondary, complementary, and conflicting types. It is assumed that an operator has a hierarchy of cues for a particular task and that primary cues are first sought when performing the task. Cues that tend to reinforce

primary cues are called secondary if they are from the same modality and complementary if they are from a different modality (motion vs. visual). Conflicting cues are those that are in opposition in terms of the information they present.

This taxonomy is useful when considered in terms of the statement made in Reference 16 that much of the concern in manual control has been with primary visual cues. However, cues of other types, though not primary, may provide critical supporting information when abstracting the quantities necessary to perform closed-loop manual control from a visual scene. Evidence that this might be the case is given by Naish (Reference 18), who constructed a geometrical model for perception of cues in a visual approach-to-landing situation. Based on the cues available from the movement of the runway in the visual field (which should be primary), the model was nevertheless unable to account for the greater level of performance exhibited by pilots. This suggests that pilots obtain other cues from the visual field that, although perhaps not primary, do contribute to enhanced task performance. Thus a methodology that considers display dynamics requirements in situations in which pictorial depictions are contemplated and which only considers the use of primary visual cues may not be adequate.

Control theoretic models that incorporate perception of primary visual cues have been successfully demonstrated in a number of instances. Wewerinke (Reference 19) has used linear perspective geometry and relative motion concepts to construct a model for the perception of cues in an abstracted approach-to-landing task. Once the basic geometry is in place that describes how the variables needed for manual control are derived from the visual scene, the OCM is used to analyze a number of visual scene configurations. The key parameters in this analysis are the perceptual thresholds associated with perceiving variables relevant to control from visual cues. These vary with the visual scene configuration and impact significantly the model-based predictions of task performance. Experimental evidence is presented to support the model developed.

Grunwald and Merhav (References 20 and 21) also attempt to incorporate the perception of visual cues into a control theoretic framework. Developed to address the problem of remote control of a vehicle using a TV image, their approach uses geometry of the visual

field to derive an expression for deviation from a prescribed flight path. To simplify the modeling, however, it is assumed that this error is always measured at a fixed distance from the vehicle. The model derived is then incorporated into the OCM framework for subsequent analysis of (remote) piloting performance. A key modeling choice made is the selection of a noise-to-signal ratio for those variables obtained from visual cues. Given the expression in Equation 2, this is a consideration equivalent to that in Reference 19. As in Reference 19, the basic model is used to evaluate possible enhancements to performance that might be obtained by augmenting the visual scene display with additional indicators, such as a velocity vector.

Finally, scene perception in the context of terrain following has been the object of study. Hess and Chan (Reference 22) analyze the use of preview in a helicopter nap-of-the-earth manual control situation. Their analysis is based on a visual field cue hypothesis. Essentially, the hypothesis asserts that the human uses visual field cues as inputs to an internal dynamic model that predicts flight path relative to the textural elements in the visual field. One of the consequences of this internal prediction is that preview compensation can be realized. A model based on this hypothesis is then developed and incorporated into the OCM framework for subsequent performance analysis.

A more fundamental approach to modeling the pilot's processing of visual flow field cues in a terrain-following context has been proposed by Zacharias (Reference 23). The approach presumes that the observer uses line-of-sight vectors to a number of textural features as the fundamental visual flow field information. From this set of vectors an impact time map is constructed internally that is analogous to the actual terrain, which in turn can be used to derive motion cues relevant for manual flight control. The approach circumvents some of the analytical difficulties that have led others to restrict visual flow field considerations to a fixed viewing distance. The complication with the impact time map concept is that a computational estimation process is required to construct the map from a given set of line-of-sight vectors. Though this does not prohibit its incorporation into the OCM framework, it is evident that some effort may be required to make the two approaches compatible for purposes of representing the use of visual cues in a control theoretic framework.

2. SPECIFIC OBSERVATION REPRESENTATIONS

In a comparative analysis to be described in Section IV, specific OCM models are used to represent various situations. Among other things, these situations are distinguished by the complement of variables assumed to be observed by the pilot. Following on the discussion in the previous subsection, this subsection considers two of the observation situations used in the Section IV analysis. They correspond to executing an approach to landing using a HUD or using out-the-window visual cues only.

a. Heads-Up Display

The flight path and attitude information provided by HUDs has been shown to improve performance in the visual approach and landing task (Reference 24). An example HUD with display symbology relevant to the flight-path tracking task embedded in the overall approach and landing task is shown in Figure 7. The pitch axis information available to the pilot from the HUD consists of the following:

1. Aircraft pitch attitude with reference to an artificial horizon: θ
2. Aircraft flight path: γ_e
3. Commanded flight path: γ_c
4. A flight director providing direct steering command information: FD

Aircraft heading and angle of attack (AOA) limiting symbols are also shown in Figure 7.

The blocks marked *Other Information* in Figure 7 provide alphanumeric displays of quantities such as calibrated airspeed, AOA, barometric and radar altitude, sink rate, and range to touchdown. Information on wind speed and direction, control configuration of the aircraft, etc., may also be provided. Although all this information is required for the successful completion of an actual landing task, these variables are not important within the framework of the task to be considered in Section IV, which is that of precise control of flight path angle.

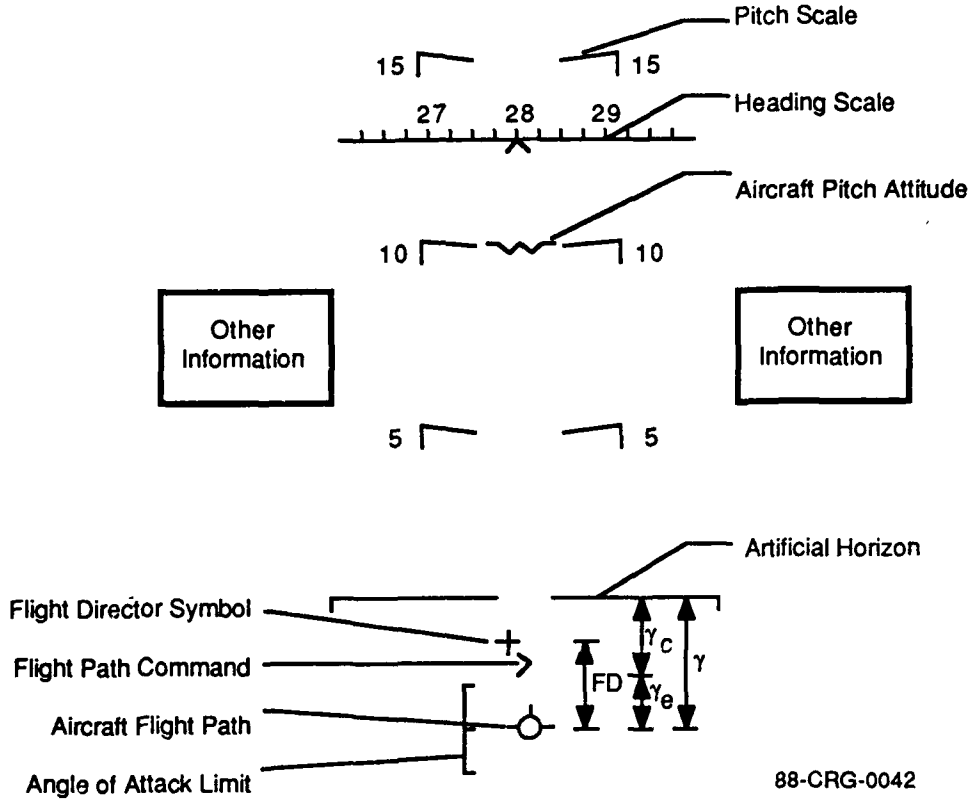

Figure 7. Example HUD Symbology for Landing Task.

With this in mind, the information assumed to be most relevant to the task and that is available from the HUD is taken to be embodied in the variables

- γ_e, $\dot{\gamma}_e$: Flight path error and rate
- γ, $\dot{\gamma}$: Flight path and rate
- θ, $\dot{\theta}$: Pitch attitude and rate

The observation vector in an OCM-based analysis of this task is therefore selected to include these elements. In addition, one of the alternatives considered in Section IV is

the assessment of the utility of the FD. Thus, depending on whether the situation under study uses it, the flight director signals FD and $\dot{FD}$ may also be included in the relevant task information and OCM observation vector.

b. Visual Approach in the Absence of HUD

In contrast to the situation where a HUD is available, executing a visual approach without one limits the information available to the pilot. In particular, accurate flight path error and flight path information is not present. Since they are assumed to be critical to the precision control of the flight path, the pilot must infer them from other more readily observable phenomena. With this in mind, the analysis presented in Section IV assumes that pitch attitude and pitch rate are available as observations (e.g., with visual reference to the horizon). In addition, the pilot is assumed to be able to sense and use normal acceleration (n_z). Finally, the pilot must have some sense of his desired flight path, even though it is not assumed that he can reliably observe actual flight path or directly observe flight path error. In an OCM framework, this is represented by declaring that the pilot is able to observe commanded flight path and commanded flight path rate (γ_c, $\dot{\gamma}_c$). Thus in the situation where a visual approach is executed without a HUD (referred to as VFR in the sequel), the OCM observation vector that models the information used by the pilot for flight path control is taken to include

- γ_c, $\dot{\gamma}_c$: Flight path command and rate
- θ, $\dot{\theta}$: Pitch attitude and rate
- n_z: Normal acceleration

3. SELECTING OCM PERCEPTUAL PARAMETER VALUES

As discussed in Section II, the OCM has three elements that model the perceptual processes of the human operator. These are cognitive/perceptual delay, observation thresholds, and observation noises. In each case these quantities are a lumped representation of complex psychophysical processes and phenomena. Though there exists a well-established set of "typical" values for these parameters, the accurate representation in OCM terms of a given task situation requires careful selection of these parameters, especially when display-related effects are of interest. For this reason, some

effort has been devoted to documenting those psychophysical factors that are lumped into OCM parameters, as well as on discussing the relationship of the two. The intended result was to provide some guidelines for choosing OCM perceptual parameters for a given modeling situation. The appendix to this report presents a first step in this direction. A summary of that discussion is presented here.

With respect to observation thresholds, the single threshold used in the OCM actually represents the effects of several psychophysical thresholds plus a cognitive-based thresholding. In the former category are included incremental, acuity, displacement, and rate thresholds. For the latter category, the thresholding effect is one of indifference. That is, the pilot may be able to distinguish changes in a variable with no difficulty but may be indifferent to these changes because they are not large enough to affect his control objectives. Thus, depending on the type of task the pilot is expected to perform, the environment in which it is to be performed, and the display design, any one of these thresholds can be the relevant or dominant thresholding effect.

The incremental threshold is defined as the minimum change in luminance that can be detected. It becomes important, for example, when a pilot's performance is limited by his ability to see display elements, such as when attempting to monitor HUD symbology against a bright out-of-cockpit scene.

The acuity threshold is defined as the reciprocal of the minimum visual angle (in minutes) that can be resolved. This threshold is important in the discrimination of fine spatial detail, such as the discrimination among alphanumeric characters or the detection of a gap between two solid lines. The latter task is performed routinely in conjunction with manual control, e.g., when the pilot is required to detect indicator displacement.

The other two thresholds become important when motion of the display indicator is a factor. When a task requires the resolution of fine spatial differences between two elements that are moving relative to each other, then the displacement threshold becomes important. Because of the additional cue that motion provides, the displacement threshold is always at least as good as the acuity threshold. Finally, a rate threshold becomes significant when it is required to determine the velocity of indicator movement.

Though the usual OCM formulation does distinguish between displacement and rate thresholds, a systematic consideration of how their values vary with respect to a number of display and environmental factors is typically not made. Moreover, the determination of which threshold effect is dominant under certain task conditions, including whether a true indifference threshold is dominant, can significantly impact the model and any subsequent model-based results. This possibility reinforces the idea of establishing guidelines for mapping several basic psychological threshold factors into a single lumped OCM threshold parameter.

With respect to perceptual/cognitive delay, the OCM lumped representation encompasses delays due to sensory, perceptual, and cognitive neural processing. Although it is possible to consider each individually, it seems that a lumped representation is sufficient for present purposes, provided that variations of this delay due to task-dependent factors, environmental factors, or changes in a pilot's vigilance state are incorporated and considered.

Finally, with respect to observation noise, a fundamental difference is apparent between this OCM quantity and usual psychological characterizations. Though it has been given a specific interpretation within the OCM, observation noise is essentially a remnant term. The significance of the -20 dB ratio as being related to fundamental human processing limitations notwithstanding, observation noise serves to characterize that part of the human operator's behavior that is not explainable using the optimal control theoretic model structure. By contrast, the interest in psychological investigations is to develop models and paradigms that systematically explain human behavior and limitations. Thus the translation of psychological factors identifiable in a given task situation into guidelines for choosing the OCM observation noise-to-signal ratios is unclear. That these factors, as well as those from the environment, do alter the effective value of this ratio is evident from Reference 20. As a first cut at establishing guidelines for selecting values of noise-to-signal ratios, therefore, it is assumed that the factors considered in the appendix have similar effects on observation noise and perceptual/cognitive delay.

The factors considered in the appendix include those of luminance, color, angle of view, pilot pupil size, display indicator size and shape, display clutter, display layout, display motion, saccadic eye movements, and display variability. Each factor is discussed in turn, and its specific impact on observation thresholds and observation delay is considered, with the impact on observation noise being taken as qualitatively the same as that on delay. As indicated earlier, the intent of the discussion is to take a first step toward developing guidelines that would permit the systematic selection of OCM perceptual parameters in a comprehensive display dynamics analysis methodology.

SECTION IV

MODEL-BASED ANALYSIS OF DISPLAY DYNAMICS EFFECTS USING THE COOPERATIVE APPROACH

In this section, results of a case study are presented in which a variety of display options are considered for a representative short take-off and landing (STOL) vehicle in an approach and landing situation. A first set of results explores how performance and workload can improve over a basic VFR display situation when the additional information available on a HUD is used in performing the approach. This additional information is obtained at some cost in processing for computation and formatting, however. Indeed, when realistic delays are included for this processing, the advantage in having the additional information quickly becomes questionable.

This deterioration in performance is the object of a second investigation, in which the Cooperative methodology is exercised in various ways to attempt to compensate for the HUD delay. One of these is to design a flight director (FD) signal, with its own set of augmented dynamics, to be included on the HUD. Another is to augment the basic vehicle dynamics using the Cooperative procedure. Finally, a simultaneous selection of vehicle control and display augmentation gains is made using the Cooperative approach. In the first two cases, some compensation for the HUD delay is achieved, though the workload induced by the FD design is in some cases probably not acceptable for a Level 1 flying qualities rating. In the third case, where vehicle control and display augmentation are selected simultaneously, the full benefits of having the additional HUD information are nearly recovered.

The results of this case study serve to illustrate that HUD formatting and computational delays can have a significant (negative) impact on flying qualities. They also show that it is possible to compensate for these effects. Finally, the Cooperative approach used to effect this compensation illustrates one approach to the systematic selection of display dynamics.

This section is organized as follows. First, the basic airframe dynamics are considered and a baseline control augmentation system is defined that satisfies a Level 1 flying qualities specification. Next, this baseline system is used in a model-based analysis for a variety of perceptual situations, e.g., with and without a HUD. Finally, the use of the Cooperative approach to investigate HUD compensation alternatives is discussed. All of this work is documented in detail in Reference 25; the presentation here will summarize the key results.

1. VEHICLE DYNAMICS AND CONVENTIONAL CONTROL DESIGN

As indicated above the vehicle used in this case study is a STOL aircraft with an airframe representative of a modern fighter aircraft. For present purposes, a linearized dynamic model in the longitudinal axis has been used, expressed in body axis system coordinates. A typical approach-to-landing trim condition has been used as well. Specifically, velocity was set to 202 ft/sec, attitude to 4.7 deg, angle of attack to 7.7 deg, flight path to -3 deg, and aircraft weight to 28,000 lb. In this configuration, the vehicle is statically unstable and clearly not acceptable according to flying qualities specifications. A block diagram of the aircraft with its control augmentation system is shown in Figure 8. The basic vehicle dynamics for the linearized model is given in state space form as:

$$A_v = \begin{bmatrix} -0.0575 & -0.2023 & -0.4656 & -0.5600 \\ -0.2900 & -0.3237 & 3.4399 & -0.0459 \\ -0.1727 & 0.3317 & -0.6121 & 0.0061 \\ 0.0 & 0.0 & 1.0 & 0.0 \end{bmatrix} \tag{8}$$

$$B_v = \begin{bmatrix} 0.1237 & -0.0299 & -0.1134 & -0.2940 \\ -0.3208 & -0.1701 & -0.3565 & -0.0298 \\ -1.7627 & -1.4325 & 0.2021 & -0.2481 \\ 0.0 & 0.0 & 0.0 & 0.0 \end{bmatrix} \tag{9}$$

$$C_v = \begin{bmatrix} 1.0 & 0.0 & 0.0 & 0.0 \\ 0.0 & 0.284 & 0.0 & 0.0 \\ 0.0 & 0.0 & 1.0 & 0.0 \\ 0.0 & 0.0 & 0.0 & 1.0 \\ 0.0 & -0.284 & 0.0 & 1.0 \end{bmatrix} \tag{10}$$

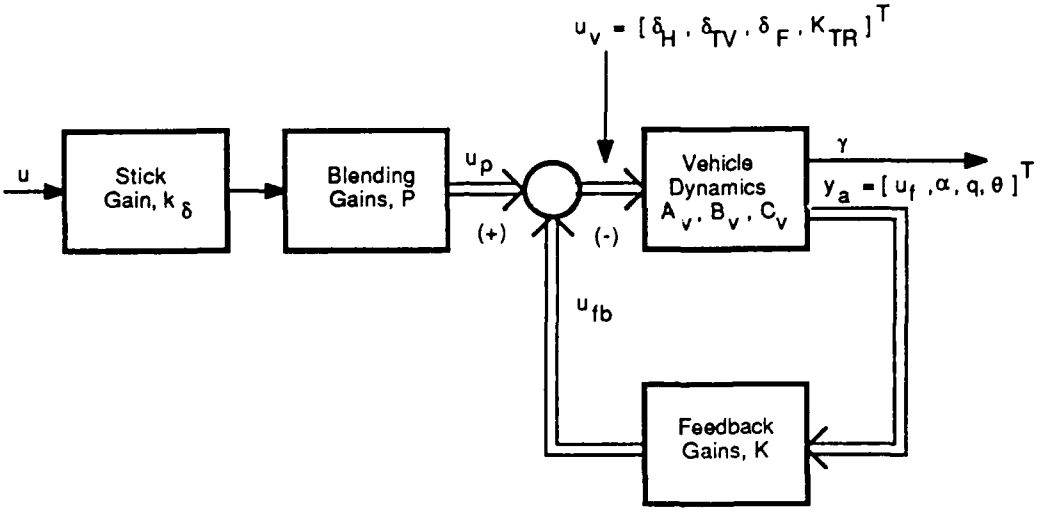

Figure 8. Block Diagram of Vehicle and Control System.

The state vector for the vehicle consists of forward speed in ft/sec (u_f), vertical speed in ft/sec (w), pitch rate in deg/sec (q), and pitch angle in deg (θ). The four control inputs are horizontal tail deflection in deg (δ_H), thrust vector angle in deg (δ_{TV}), trailing edge flap deflection in deg (δ_F), and thrust reverser expressed as the percentage of flow split (K_{TR}). Finally, the vehicle responses of interest are u_f, α, q, θ, and γ, where α and γ are angle of attack in deg and flight path angle in deg, respectively. Key transfer functions for the STOL vehicle are listed in Appendix B, which also contains relevant closed-loop transfer functions for the three augmentation cases considered in this section.

As a baseline case, the vehicle dynamics are augmented with a set of feedback gains, K, and a set of blending gains, $P \cdot k_\delta$, such that Level 1 flying qualities are achieved according to existing handling qualities specifications. Short period and phugoid criteria in Reference 26 were used to meet attitude stability and phugoid mode specifications. The parameter $\tau_{\theta 2}$, which governs the γ-to-θ relationship, was selected according to the

discussion in Reference 27, which suggests a value less than 0.75 to achieve rapid flight path control. The gains selected that accomplish this are given as:

$$K = \begin{bmatrix} 0 & -1.06 & -0.28 & 0 \\ 0 & -3.18 & -0.84 & 0 \\ 0 & -2.11 & 0 & 0 \\ -0.6 & 0 & 0 & 0 \end{bmatrix} \tag{11}$$

$$P \cdot k_{\delta} = \begin{bmatrix} -3.5 \\ -10.5 \\ 0 \\ 0 \end{bmatrix} \tag{12}$$

As a further indication that the baseline augmented vehicle has the desired property of a good flying qualities rating, its augmented dynamics have been compared with the configurations in the LAHOS data base. Based on a number of comparison points, such as frequency response, time histories, and system modes, the baseline augmented vehicle was similar to the LAHOS 2-1 configuration, which itself achieved a pilot rating of 2 on the Cooper-Harper scale. In the sequel, the augmented vehicle system represented by *Equations 8 through 12 will be referred to as the baseline aircraft.*

2. MODEL-BASED EVALUATION AND HUD TIME-DELAY EFFECTS

In this subsection, performance of the approach and landing task is considered using the baseline aircraft and several perceptual alternatives. One of these alternatives is where a conventional attitude indicator is assumed for a display. A second is one that assumes a HUD. *In the latter, a number of variations will be considered, corresponding to the* effective HUD processing delay, denoted τ_d. The two classes will be referred to as VFR and HUD, respectively.

a. Modeling Procedure

An extensive model-based study of pilot/vehicle interaction in the approach and landing task was performed by Anderson and Schmidt and is reported in Reference 5. In that study, it was hypothesized that for a given vehicle dynamic configuration, the ability to precisely control flight path angle is a necessary condition to obtain good pilot ratings in the approach, flare, and landing task. Under such a hypothesis, the pilot's task has been modeled as that of tracking a flight path angle command. Representing this in terms of the OCM the configurations considered in the LAHOS study (Reference 8) were evaluated. As shown in Reference 5, this procedure led to excellent correlation between pilot ratings and model results, such as pilot phase compensation and closed-loop RMS flight-path error. A similar modeling approach will be used in the study presented in this section.

In the formulation of the OCM approach, the task of precisely tracking a flight path angle command is represented by selecting the following cost function:

$$J_p = \lim_{T\to\infty} E\left\{ \frac{1}{T} \int_0^T \left(\gamma_e^2 + r\dot{u}^2 \right) dt \right\} \tag{13}$$

where γ_e is the flight path tracking error ($\gamma_e = \gamma_c - \gamma$) and g is selected to yield a reasonable pilot controller bandwidth. This selection is reflected in the value of the neuromotor lag time-constant, τ_N. As described earlier in Section II, Reference 5 uses a prefilter driven by white noise to generate a hypothesized flight-path-angle command signal, with a frequency content that is representative of a VFR landing task. The command dynamics are the same as those used in Section II and are repeated below in state space form:

$$\begin{bmatrix} \dot{\theta}_c \\ \ddot{\theta}_c \\ \dot{\gamma}_c \end{bmatrix} = \begin{bmatrix} 0 & 1 & 0.5 \\ -0.25 & -0.5 & 0 \\ 0.5 & 0 & -0.5 \end{bmatrix} \begin{bmatrix} \theta_c \\ \dot{\theta}_c \\ \gamma_c \end{bmatrix} + \begin{bmatrix} 0 \\ 0.25 \\ 0 \end{bmatrix} w_c \tag{14}$$

Recall that w_c is a zero-mean white Gaussian random process with intensity equal to 64. This results in an RMS value for γ_c of 3.25 deg, which is intended to be representative of the effective variability associated with the actual flight path tracking task.

1) VFR Case–As discussed in Section III, in the conventional VFR task the responses sensed by the pilot are assumed to be pitch attitude, pitch rate, and normal acceleration. Also, since the pilot does not have any instrument giving him flight-path command information, the desired flight path is assumed to be generated internally. For this case, referred to as the VFR case, the pilot's observation vector for OCM analysis is then given as:

$$y^T = \left[\gamma_c, \dot{\gamma}_c, \theta, \dot{\theta}, n_z\right]^T \tag{15}$$

2) HUD Case–A second perceptual situation of interest is where a HUD is used to assist in the approach and landing. Discussion of the selection of an OCM observation vector to represent this situation has been given in Section III. The outcome of that discussion has been to assume that the pilot obtains and uses flight path error and error rate, flight path angle and rate, and pitch attitude and rate as inputs when deciding his control action. For this case, referred to as the HUD case,

$$y^T = \left[\gamma_e, \dot{\gamma}_e, \gamma, \dot{\gamma}, \theta, \dot{\theta}\right] \tag{16}$$

Assuming a time-delay of τ_d sec in the HUD, a block diagram for pilot/vehicle interaction in the HUD case is shown in Figure 9a. Within the framework of the OCM, the time-delay can be accounted for in terms of a Padé approximation. Since it is assumed that the pilot still derives all the information relevant to the task from the HUD, the time-delay can be reflected at the plant input to obtain the equivalent system shown in Figure 9b. This model, with a second-order Padé approximation for the time delay, was used to assess the effects of HUD delay.

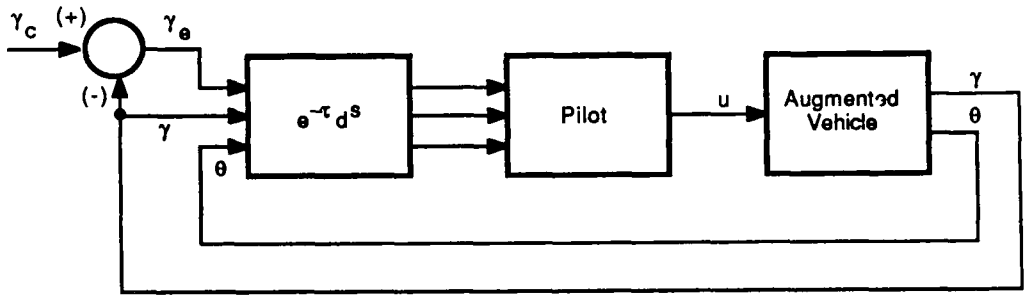

a. Time delay at pilot observations.

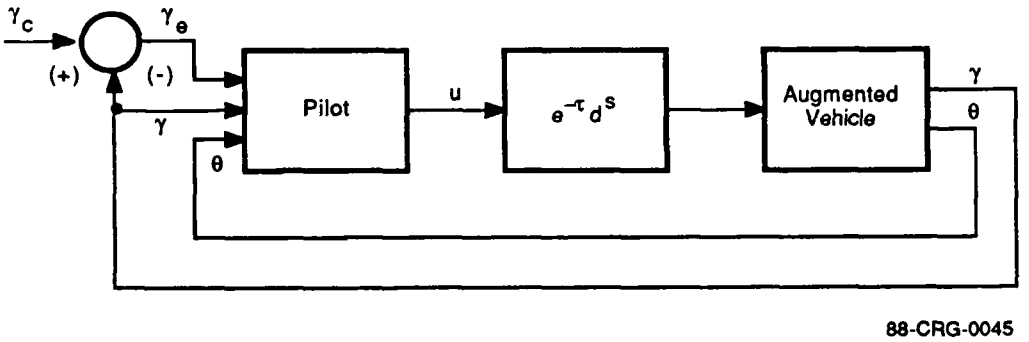

b. Time delay at pilot input.

Figure 9. Block Diagrams for Modeling HUD Time Delay.

3) Other OCM Parameters–The remaining model parameters were set to values typical of those found in the literature. These are as follows. Observation thresholds for angular deflections and angular rates are set to 0.05 deg and 0.18 deg/sec, respectively, which is consistent with the choice in Reference 5. In the VFR task, the observation threshold for n_z was chosen to be 0.05 g's (1.6 ft/sec^2). The full attention observation noise-to-signal ratio was chosen to be -20 dB for each observation. The pilot's full attention was assumed to be devoted to the control task, with the attention allocation between the various observations optimized using the procedure in Reference 28. For the attention optimization, the angular deflection and rate observations were considered in pairs. Since the pilot generates the command internally in the VFR task, ideal knowledge of the command (γ_c and $\dot{\gamma}_c$) was assumed, and the attention allocation

division was considered between θ and n_z only. Finally, the motor noise ratio was set at -25 dB and observation time delay, τ_p, was set at 0.2 sec.

This leaves only the value of the neuromuscular time constant, τ_N, unspecified. Typical values for this parameter range from 0.1 to 0.25, depending on the OCM application. In Reference 5, a value of 0.1 was chosen to reflect aggressive pilot behavior, which would in turn tend to expose handling qualities cliffs in the model-based analysis. Here an alternative scheme for selecting τ_N has been used, based on an observed performance/workload tradeoff that is apparent as a function of τ_N. This tradeoff was introduced in Reference 29 and is illustrated in Figure 10 for the baseline aircraft. Normalized workload is plotted on the abscissa, where workload is defined as RMS $\dot{u}$ and where the normalizing factor is the model-based value of $\sigma_{\dot{u}}$ obtained when $\tau_N = 0.1$.

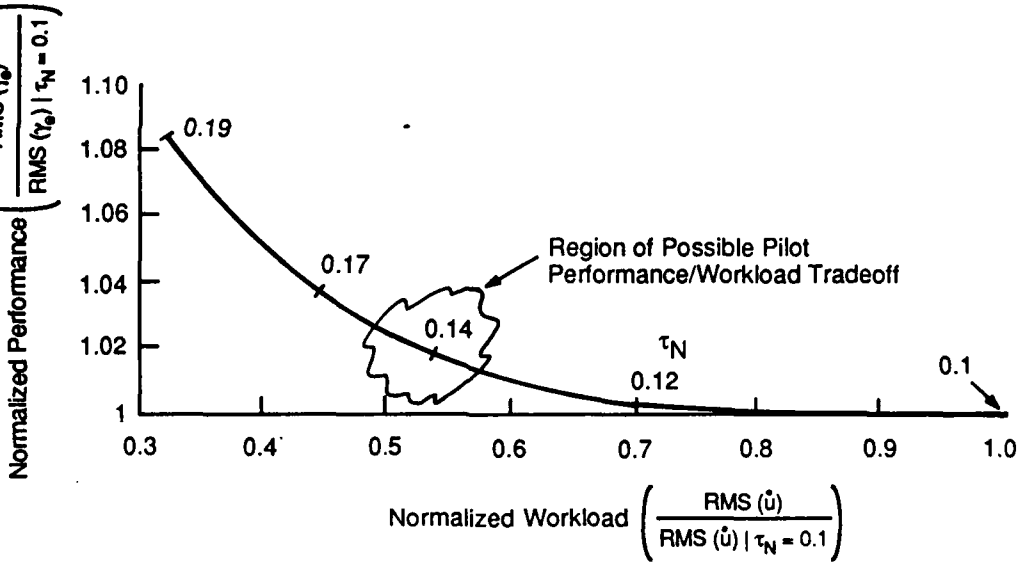

Figure 10. Performance/Workload Tradeoff by Varying τ_N.

Similarly, a normalized performance is defined and plotted on the ordinate axis using $\sigma_{\gamma e}$ as the performance measure for this task. The plot shown in Figure 10 is that of normalized workload vs. normalized performance as a function of τ_N. The interesting feature of the plot is that, up to a point, a substantial reduction in workload can be realized with only a slight degradation in performance. Assuming that a well-trained pilot will work just hard enough to achieve an acceptable level of performance, choosing a value of τ_N somewhere near the knee in the curve of Figure 10 represents a reasonable approach to modeling this performance/workload tradeoff. The viability of this model-based adjustment procedure is supported by experimental evidence in Reference 29, and it has been used to select τ_N in the analysis reported in this section.

b. Model-Based Evaluation Results

Four cases involving the baseline aircraft were analyzed. Included were the VFR case and three HUD cases where τ_d was set to 0.0, 0.1, and 0.2 sec. In addition, for comparison purposes the LAHOS 2-1 case was examined using the VFR and no-delay HUD observation situations. The results of this analysis are summarized in Table 4. The values of τ_N were obtained using the adjustment procedure described earlier. RMS

TABLE 4. MODEL-BASED EVALUATION RESULTS

Aircraft	Observation Case	τ_N (sec)	RMS γ_e (deg)	RMS $\dot{u}$ (in/sec)	ω_c (rad/sec)	ϕ_{peq} (deg)
Baseline	VFR	0.14	0.71	3.62	2.0	29.0
	HUD+τ_d=0	0.14	0.57	3.73	1.9	28.8
	HUD+τ_d=0.1	0.19	0.69	2.49	1.7	38.8
	HUD+τ_d=0.2	0.26	0.83	1.65	1.5	50.1
LAHOS 2-1	VFR	0.14	0.71	3.47	2.0	44.0
	HUD+τ_d=0	0.14	0.51	3.49	2.1	46.2

values of flight path error and control rate were obtained directly from the OCM analysis output. The frequency domain results of crossover frequency (ω_c) and equivalent pilot phase compensation ($\angle peq$) were obtained using the procedure defined in Reference 5. This procedure involves the construction of an equivalent single-loop pilot transfer function from γ_e to u from the multivariable OCM model. From this transfer function, crossover frequency and equivalent phase compensation can be measured. The latter is defined as the maximum pilot phase compensation in the region of crossover and is used as an indication of workload for this task.

To better understand the results in Table 4, a plot of RMS γ_e versus $\angle peq$ is shown in Figure 11, and a plot of RMS γ_e vs. RMS $\dot{u}$ is shown in Figure 12. From the figures, it is first of all evident that the baseline vehicle is comparable to the LAHOS 2-1 vehicle as was intended, both for the VFR and HUD cases. This is particularly evident in Figure 12, where τ_N is the same for all four cases and thus makes RMS $\dot{u}$ comparable across these cases.

Also evident from the figures is the improvement in performance possible with extra information provided by the HUD (with no delay). This is indicated for both the baseline and LAHOS 2-1 aircraft. The mechanism for this improvement is best understood by an inspection of Figure 13. Shown there is the power spectra of the pilot control input (u) as obtained for the VFR and the HUD observation cases using the baseline aircraft dynamics. Both the total spectra as well as the remnant reflected at the pilot stick input are shown. (Remnant is defined as that part of pilot stick input which is not correlated with the command in the control task (Reference 30).) Note that, although the total power spectra is the same for both the VFR and HUD cases, the remnant is significantly lower for the HUD case in the command signal bandwidth region. Thus, the apparent effect of providing direct flight path information is to reduce the amount of error (noise) injected by the pilot into the system, which results in improved tracking performance.

Finally, as the HUD delay increases, deteriorations in both performance and workload are evident in the figures. Because of differences in the current modeling procedure from those used to construct the flying qualities correlations given in Section II and in

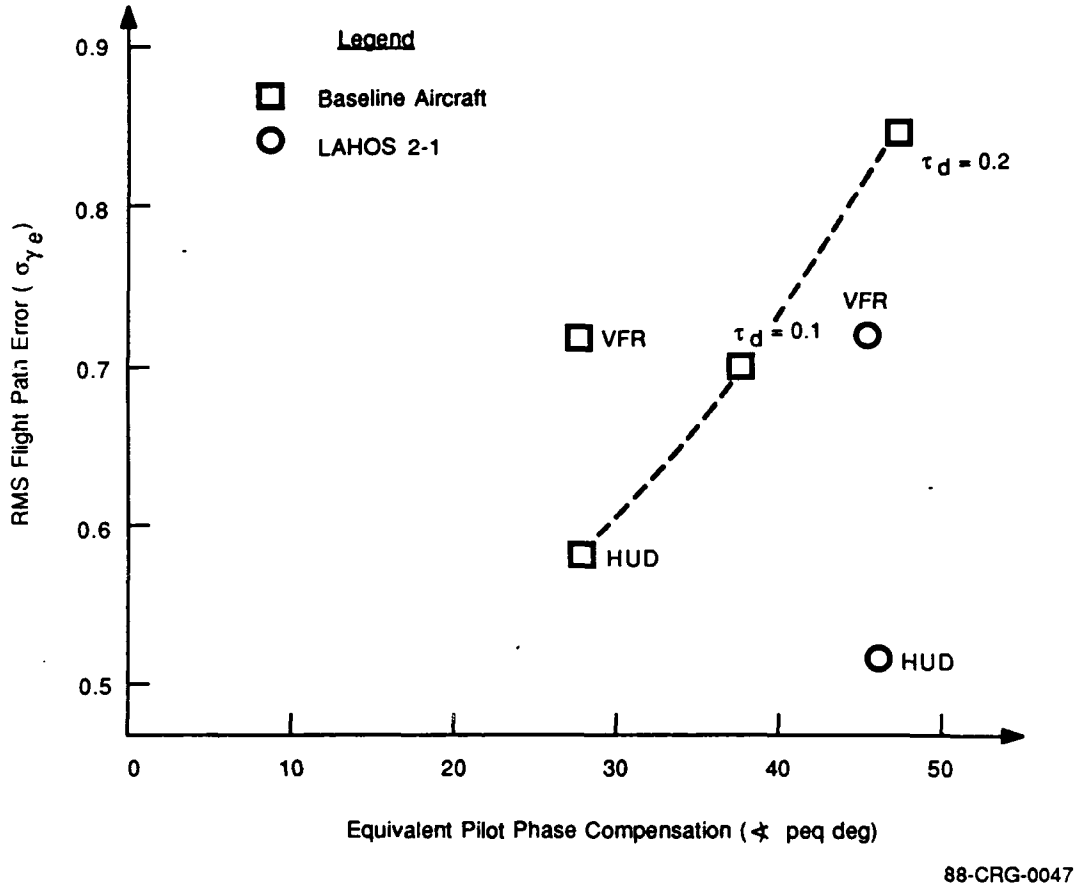

Figure 11. Model-Based Performance/Workload Results I.

Reference 5, direct comparison of Figures 11 and 12 with those correlations is not possible. (The differences are due to the τ_N adjustment procedure and to using different values for stick sensitivity.) In addition, because the selection of τ_N directly impacts RMS $\dot{u}$ (through its relationship to the cost function weighting on $\dot{u}$), the results for the nonzero HUD delay cases are not directly comparable in Figures 11 and 12. However, Figure 11 in particular indicates that pilot workload increases with increasing τ_d, even when the pilot is assumed to be making a reasonable performance/workload tradeoff. Note also that for $\tau_d = 0.1$, Figure 11 indicates that the HUD is similar to the VFR case.

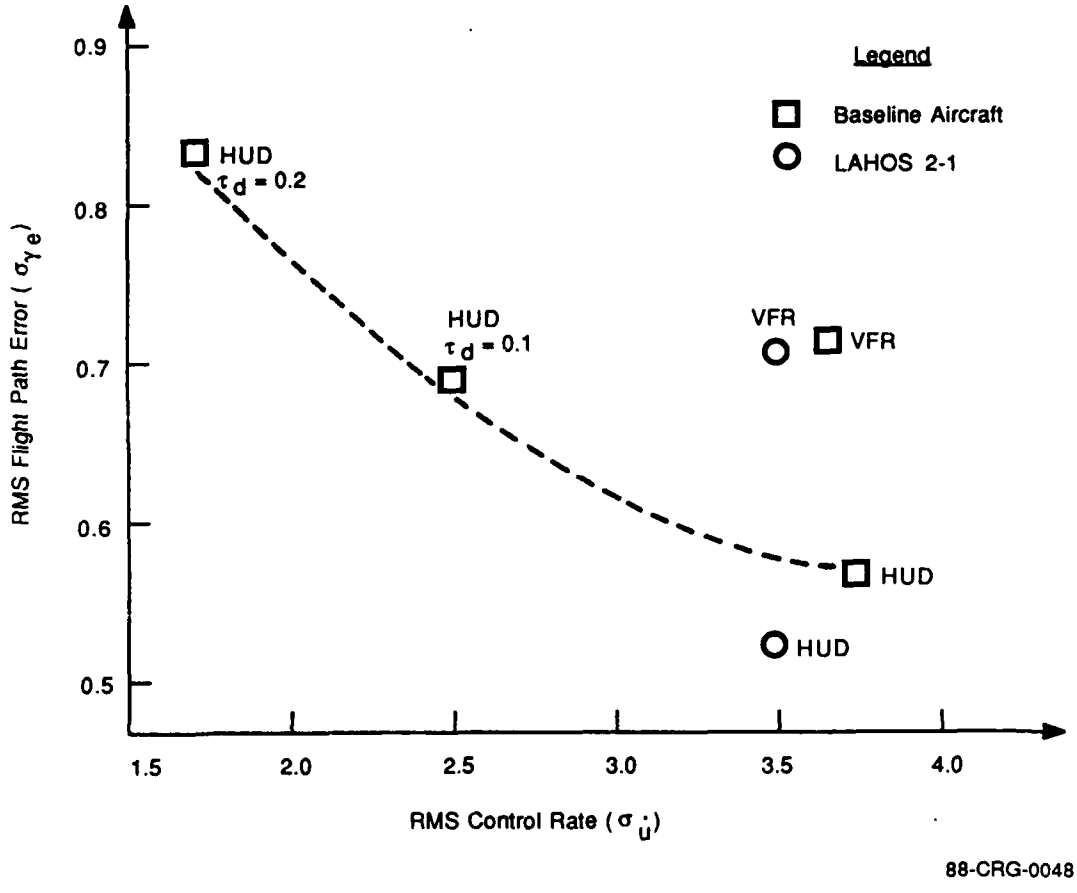

Figure 12. Model-Based Performance/Workload Results II.

The interpretation here is that for low values of HUD time delay, there should be little deterioration in pilot rating. This is in agreement with experimental results reported in Reference 31.

In sum, the evaluation results depicted in Figures 11 and 12 indicate that while additional information displayed to the pilot can significantly improve performance, the computational and formatting overhead to do this, as manifested in a transport delay, can severely compromise the advantages of presenting the information. This is a case then, where the display dynamics inherent in a system are undesirable. The next subsection

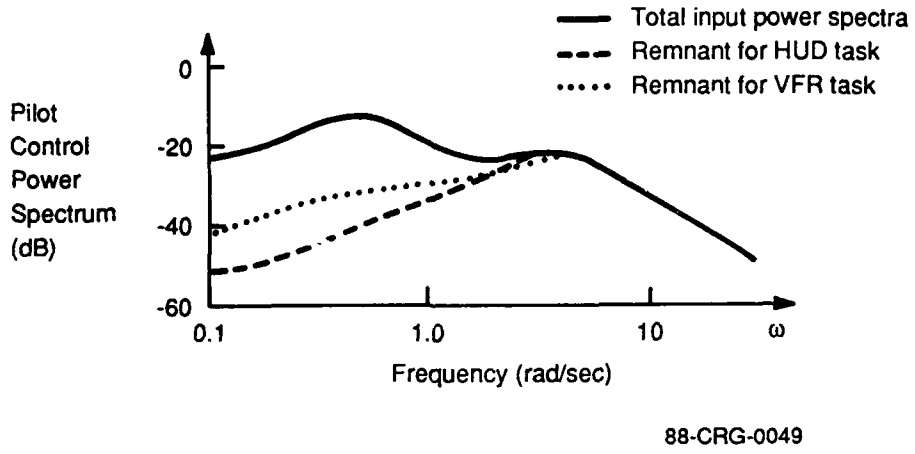

Figure 13. Pilot Control Input Power Spectra Comparison.

considers how compensation with additional display dynamics can overcome this situation.

3. COMPENSATION FOR HUD DELAY USING COOPERATIVE SYNTHESIS

The results obtained in the previous subsection indicate that for the baseline aircraft a HUD delay of 0.2 sec will considerably increase tracking error. This section uses the Cooperative approach to explore several alternatives for avoiding this effect. One alternative is to introduce an FD on the HUD (see Figure 7) and specify its dynamics such that performance is improved. Another (nondisplay related) alternative is to modify the vehicle's augmentation gains to be in concert with the pilot's compensation. A third alternative is to simultaneously adjust FD and vehicle augmentation dynamics to obtain a system in which pilot, vehicle, and display complement each other.

After a brief review of the Cooperative Synthesis methodology, the following paragraphs discuss each of these alternatives in turn. Of primary interest here is verifying that the introduction of compensating display dynamics can overcome undesirable inherent display system dynamics and that this introduction can be accomplished using a systematic, model-based approach.

a. Cooperative Synthesis Approach

The Cooperative Synthesis technique for simultaneous design of pilot-optimal control and display augmentation is structured as depicted in the block diagram of Figure 14. In the figure, Controller 1 is a simplified pilot model similar to the OCM. The objective of the synthesis technique is to find the "best" combination of the control augmentation gains, G_a, and the display augmentation gains, G_d, that simultaneously minimize 1) an appropriately defined pilot objective function, and 2) an augmentation cost function that reflects the task being performed. A detailed description of the synthesis procedure is contained in Reference 25. The following will review only basic concepts to establish notation and context for subsequent discussion.

In Figure 14, vehicle and display dynamics are assumed to be linear, time-invariant, and finite dimensional. Hence they can be expressed in standard state-space form. In this context, the C matrices correspond to mappings of the various state variables x and control variables u into the variables observed by the pilot (y). Furthermore, the control laws G_a and G_d are constrained to be matrix gain elements. The pilot receives noisy observations of vehicle and display states and the display control u_d. The noise process v_y is assumed to be a zero-mean white gaussian process with intensity V_y. Thus the form of the controller (y_p to u) is that of a linear-quadratic-gaussian (LQG) compensator (linear full-state feedback in series with a linear, least-squares state estimator), where K_p is a matrix of state feedback gains used in conjunction with a Kalman estimator. With the addition of the neuromotor lag element, Controller 1 closely approximates the OCM, with the major difference being that of neglecting the perceptual/cognitive delay element, and the predictions associated with it.

The Cooperative Synthesis problem is set up by formulating dual cost functions, one that reflects the objectives of the pilot and one that reflects objectives for the display and vehicle controllers. Formally stated, these cost functions are given as follows.

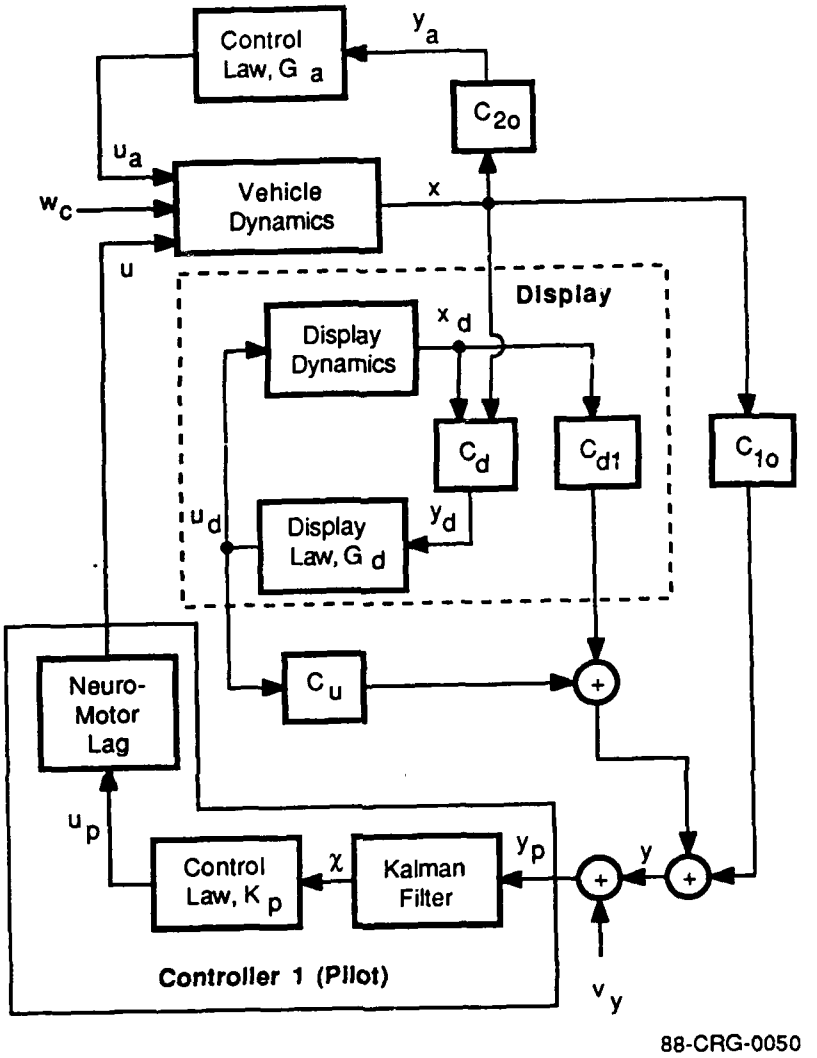

Figure 14. Cooperative Control/Display Augmentation Block Diagram.

Cost function 1 (pilot):

$$J_1 = \lim_{T \to \infty} E\left\{ \frac{1}{T} \int_0^T \left(x^T Q_{10} x + x_d^T Q_{1d} x + u^T R_1 u + u_a^T F_1 u_a \right) dt \right\} \qquad (17)$$

Cost function 2 (display and vehicle);

$$J_2 = \lim_{T\to\infty} E\left\{\frac{1}{T}\int_0^T \left(x^T Q_{20} x + x_d^T Q_{2d} x_d + u^T R_2 u + u_a^T F_2 u_a + u_d^T F_{2d} u_d\right) dt\right\} \quad (18)$$

In Equations 17 and 18, the weighting matrices Q_{10}, Q_{20}, Q_{1d}, Q_{2d}, R_2, and F_1 are chosen to be positive semi-definite, and the matrices R_1, F_2, and F_{2d} are chosen to be positive definite.

The Cooperative Synthesis problem, then, is to find an equilibrium solution, where J_1 is to be minimized through selection of u and J_2 is to be minimized with respect to u_a and u_d. Formally, this problem is that of a multiplayer nonzero sum game and the Cooperative Synthesis solution finds a Nash point (Reference 32).

Details of an algorithm to find a Nash solution are given in Reference 25. Here it is sufficient to note that there are several variations on the problem that will be of interest in the sequel. Besides the full cooperative formulation represented by the cost functions in Equations 17 and 18, it is possible to consider a *display-only solution*, e.g., selecting control laws for u and u_d only, assuming that G_a is known. Similarly, it is reasonable to seek a vehicle-control-only solution, where the display control law is either fixed or the display is unaugmented. Both of these cases will be considered subsequently. Finally, though the Cooperative Synthesis procedure uses an approximation to the OCM, any subsequent analysis using synthesized control laws for G_a and G_d does use the full OCM structure. In order to ensure that the synthesis results are consistent with the full structure, the algorithm described in Reference 25 modifies the noise-intensity parameters V_y (see Figure 3 and Equation 1) at each iteration in the synthesis solution procedure.

b. Formulation of Cooperative Synthesis Problems

1) Flight Director–The first compensation alternative considered for overcoming the effects of HUD delay has been that of adding an FD to the HUD display. A Cooperative

Synthesis problem was formulated as follows for a display augmentation-only solution in order to investigate this alternative. Based on the work reported in References 33 and 34, the FD signal was chosen to have dynamics of the form

$$FD = \gamma_e + g_{\dot{\gamma}e}\dot{\gamma}_e + g_\theta\theta + g_q q \tag{19}$$

where the g's are the FD gains to be determined. q and θ have been included in Equation 19 to account for the fact that the pilot might be closing the pitch attitude loop in the flight path tracking task. $\dot{\gamma}_e$ has been included to provide lead information. (Note that when implementing an FD of this form, the pitch attitude signal will also be passed through a wash-out filter, and then the FD signal will approach γ_e in steady flight.) A block diagram description of the system with an FD is given in Figure 15.

In order to represent Equation 19 in a form compatible with the Cooperative Synthesis approach, the FD signal is passed through an additional first-order lag at 100 rad/sec. This yields a time domain description for FD of

$$\dot{FD} = -100\,FD + 100\,\gamma_e + 100\,u_d \tag{20}$$

The display control law u_d is now defined as $G_d y_d$, where $G_d = [g_{\dot{\gamma}e}, g_\theta, g_q]$ and $y_d = [\dot{\gamma}_e, \theta, q]^T$.

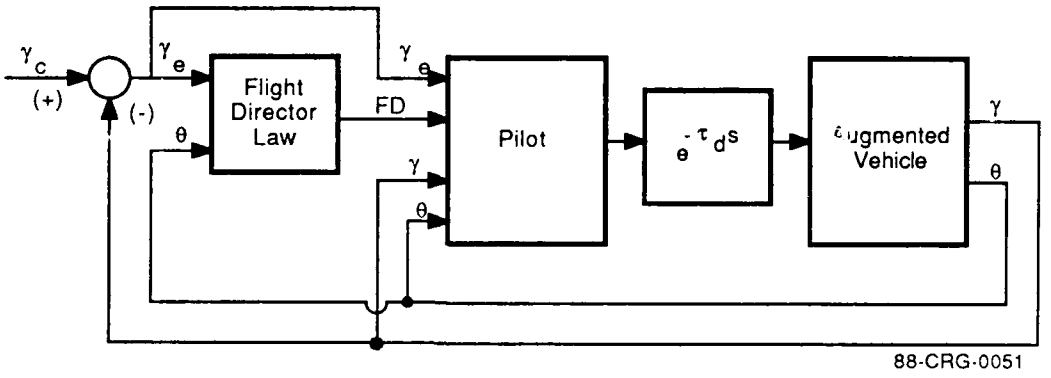

Figure 15. Block Diagram for Flight Director Design.

With the FD on the HUD, the pilot's observation vector is modified to include FD and $\dot{FD}$:

$$y^T = \left[\gamma_e, \dot{\gamma}_e, \gamma, \dot{\gamma}, \theta, \dot{\theta}, FD, \dot{FD}\right] \tag{21}$$

The cost function J_1 for the pilot (model) is (see Equation 17):

$$J_1 = \lim_{T\to\infty} E\left\{\frac{1}{T}\int_0^T \left(\gamma_e^2 + n\dot{u}^2\right) dt\right\} \triangleq J_p \tag{22}$$

That is, even with the FD, the pilot's task is modeled as that of tracking the flight path command rather than the FD signal.

The cost function to be minimized by the display control law u_d is defined to be

$$J_2 = J_p + \lim_{T\to\infty} E\left\{\frac{1}{T}\int_0^T \left(F_{2d}u_d^2\right) dt\right\} \tag{23}$$

This definition is consistent with the desire to design an FD signal that improves the pilot rating of the system. In Equation 23, F_{2d} is a scalar and its value determines the display (e.g., FD) gains. The requirements for the FD design are that the FD signal should be consistent with γ_e and that the FD should not appear to be busy (i.e., FD RMS values should not be too high). These requirements place constraints on the magnitude of the display control gains G_d.

Using the above formulation, Cooperative Synthesis was performed using three values of F_{2d}, together with the baseline aircraft and a 0.2-sec HUD delay. The F_{2d} values and the resulting gains, G_d, are listed in Table 5. For the purposes of further discussion, these three cases will be referred to as FD1, FD2, and FD3, respectively, in the order of decreasing F_{2d}, or decreasing gains. In Table 5 note that the gains g_q and g_θ are $\simeq 0$ for

TABLE 5. COOPERATIVE DISPLAY SYNTHESIS RESULTS

Class	F_{2d}	g_{γ_e}	g_θ	g_q
FD1	2.0	0.18	0.0	-0.01
FD2	1.0	0.35	0.0	-0.02
FD3	0.5	0.57	0.0	-0.04

all the three cases, showing that little improvement in pilot performance or workload can be expected by incorporating θ or q information into the FD.

An indication of the benefit of an FD is shown in Figure 16, where two frequency responses are plotted. One is the FD to pilot stick for FD2, and the other is the flight path angle to pilot stick. From the figure it is evident that FD clearly extends the k/s like magnitude behavior and provides phase lead in the crossover region.

2) Vehicle Control Augmentation Only–A second alternative for overcoming the effects of HUD delay is to synthesize a different vehicle controller that will take into account the HUD dynamics. Though perhaps not a direct indication of how to select display dynamics, this alternative does indicate how including the display (and pilot) as part of the vehicle control design can improve flying qualities. It furthermore provides an additional comparison point for the case where vehicle and display augmentation are considered simultaneously.

With reference to Figure 8 and the discussion in subsection 2a, it is evident that the Cooperative Synthesis formulation for augmentation gains K is a direct one, with a straightforward modification to include the HUD delay. Furthermore, the synthesis procedure has been set up such that the control blending gains, P, could be obtained from the optimization process as well (see Reference 25). However, the stick gain, k_δ, was adjusted after the synthesis to yield reasonable values of control sensitivity.

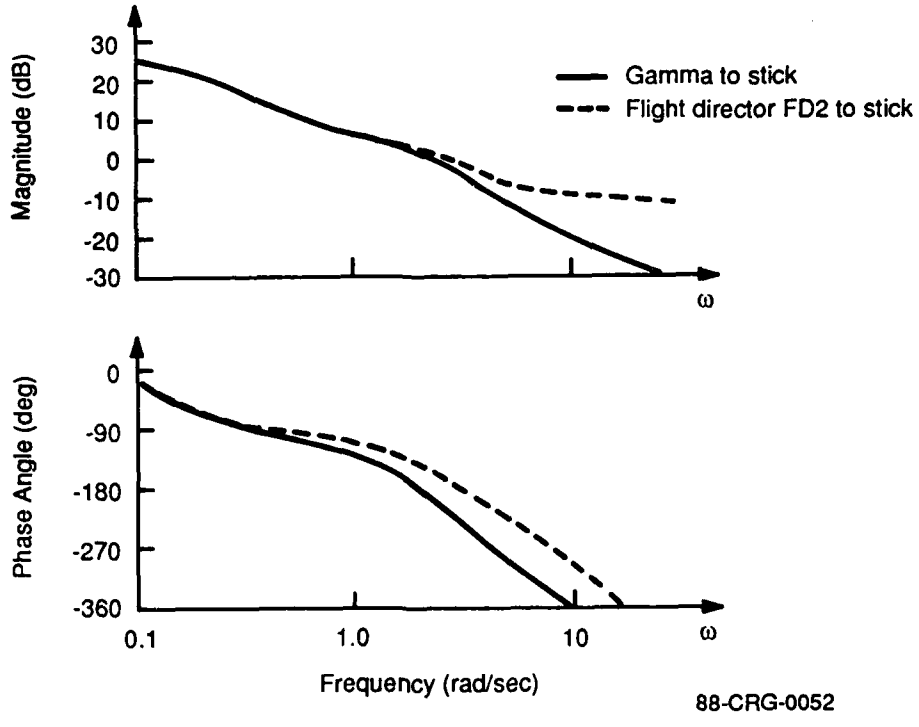

Figure 16. Flight Path and Flight Director Frequency Response Comparison.

For this problem, the pilot's cost function was unchanged from that used previously, i.e., $J_1 = J_p$. The second cost function has been formulated as

$$J_2 = J_p + \lim_{T\to\infty} E\left\{\frac{1}{T}\int_0^T \left(u_a^T F_2 u_a\right) dt\right\} \tag{24}$$

where, because of the reformulation of the problem to include blending gains (P), u_a in this case is u_v in Figure 8. F_2 is chosen based on maximum allowable control deflections (see Reference 25 for details):

$$F_2 = \text{diag}\left[\frac{1}{\left(u_{v_{max}}\right)^2}\right] = \begin{bmatrix} 0.01 & 0 & 0 & 0 \\ 0 & 1.11\text{e-}03 & 0 & 0 \\ 0 & 0 & 0.04 & 0 \\ 0 & 0 & 0 & 4.0\text{e-}04 \end{bmatrix} \tag{25}$$

For this formulation, the Cooperative solution yielded

$$K = \begin{bmatrix} 0.248 & -0.342 & -0.729 & -0.443 \\ 0.697 & -0.600 & -0.244 & -0.922 \\ -0.323 & 0.235 & 0.216 & 0.366 \\ -0.559 & 0.106 & -0.153 & 0.024 \end{bmatrix} \quad (26)$$

and

$$P \cdot k_\delta = \begin{bmatrix} -6.36 \\ -9.43 \\ 7.36 \\ -5.43 \end{bmatrix} \quad (27)$$

In Equation 27, k_δ has been selected to be 10.

An interesting outcome of this synthesis problem is that the closed-loop aircraft dynamics obtained as the solution are quite different from the classical longitudinal modes, of which the baseline aircraft is representative (Appendix B contains the closed-loop transfer functions). This is discussed further in Reference 25, where the discussion includes the observation that the control response for the Cooperatively augmented vehicle (that is, the vehicle control augmentation case just discussed) is reminiscent of the so-called gamma command laws presently being flight tested on commercial aircraft (Reference 35).

3) Simultaneous Vehicle Control/Flight Director Synthesis–Finally, the Cooperative Synthesis algorithm was applied to *simultaneously* synthesize a control augmentation law and an FD law for the STOL vehicle, again considering a HUD with a time delay of $\tau_d = 0.2$ sec. The formulation of this synthesis problem is basically a combination of the previous two cases. A modification to the FD formulation was made, however, based on the earlier results where q and θ were not found to contribute significantly to the FD. With this in mind, the display controller was defined to be

$$y_d = \dot{\gamma}_e; \; G_d = g_{\dot{\gamma}_e} \; ; \; u_d = G_d \cdot y_d \quad (28)$$

To complete the formulation, the cost functions were chosen to be J_p as in Equation 22 and

$$J_2 = J_p + \lim_{T\to\infty} E\left\{\frac{1}{T}\int_0^T \left(F_{2d}u_d^2 + u_a^T F_2 u_a\right) dt\right\} \tag{29}$$

with F_2 as in Equation 25 and $F_{2d} = 1$.

Solution of this Cooperative Synthesis problem yielded an FD gain G_d of 0.25, and vehicle augmentation matrices K and $P{\cdot}k_\delta$ of

$$K = \begin{bmatrix} 0.438 & -0.497 & -0.303 & 0.622 \\ 0.218 & -0.396 & -0.190 & -0.580 \\ -0.243 & 0.085 & 0.115 & 0.198 \\ -1.020 & 0.139 & -0.181 & 0.177 \end{bmatrix} \tag{30}$$

$$P\cdot k_\delta = \begin{bmatrix} -6.35 \\ -3.88 \\ 5.43 \\ -2.02 \end{bmatrix} \tag{31}$$

A stick gain of $k_\delta = 10$ was again found to give satisfactory flight path control sensitivity (again, refer to Appendix B for tabulation of closed-loop transfer functions).

c. Model-Based Evaluation Results

To compare the characteristics of the Cooperative problem solutions with each other, an OCM analysis similar to that performed in subsection 2 was performed. Table 6 summarizes the results of this analysis for the three FD solutions, (FD1, FD2, FD3), the vehicle control-augmentation-only solution (designated VC), and the simultaneous vehicle control/flight director (VCFD) solution. Recall that in all cases a HUD with a 0.2-sec delay has been assumed. Depictions of the data in Table 6 are given in Figures 17 and 18, which are similar to Figures 11 and 12. In fact, for purposes of further comparison, the data in Figures 11 and 12 have been included in Figures 17 and 18. In

TABLE 6. COMPARISON OF COOPERATIVE SYNTHESIS RESULTS

Case	τ_N (sec)	RMS γ_e (deg)	RMS $\dot{u}$ (in/sec)	ω_c (rad/sec)	$\measuredangle$ peq (deg)	RMS (FD) / RMS (γ_e)	RMS ($\dot{FD}$) / RMS ($\dot{\gamma}_e$)
FD1	0.26	0.73	1.56	1.7	16.3	1.01	1.10
FD2	0.26	0.70	1.52	1.7	-1.0	1.06	1.41
FD3	0.26	0.68	1.50	1.8	-14.7	1.18	1.95
VC	0.22	0.69	2.13	1.7	42.3	---	---
VCFD	0.22	0.62	2.18	1.8	34.5	1.06	1.15

considering the data in the tables and figures, note first of all that equivalent pilot phase compensation ($\measuredangle$ peq) and crossover frequency (ω_c) for the FD cases were calculated using an equivalent pilot transfer function from FD to u derived in much the same fashion as the equivalent γ_e to u function was derived in Reference 5. Second, because of the performance/workload tradeoff adjustment procedure used, the values of τ_N are not equal in all cases. Hence the values of RMS $\dot{u}$ do not provide a consistent indication of workload.

With respect to the FD-only cases, it is readily apparent that as the gain on $\dot{\gamma}_e$ increases (which is the main difference between the cases), tracking error improves and the workload measure decreases. Though this difference is more dramatic using equivalent phase as a workload measure, the results using RMS $\dot{u}$ are nevertheless comparable since τ_N is the same for all three cases. By either indication of workload, it may well be that the flight directors place operation outside of a Level 1 flying qualities region, however. This is because a low value on some scale that indicates workload (i.e., a control system that is highly sensitive to pilot inputs) may be as unsatisfactory as a high value (a sluggish control system), as the results in Section II and Reference 5 indicate. Finally, the last two columns in Table 6 also indicate that increasing the FD gain may be undesirable. One of the goals for FD design was that the FD signal not be too busy. The ratios in Table 6 indicate that higher values of gain on $\dot{\gamma}_e$ may result in an FD signal with unacceptable variability.

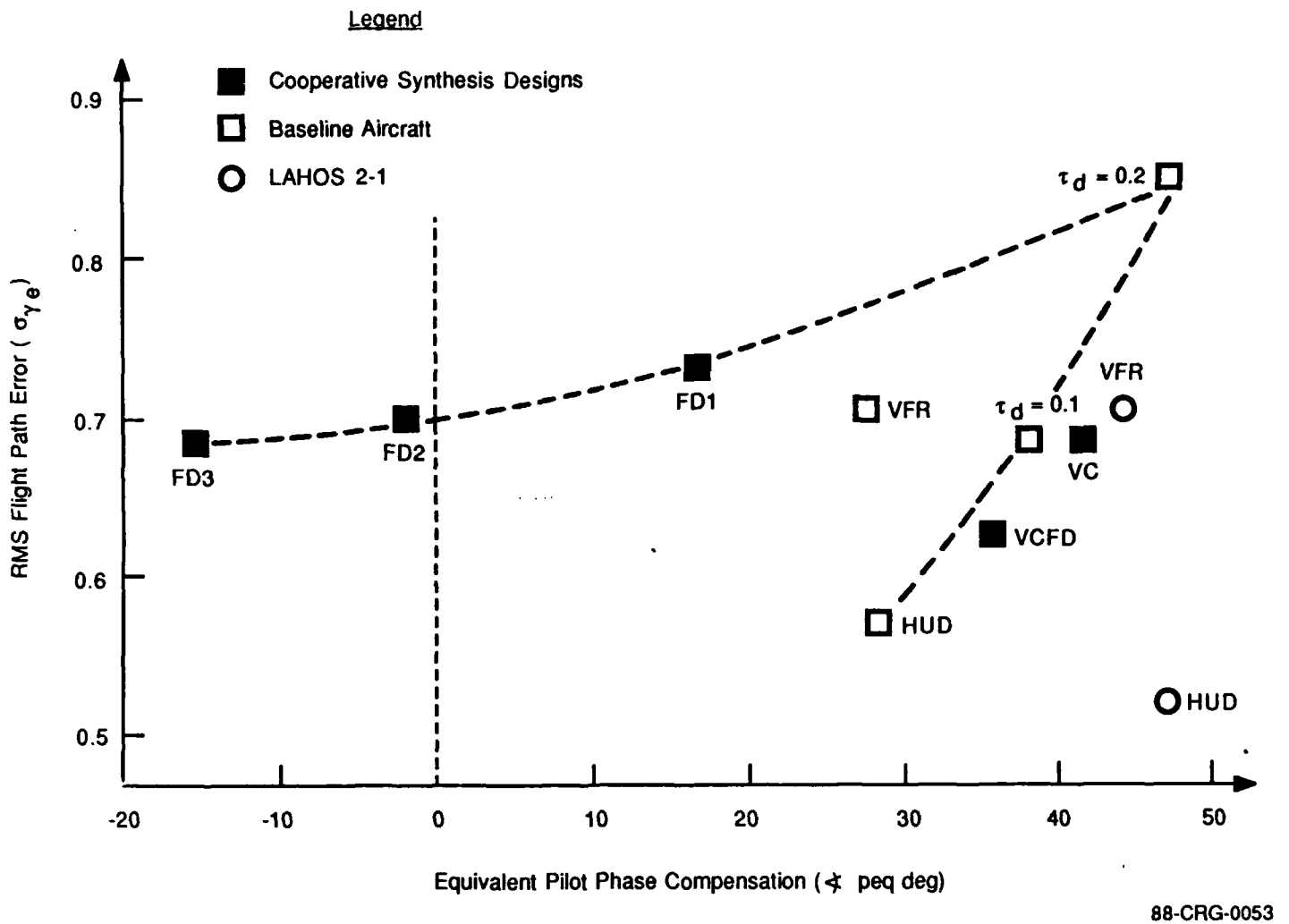

Figure 17. Model-Based Performance/Workload Results for Cooperative Synthesis Designs (I).

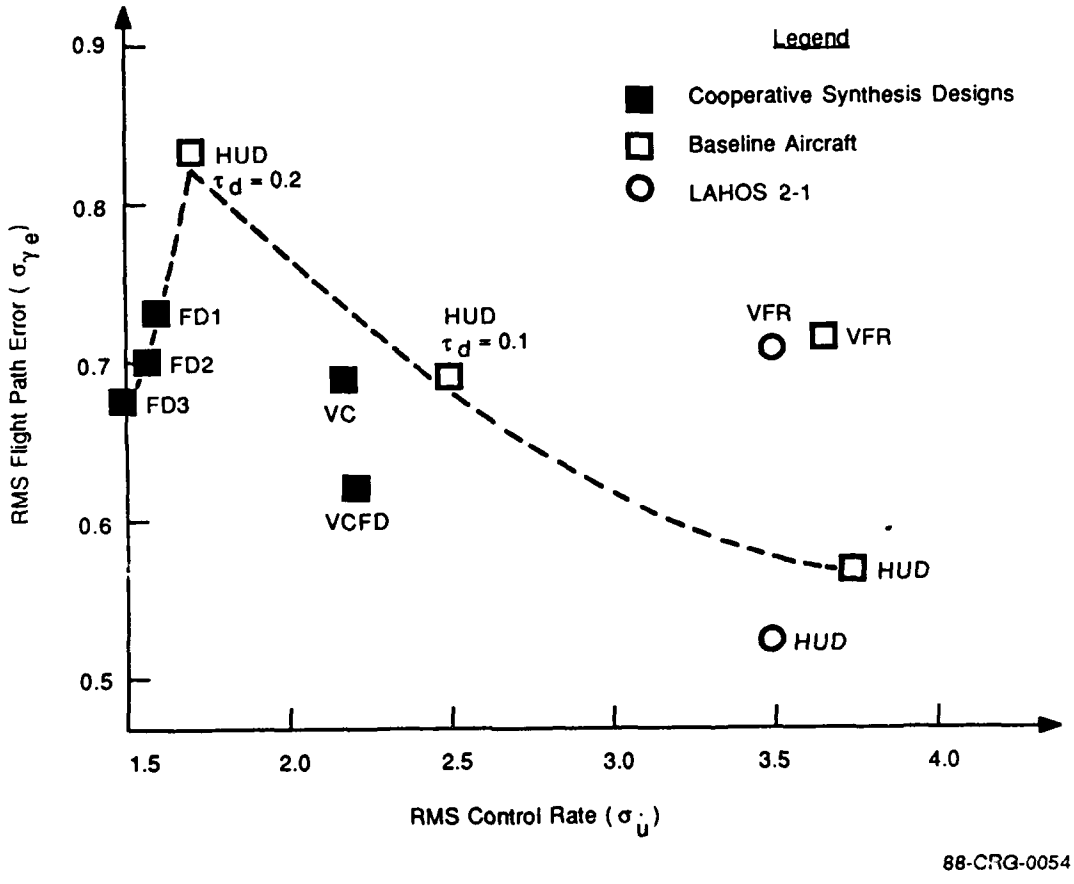

Figure 18. Model-Based Performance/Workload Results for Cooperative Synthesis Designs (II).

Considering the case of vehicle control augmentation only (VC), it is evident that adjusting the vehicle controller can provide compensation for the HUD delay. From both figures, it appears that tracking error performance exhibits the most improvement, with a relatively smaller apparent change in workload. It is also interesting to note that the locations of the HUD with 0.1-sec delay and for case VC are proximate in both figures (values of τ_N are comparable for VC, VCFD, and HUD + 0.1). Loosely speaking, this might indicate that the cooperative vehicle control augmentation is able to compensate for roughly 0.1 sec of HUD delay.

Finally, the VCFD case exhibits additional improvement in performance and workload over both the FD and VC cases. This is especially true with respect to tracking error. The simultaneous synthesis of vehicle control and display gains substantially recovers the losses incurred by including a realistic delay for the HUD (Figure 17), and it does so by selecting a relatively low gain on $\dot{\gamma}_e$ for the FD (half that of FD1). Not only does this keep workload within expected limits, it also satisfies the FD variability design goal (see Table 6).

In sum, the various cases considered in this subsection illustrate how the introduction of additional dynamics or the modification of existing dynamics can compensate for the degrading effects of HUD delay. The synthesis of a flight director was shown to partially compensate by providing additional information to the pilot. The modification of existing dynamics through the Cooperative Synthesis of a vehicle controller also partially compensated for the HUD delay. A significant aspect of this latter case is that by effectively considering the display as part of the airframe when deciding vehicle augmentation, an improvement in pilot-in-the-loop system performance can be realized. Synthesizing both vehicle control and display control simultaneously was shown to substantially remove the effects of the HUD delay. A key point here, and actually in all the cases considered, is that a systematic, model-based approach has been used to consider display dynamics issues in particular contexts. Section V continues on this theme by describing a different approach for systematically considering display dynamics requirements.

SECTION V

INVESTIGATION OF DISPLAY DYNAMICS REQUIREMENTS USING THE STRUCTURED SINGULAR VALUE

1. INTRODUCTION

The previous section has described the use of an OCM-based approach for examining the effects of display dynamics, including the simultaneous consideration in a synthesis process of display augmentation, vehicle augmentation, and pilot manual control behavior. Specific structures for display, vehicle, and pilot were assumed and the analysis and synthesis results, though able to provide considerable insight into certain display-related effects and how to compensate for them, are nevertheless tied to this model structure. An important consideration arises, however, when the models used are likely to be incorrect or are known to be inexact. This might be the case, for example, when the vehicle model is not complete (e.g., there are unknown or unmodeled dynamics) or when pilot behavior is likely to deviate from that assumed (e.g., as modeled by the OCM). Understanding system behavior in the face of such deviations can become a key consideration in these situations, and designing a system to perform acceptably when given a possible range of vehicle dynamics or pilot behaviors can present a severe challenge.

Specifically, when examining the potential effects of existing or contemplated display dynamics, a significant criterion for evaluation might be whether the display is sensitive to pilot and vehicle variations. That is, does the display tend to exacerbate the impact of such variations to the point where performance and workload deteriorate, or does it provide a tolerance within the system to these effects such that acceptable flying qualities are maintained? This section presents an approach (in a preliminary state of development) that addresses this question. The approach provides an analysis capability that is useful for the comparative consideration of alternative sets of display dynamics. It also includes the possibility of synthesizing a set of display dynamics that balances performance and stability considerations in view of uncertainties in system elements.

The quantity fundamental to this approach is the so-called structured singular value (SSV). In the following subsections, a brief review of the SSV and its use is given. Next, an approach for considering display dynamics using the SSV is outlined. Third, an example synthesis problem is formulated and two candidate displays are derived based on SSV considerations. Finally, a comparative analysis with other candidate displays is presented, along with a brief discussion of how the predicted effects of pilot variability might be tested.

2. THE STRUCTURED SINGULAR VALUE

This subsection reviews the fundamental concepts of the SSV as they are applied to multivariable systems analysis. Since they have been documented in detail elsewhere (References 36 and 37), only those that are relevant to the present context are considered. Discussion is divided into the consideration of the SSV for analysis purposes and for purposes of synthesis. The former is well-established both mathematically and numerically. The latter is less so, although reliable procedures are available for experimental purposes.

a. Analysis using the SSV

1) Perturbation Structure–To establish the use of the SSV in the present context, consider the system shown in Figure 19. The figure depicts a situation similar to the formulation used in Section II to correlate flying qualities data from the Neal-Smith study with model-based evaluation results. In that analysis, the pilot was assumed to have available as observations the position-rate pairs of θ and θ_e and to exercise control in a single dimension (u). A pitch tracking command signal θ_c was used to model the actual pitch tracking task and was generated by passing white noise through a shaping filter. All of these features are reflected in Figure 19, as well as the system performance and pilot workload signals of interest: pitch tracking error, θ_e, and control rate, $\dot{u}$.

Besides the elements of the formulation used in Section II, Figure 19 includes additional features that are of interest with respect to the present discussion. One of these, of

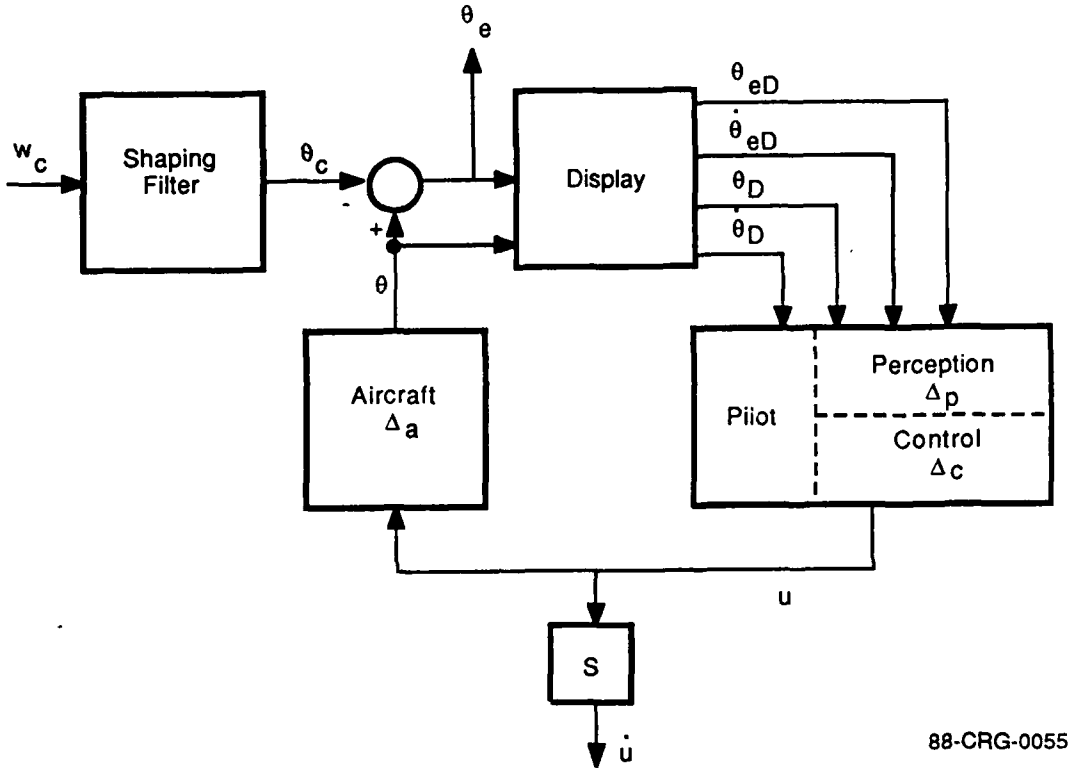

Figure 19. Representative Pilot/Aircraft/Display Structure.

course, is the display element. Another is the indication (by a Δ) that the pilot and aircraft models may have uncertainties associated with them. For example, Δ_a indicates that the aircraft model may be inaccurate due to unmodeled or unknown dynamics. In addition, the pilot may deviate from assumed (e.g., OCM) behavior through variations in perception (Δ_p) or through variations in the selection of a control action (Δ_c).

In the SSV analysis framework, Δ variations are always with respect to a nominal model that is finite-dimensional, linear, and time-invariant. The specific mathematical form of the Δ perturbations is unstructured, multiplicative. That is, if G is a (possibly)

multi-input, multi-output transfer function for a system element, then the set of perturbed transfer functions $\tilde{G}$ possible due to Δ are typically of the form

$$\tilde{G} = G(I + \Delta) \tag{32}$$

Though the structure of the matrix Δ can be arbitrary, it is usually possible and desirable to represent what is known about anticipated uncertainties or to consider certain frequencies or combinations of variables that are of particular interest with respect to uncertainty. A common instance where this occurs is when the model (G) is known to be highly accurate at low frequencies but is unreliable at higher frequencies. For this case Δ is structured in frequency-dependent terms to be negligible at low frequencies but dominant (in Equation 32) at high frequencies. The usual way of representing characterizations of this type is to assume Δ to be of the form

$$\Delta = \Delta' W_{\Delta} \tag{33}$$

where W_{Δ} is a frequency-dependent weighting matrix that reflects what is known or of interest with respect to the possible perturbations, and Δ' is constrained to be such that its magnitude is less than 1. Other technical restrictions of a mathematical nature apply to W_{Δ} and Δ', but, while important in that context, they will not be a factor in the sequel.

Since the selection of weights W_{Δ} is where a great deal of qualitative knowledge about the system under consideration is encoded, this process is a significant part of any analysis using the SSV. Indeed, the selection of weights, as well as the positioning of Δ elements to meaningfully reflect variabilities in the system (particularly with respect to the pilot), has been a significant part of the present effort in investigating the applicability of the SSV in examining display dynamics effects. This issue is taken up in a specific problem context subsequently.

2) **Robust Stability**–With a specific model and perturbation structure in place, several analysis questions are of interest. One of the most important is that of whether the system remains stable in the face of all possible perturbations Δ. For the system in

Figure 19, robust stability means that no possible combination of values for Δ'_i will destabilize the system, given a selected set of weights W_a, W_p, and W_c.

Because of the multivariable nature of the problem, robust stability is nontrivial to determine without being overly conservative. A conservative assessment can be obtained by reflecting all the perturbations to a single point in the loop. Doing this in a tractable way generally means that the original perturbation structure is lost, however. The alternative is to use the structured singular value, often referred to as μ, to make a determination of robust stability.

Under the assumption that the system in Figure 19 is finite-dimensional and linear, time-invariant, it can be rearranged into the equivalent form shown in Figure 20. Essentially,

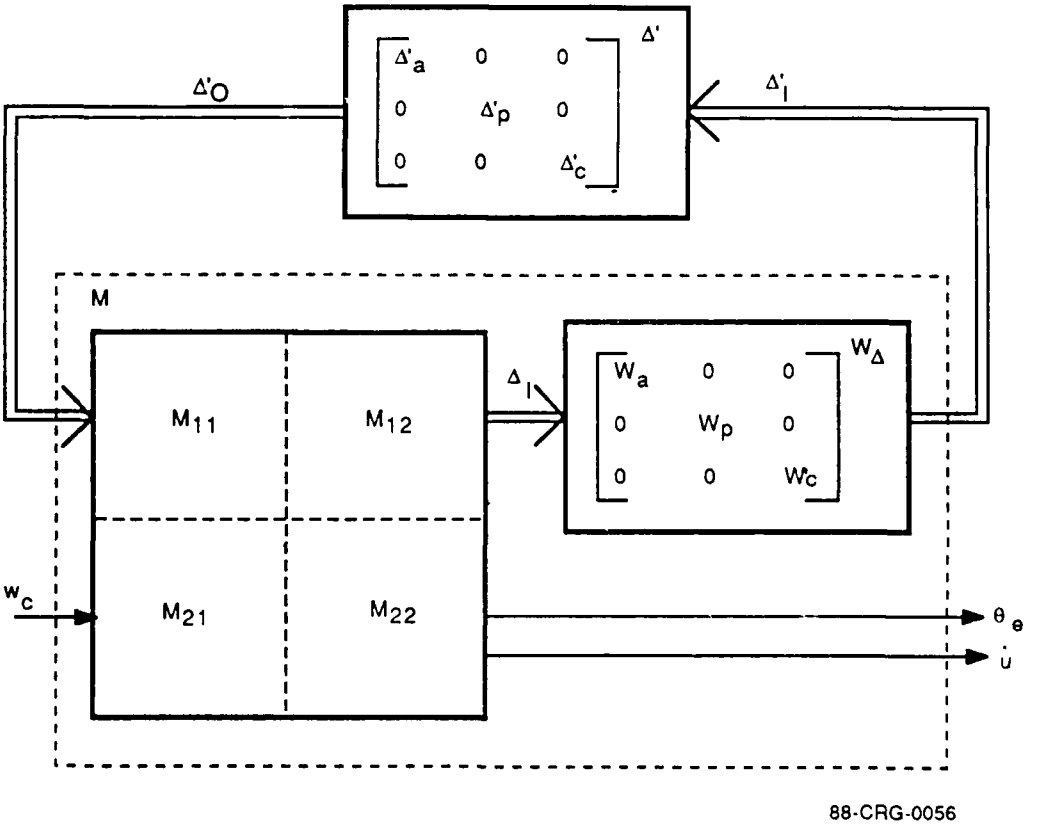

Figure 20. Equivalent Representation for System in Figure 19.

the idea is to arrange the perturbations $\Delta'_i W_i$ into a single block-diagonal structure and to derive the matrix transfer for functions M_{ij} that correspond to this structure. For example, M_{11} designates the transfer function from diagonally arranged Δ block outputs to Δ block inputs. Taking the structure of each Δ_i block into account ($\Delta_i = \Delta_i' W_{\Delta i}$), M_{11} is such that

$$\Delta_I' = W_\Delta M_{11} \Delta_O' \tag{34}$$

Similarly, M_{22} designates the transfer function from w_c to θ_e and $\dot{u}$. Finally, M_{12} and M_{21} designate the cross-transfer functions from w_c to Δ_I and from Δ_O' to θ_e and $\dot{u}$, respectively.

Neglecting the block diagonal structure of the Δ' element, a conservative condition of stability robustness is to require that

$$\bar{\sigma}\left(M_{11}(j\omega) W_\Delta(j\omega) \right) < 1 \; \forall \omega \tag{35}$$

In Equation 35, $\bar{\sigma}(A)$ denotes the largest singular value of the matrix A, and M_{11} and W_Δ are defined in Figure 20. (The largest singular value of A is the maximum output magnitude possible from a unit magnitude input to A.) The condition in Equation 35 depends on the assumption that $|\Delta'| \leq 1$ (i.e., $\bar{\sigma}(\Delta') \leq 1$).

The conservatism in Equation 35 is that all input vector directions to M_{11} (outputs from Δ') are assumed possible. This is equivalent to ignoring the special structure of Δ'. A less conservative condition for stability robustness, and one that takes advantage of the actual structure of Δ', is to require that

$$\det \left(I - \text{diag}\left(\Delta'_i(j\omega)\right) M_{11}(j\omega) W_\Delta(j\omega) \right) \neq 0 \quad \forall \omega, \; \forall \Delta_i \tag{36}$$

The condition in Equation 36 can be expressed in an equivalent way by defining a new matrix function μ and requiring that

$$\mu\left(M_{11}(j\omega) W_\Delta(j\omega) \right) < 1 \quad \forall \omega \tag{37}$$

In words, μ denotes the largest singular value in the space spanned by the block diagonal perturbation structure. Ensuring that μ is less than 1 also ensures that no perturbation Δ' can destabilize the system. Conversely, if $\mu > 1$, there exists a Δ' that is destabilizing.

3) **Nominal Performance**–One of the consequences of analyzing systems in terms of the block diagonal structure outlined above is that system performance can be analyzed as well as stability. This requires, however, that performance specifications or goals be expressed in terms of weighting matrices in the same fashion that model perturbations and uncertainties were assigned such weights. Once this is done, the weighted performance signals are passed through a perturbation matrix Δ'_0 and fed back as the system's disturbance signal. If this does not "destabilize" the system, the performance specifications are considered to be satisfied, since the system is robust with respect to performance perturbations.

In terms of the system in Figure 19, there are two performance specifications of interest. The first is that RMS θ_e should be small. The second is that RMS control rate should be within a given range. Following on the discussion in Section II these specifications ensure that desirable flying qualities will result. Translating these performance goals into frequency-domain weights is a nontrivial matter, as will be discussed later, but for now consider the goal of keeping RMS θ_e small and how a weighting function might be specified to do this. Qualitatively, it is reasonable to assume in this system that it is undesirable for θ_e to have substantial low-frequency spectral content, but that there is indifference to its spectral content at high frequencies. This derives from the limited bandwidth of other system elements, including the pilot. Thus a performance weighting for θ_e might be as shown in Figure 21. In the figure, ω_o designates some transition frequency for separating low from high. The low frequency weighting value is typically selected to be the reciprocal of the size of θ_e permitted or desired.

With performance weights in place for the example system, its revised block diagram is given in Figure 22. As indicated in the above, the nominal system meets the

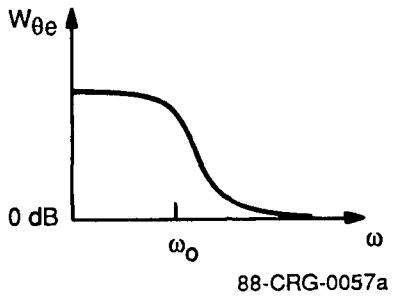

Figure 21. Possible Weighting for θ_e.

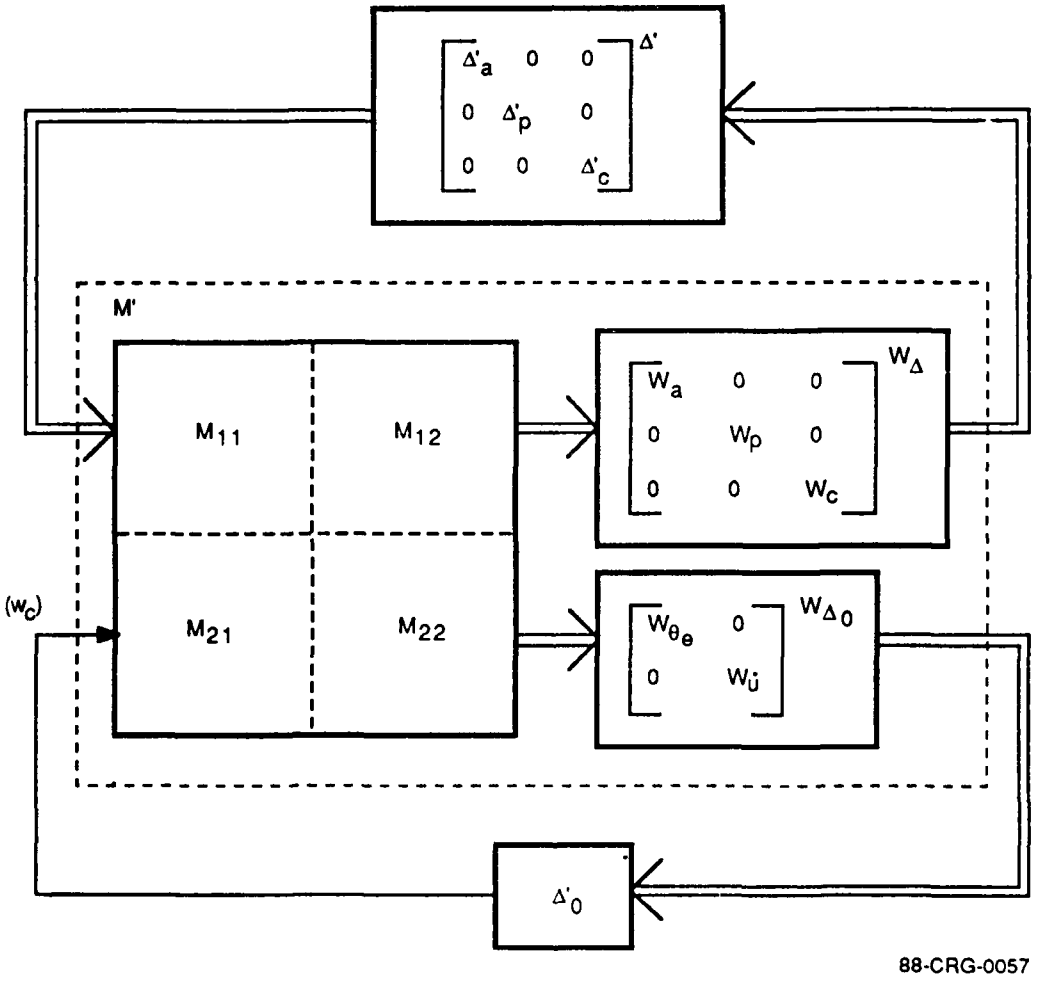

Figure 22. Stability and Performance Robustness Block Diagonal Form.

performance specifications (as they have been encoded in $W_{\theta c}$ and $W_{\dot{n}}$) if there is no Δ'_0 that destabilizes the system. Specifically, the condition

$$\bar{\sigma}\left(M_{22}\,(j\omega)\, W_{\Delta 0}\,(j\omega)\right) < 1 \tag{38}$$

for $|\Delta_0'| \leq 1$ is the test for nominal performance, where M_{22} and $W_{\Delta 0}$ are as indicated in Figure 22.

4) **Robust Performance**–The combination of robust stability and nominal performance represents a final SSV-based characterization of interest. Termed robust performance, a system with this property not only remains stable in the face of all perturbations Δ', but also remains within its performance specifications. The test for this property is to apply the SSV to M', the matrix of combined transfer functions M and performance and stability weights. That is,

$$\mu\left(M'\,(j\omega)\right) < 1 \;\; \forall\omega \tag{39}$$

guarantees robust performance, where μ is calculated using the block diagonal perturbation structure of $\bar{\Delta} = \text{diag}\,(\Delta'_i, \Delta'_0)$ and where $\bar{\Delta}$ is constrained to be such that $|\bar{\Delta}| \leq 1$.

b. Synthesis using the SSV

Given the analysis framework outlined above, it is a natural step to consider the synthesis of a dynamic element (i.e, a controller) that augments the system to achieve robust performance. A technique that accomplishes this, called μ-synthesis, is described in Reference 38. Basically, it combines the SSV-analysis framework with H_∞ synthesis methods to formulate an optimization problem that solves for a controller. The H_∞ synthesis approach is a multivariable generalization of the single-input, single-output goal of achieving maximum gain over all frequencies. The equivalent performance

measure in the H_∞ case is the maximum singular value of the closed-loop transfer function. When this performance measure is optimized, for a stable system, the ratio of the bounded power of output signals to input signals is minimized.

In terms of the example system, the H_∞ synthesis formulation is depicted in block diagram form in Figure 23. Note that a manipulation has been performed similar to that used to obtain the representation in Figure 20. In this case, however, the element to be synthesized (the controller K), has been isolated. In anticipation of combining H_∞ with μ-analysis, the block-diagonal perturbation structure has also been maintained as a separate element, which is shown implicitly by the Δ'_O and Δ'_I inputs and outputs. They designate the outputs from the perturbation matrix Δ' and the inputs to it, respectively.

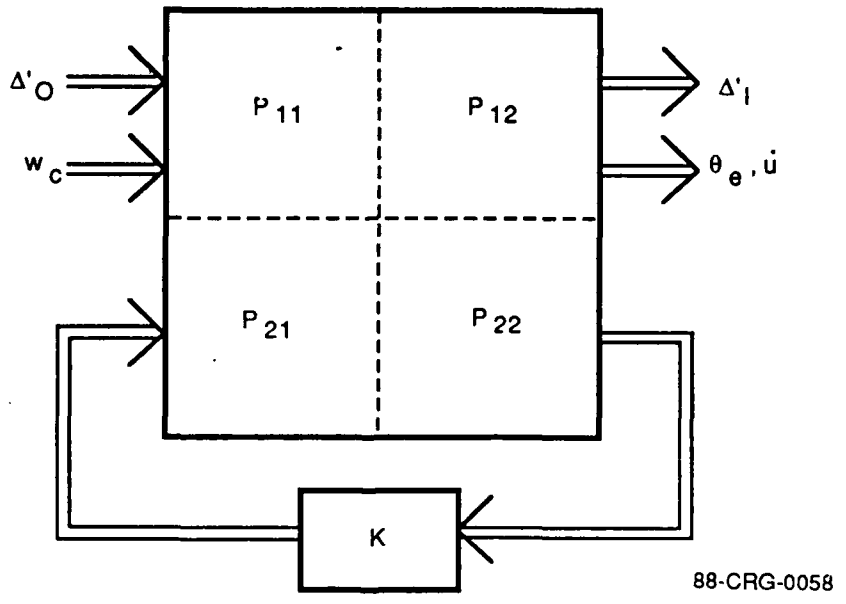

Figure 23. Framework for H_∞ Synthesis.

Neglecting the Δ'_O to Δ'_I transfer function elements in P, the H_∞ synthesis formulation seeks a stabilizing K that minimizes

$$\| \tilde{P}_{11} + \tilde{P}_{12} K \left(I - P_{22} K \right)^{-1} P_{21} \|_\infty \tag{40}$$

where $\| \cdot \|_\infty$ denotes the infinity norm. In Equation 40, K is in general frequency dependent, and $\tilde{P}_{11}$ and $\tilde{P}_{12}$ denote modified versions of P_{11} and P_{12} that remove Δ_O' inputs and Δ_I' outputs. Doing this yields an "optimistic" H_∞ solution in the sense that perturbations are not taken into account. Using P_{11} and P_{12} yields a conservative solution, however, because the block diagonal structure of Δ' is not taken into account. Therefore, to combine H_∞ synthesis methods with the nonconservative but meaningful consideration of uncertainties provided by μ-analysis, the following problem is formulated and solved as the μ-synthesis problem:

$$\min_{K,D} \| D \left[P_{11} + P_{12} K \left(I - P_{22} K \right)^{-1} P_{21} \right] D^{-1} \|_\infty \tag{41}$$

In Equation 41, D is a scaling matrix with the same block diagonal structure as Δ' (Reference 36), and it happens that minimizing over D in Equation 41 is equivalent to calculating an upper bound on μ which under certain conditions is exact. Thus the solution to Equation 41 yields (in principle) not only an H_∞ optimal controller, but a controller whose properties with respect to robust stability, nominal performance, and robust performance are also the best achievable within the problem structure. Because these objectives are often conflicting, the solution to Equation 41 is in reality a compromise between performance and robustness. Finally, solution for the global optimum in Equation 41 is a nontrivial problem, and methods are currently under development (Reference 39). The μ-synthesis results presented in the sequel have been generated using a set of experimental algorithms that are reliable for present purposes, however.

3. AN SSV-BASED APPROACH FOR DECIDING DISPLAY DYNAMICS REQUIREMENTS

From the above discussion, the SSV appears to have applicability to the consideration of display dynamics. In particular, SSV-based analysis provides a method for doing performance comparisons of candidate displays in task situations that are characterized by ranges of vehicle dynamics and pilot behaviors. From such a comparison, one display might emerge as superior and satisfactory for the task at hand. This use of the SSV relies on generating candidate displays through other means, however. Although a variety of reasonable approaches exist and have been used to determine dynamic compensation within a display element, including the Cooperative approach and other FD design techniques, the potential also exists to use the SSV-H_∞ synthesis approach to decide display dynamics.

One of the advantages of using μ-synthesis to explore display dynamics alternatives is that a minimum of structure is imposed a priori on the controller to be synthesized (in this case a display). While this places an additional emphasis on interpreting the synthesis result, it also permits the possible derivation of control schemes that were not anticipated. This is especially attractive when a multivariable situation is under consideration, since those interactions of variables that achieve robust performance are often not obvious. Indeed, the ability to systematically consider robustness in the course of design is also an important advantage of μ-synthesis.

For these reasons, use of the μ-synthesis technique has been pursued as a means of deciding display dynamics. The remainder of this subsection outlines such an approach and discusses critical issues with respect to its use. Because the μ-synthesis subsumes the use of the SSV for analysis purposes, many of the issues with respect to the former are also critical to the latter. This will be especially apparent when a specific example is presented in the next subsection.

An approach for deciding display dynamics using μ-synthesis is suggested in general terms in Figure 24. In addition to using the μ-synthesis technique, this approach assumes that the manual control task of interest can be represented appropriately in terms of a

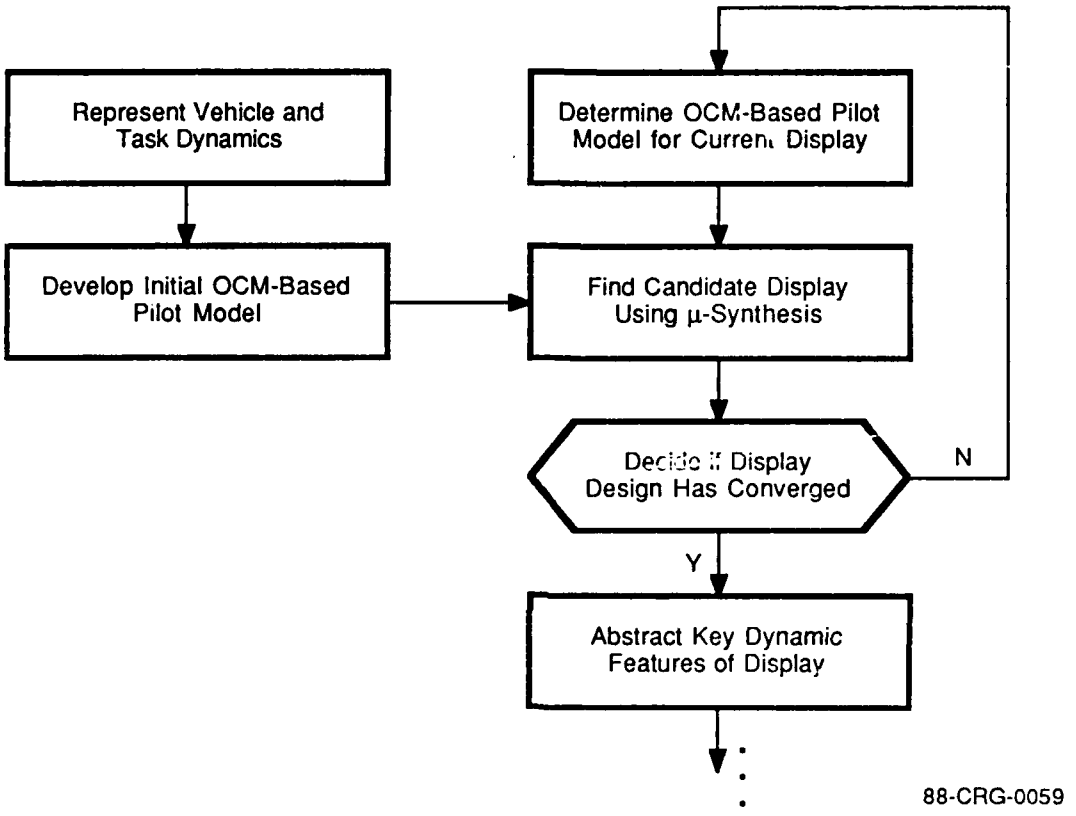

Figure 24. A μ-Based Approach for Deciding Display Dynamics.

linear system along the lines of the representations used earlier. Also integral to the approach is the use of the OCM as a model of pilot behavior.

As indicated in the figure, a linear system representation of the task situation is the first basic step. This includes developing a model of aircraft dynamics, as well as a model that characterizes the actual manual control task. This could involve, for example, the definition of a command signal that approximates the frequency content of a realistic pitch tracking task. It is also necessary in this step to make a preliminary determination

of those variables that the pilot will observe and those that he will control. This can be done by prior analysis of the type discussed in Section III.

Once a basic representation of the task situation is in place, the next step is to develop an initial OCM-based pilot model. At the least, this step involves a usual OCM formulation and solution, where the resulting pilot control gains and Kalman estimator gains are then used to construct an initial pilot model. One of the constraints on this model is that it be expressed in state space terms. This requires some adaptation of the OCM framework, which will be discussed in the context of the example presented later.

Since the initial pilot model will serve as a starting point in an optimization process, it may be desirable to perform some additional analysis to select this point. For example, pre-analysis with various classes of display dynamics may give an indication regarding the type of dynamics that will be consistent with performance and robustness goals. Introducing such a bias may, of course, inhibit the emergence of other, qualitatively different display dynamics solutions. The point here is that any initial pilot model introduces some biases into the iterative optimization process. It is therefore important to recognize them and possibly determine them at this step in the approach.

Given an (initial) pilot model, a μ-synthesis problem is then formulated to determine a candidate set of display dynamics. This involves the definition of a specific uncertainty structure within the aircraft and pilot elements, including the definition of weighting functions for each Δ block. It also involves the selection of weighting functions on the performance signals of interest. Once the problem has been formulated and solved, the resulting set of display dynamics can be compared to the set obtained at the previous iteration. If the two are sufficiently dissimilar, then the iterative process continues with the determination of an OCM-based pilot model that matches the current display. This is then used as a basis for formulating and solving another μ-synthesis problem for a new display, and so on.

When convergence of the iterative process is decided, the set of display dynamics that has resulted can then be examined for its key features. This is necessary for two reasons.

First, the μ-synthesis process in general produces controllers of high order for which model reduction is essential. Reducing the order of the display requires that its key features be identified and retained. Second, and more importantly, it is the qualitative interpretation of a display's dynamic characteristics that is of primary interest for deciding requirements. That is, for the given task under consideration, what kind of dynamics does the synthesis process indicate as appropriate for the display? Does the display provide lead information? Are there particular combinations of observed variables suggested by the display design? Does the display limit bandwidth or otherwise emphasize certain frequency bands in the variables it processes? These types of observations with respect to the synthesis result are of greater value in deciding display dynamics requirements than the specific transfer functions obtained for a given problem.

The validity of the methodology stated above depends on several factors. One of these is the ability to represent the key aspects of the manual control problem under consideration in terms of the μ-synthesis framework. This is particularly relevant to the problem of defining a perturbation or uncertainty structure within the pilot model. Because the OCM is essentially a time-domain model, its parameterization is not necessarily directly compatible with a frequency-domain SSV-based approach. Thus, deciding the position of a Δ element and its corresponding weighting function does not equate to a straightforward translation of perturbations in OCM parameters. On the other hand, pilot deviations from nominal behavior (i.e., from constrained optimality) are not necessarily best understood in the time domain. Rather, they may be more naturally expressed in terms of the frequency-domain. Resolution of this issue probably requires a careful examination of human variability in piloting contexts from first principles, so that a faithful characterization of this variability can be made for purposes of SSV-based analysis.

A second factor with respect to the validity of the suggested methodology is whether the iteration process is one that will have reasonable convergence properties. Using the OCM itself as an indicator, where iteration is required to achieve equilibrium with respect to noise-to-signal ratios, the expectation is that the process in Figure 24 will

indeed converge. However, experience to date with the example problem described in the next subsection has not offered substantial support for this expectation. An alternative process, and one that is much more desirable from an optimization point of view, is to consider the pilot and display elements simultaneously, in much the same fashion that the Cooperative Synthesis approach does in its own right. Limitations on resources have not permitted the exploration of this possibility, although it would appear to be a promising research issue.

A third issue that arises in considering the validity of the approach in Figure 24 is that of comparative analyses of transfer functions. This question is relevant to the determination of whether the result from the previous synthesis iteration is similar enough to the present iteration result. It is also relevant to the determination of what constitute the key dynamic features in a given transfer function. In both cases, the problem is particularly nontrivial when a multivariable transfer function is under consideration.

Since the approach suggested in this subsection is in a preliminary state of development, the issues discussed above have not been resolved in a general way. They have been addressed in the context of a specific example, however, which is described in the next subsection.

4. EXAMPLE

As a means of exploring the usefulness of SSV-based analysis and synthesis methods for considering display dynamics requirements, an example problem has been investigated. This section documents that investigation and is organized as follows. First, the task situation is described and modeled, followed by a discussion of the model structure used to represent pilot behavior. Next, the uncertainty structure used is presented, which includes not only the choices made with respect to the placement of Δ blocks but also their characterization through weighting functions. A discussion of the selection of weights on performance signals then follows, which completes the problem formulation. Discussion of synthesis results is then offered, followed by a comparative analysis of several candidate sets of display dynamics using SSV methods. Finally a brief

discussion is given on how some of the hypotheses implicit in the comparative analysis results might be experimentally tested.

a. Formulation

1) Task–The manual control task to be considered is one adapted from recent investigations within the Flying Qualities Group at Wright-Patterson AFB (Reference 40). That effort has focused primarily on the experimental analysis of display dynamics effects in a pursuit tracking task. A number of cases have been considered, distinguished according to the plant and display dynamics selected. One of the selections for plant dynamics used in Reference 40 will form the basis of the manual control task considered here. In doing so, the results and hypotheses that are obtained will presumably be complementary to the experimental set-up and results in Reference 40 and will also be complementary to the analysis performed in Reference 29.

A general depiction of the manual control task to be examined is shown in Figure 25. The pilot is required to minimize the difference between a command signal, θ_c, and the plant output, θ_a. This difference is designated as the error signal θ_e. However, the pilot must do so using the displayed versions of these signals. To simplify the synthesis

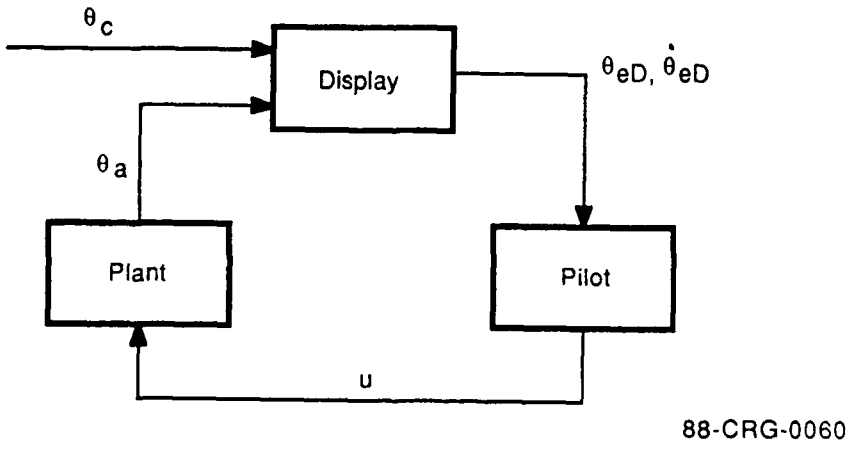

Figure 25. Depiction of Manual Control Task.

problem, it is assumed that the pilot selects his control actions based only on the position/rate pair θ_{eD}, $\dot{\theta}_{eD}$, which are θ_e and $\dot{\theta}_e$ as modified by the display. This reduces the synthesis problem to a single input–single output formulation, which is done to facilitate the interpretation of the synthesis result. This assumption is also reasonable from a modeling point of view, since OCM attention fraction optimization in problems of this type would typically assign an attention fraction of 0.9 or better to θ_e.

Given this basic setup, the specific structure for the plant and the command signal is shown in Figure 26. As indicated earlier, this structure is adapted from Reference 40 with additional information obtained from Reference 41. Working from right to left on the θ_a path in Figure 26, the analog to digital conversion used in the experimental analysis introduces a gain into the system. An additional stick gain is also present. Both the stick gain and the conversion gain are taken directly from the experimental setup described in Reference 40. ("MAGIC" refers to a general-purpose facility for experimental analysis of, among other things, cockpit displays.) The element G_a represents the basic plant dynamics, which were under experimental control. The case selected for consideration here sets G_a to be

$$G_a(s) = \frac{2.15}{s(s+4)} \tag{42}$$

which matches one of the cases in Reference 40.

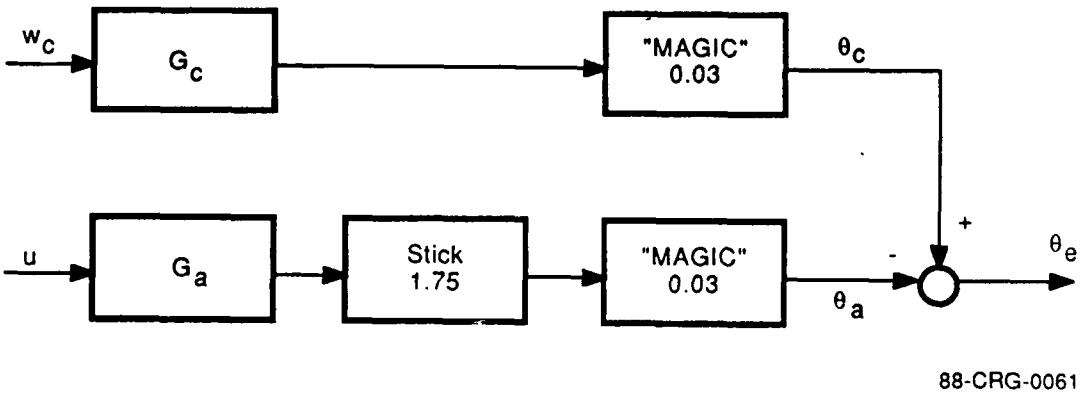

Figure 26. Plant and Command Signal Structure.

The command signal θ_c used in Reference 40 was a sum of sines. For present purposes, however, an OCM-compatible equivalent of this command signal is necessary, such as was used in Reference 28. Assuming w_c to be zero-mean, white Gaussian noise with intensity 1, a shaping filter was devised such that θ_c as modeled here would have a bandwidth and total power similar to that of θ_c in Reference 40. The filter selected for this purpose is

$$G_c(s) = \frac{0.6}{\left(\frac{s}{3.8}\right)^2 + 2(.7)\frac{s}{3.8} + 1} \tag{43}$$

2) Pilot Model–The discussion in subsection 1 above essentially completes the first step of the approach depicted in Figure 24. The next step involves the selection of an initial pilot model. As discussed earlier, this step may include an amount of pre-analysis in order to arrive at a good starting point for the iteration process. This analysis is envisioned to be that of using the standard OCM formulation with preliminary display candidates. An example of this will be given later. For now, attention is focused on how the state space representation of the OCM is constructed, which is the final consideration in forming an initial pilot model.

The OCM formulation for the task situation under consideration proceeded as follows. A cost function of

$$J = \lim_{T \to \infty} E\left\{\frac{1}{T}\int_0^T \left(\theta_{eD}^2 + ru^2\right) dt\right\} \tag{44}$$

has been used to model the pilot's objectives, where the value of r is adjusted so that the neuromuscular time constraint (τ_N) is equal to 0.1. Other OCM parameter values are set equal to those cited as typical in Table 1, with the exception of the observation thresholds. These latter parameters have been selected as 0.021 in. and 0.075 in./sec for θ_{eD} and $\dot{\theta}_{eD}$, respectively, in order to more closely reflect the original experimental situation in Reference 40.

With these definitions and parameter assignments, an OCM solution is obtained that gives pilot control gains, Kalman estimator gains, and actual observation and motor noise intensities. Next, these model elements are substituted into the block diagram structure shown in Figure 27. In the figure, A_1, B_1, and C_1 denote the state-space model of plant, disturbance, and display dynamics as augmented with the pilot's control input u. H_1 is the matrix of Kalman estimator gains, which depends on the observation noise intensities V_y. The quantity L* is the vector of optimal pilot gains and the quantity τ_p denotes the perceptual/cognitive delay.

All of the elements in Figure 27 are part of the usual OCM formulation. For more detail regarding their definition and derivation, particularly with respect to the augmentation of the basic state-space model with the control u, see Reference 1. Here it is sufficient to note that the position of the delay in the model structure has been decided for numerical reasons. In addition, a 4th order Padé approximation has been used for this delay in

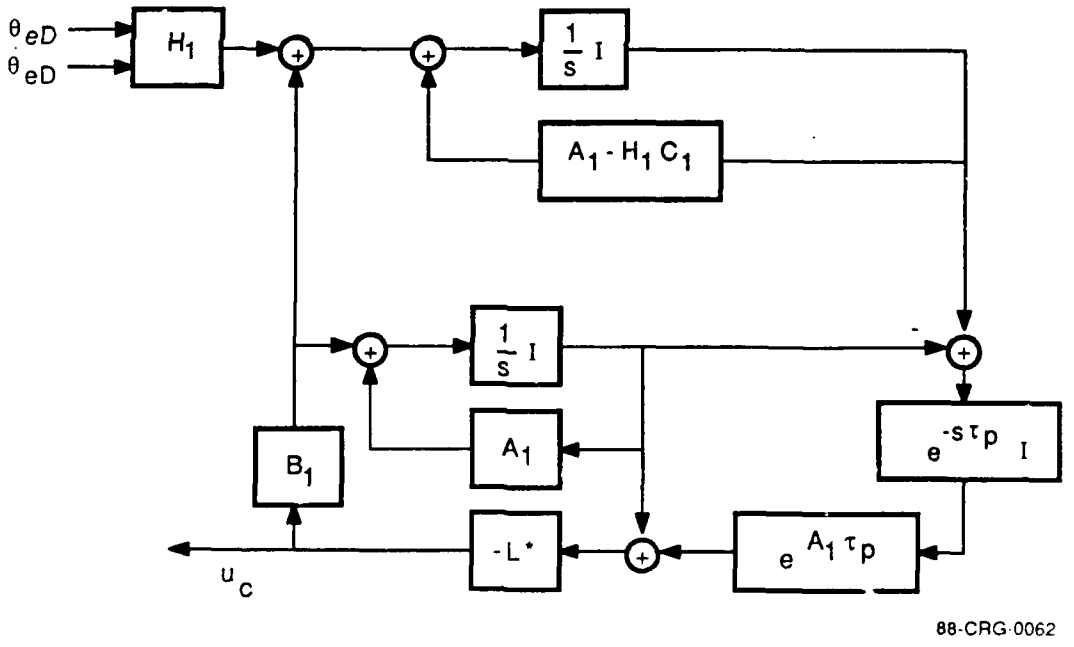

Figure 27. OCM Block Diagram Structure.

order to obtain a finite-dimensional state-space representation. Note also that the observation and motor noises, along with the neuromuscular lag, are not shown in Figure 27. They will be included subsequently, when the synthesis problem formulation is completed.

Finally, after using the OCM to generate the model elements in Figure 27, and after forming a state-space representation of pilot behavior according to the interconnection structure shown there, one other step remains before consideration can proceed to the μ-synthesis problem formulation. The OCM is in general a nonminimal system, due primarily to the presence of a relatively small time delay. To be compatible with μ-synthesis methods, however, a minimal pilot model is required. Thus a model-reduction procedure must be executed on the structure shown in Figure 27. The reduction method used in the present investigation was the so-called balanced model reduction procedure, as outlined in Reference 42. Essentially, this method first forms a balanced realization of the system under consideration and then truncates the least controllable and observable states. Using a minimal pilot model in μ-synthesis is consistent with the neglect of the time delay element in the Cooperative Synthesis formulation (Reference 25) and with the simplified OCM structure presented in Reference 43.

3) Uncertainty and Performance Weights–

i) Uncertainties–With an OCM-based pilot model derived and a representation of the task situation in place, attention now focuses on the step where a display is synthesized using SSV-based techniques. Completion of this step requires the definition and characterization of uncertainties in system elements. It also requires that performance goals be specified in terms of frequency domain weighting functions.

The uncertainty structure selected for the present problem is shown in Figure 28. As is evident from the figure, two types of uncertainty are represented, both of which reflect possible deviations of pilot behavior from the constrained optimality implicitly assumed by the OCM. One of these types is a deviation in the fidelity with which the signals θ_{eD}

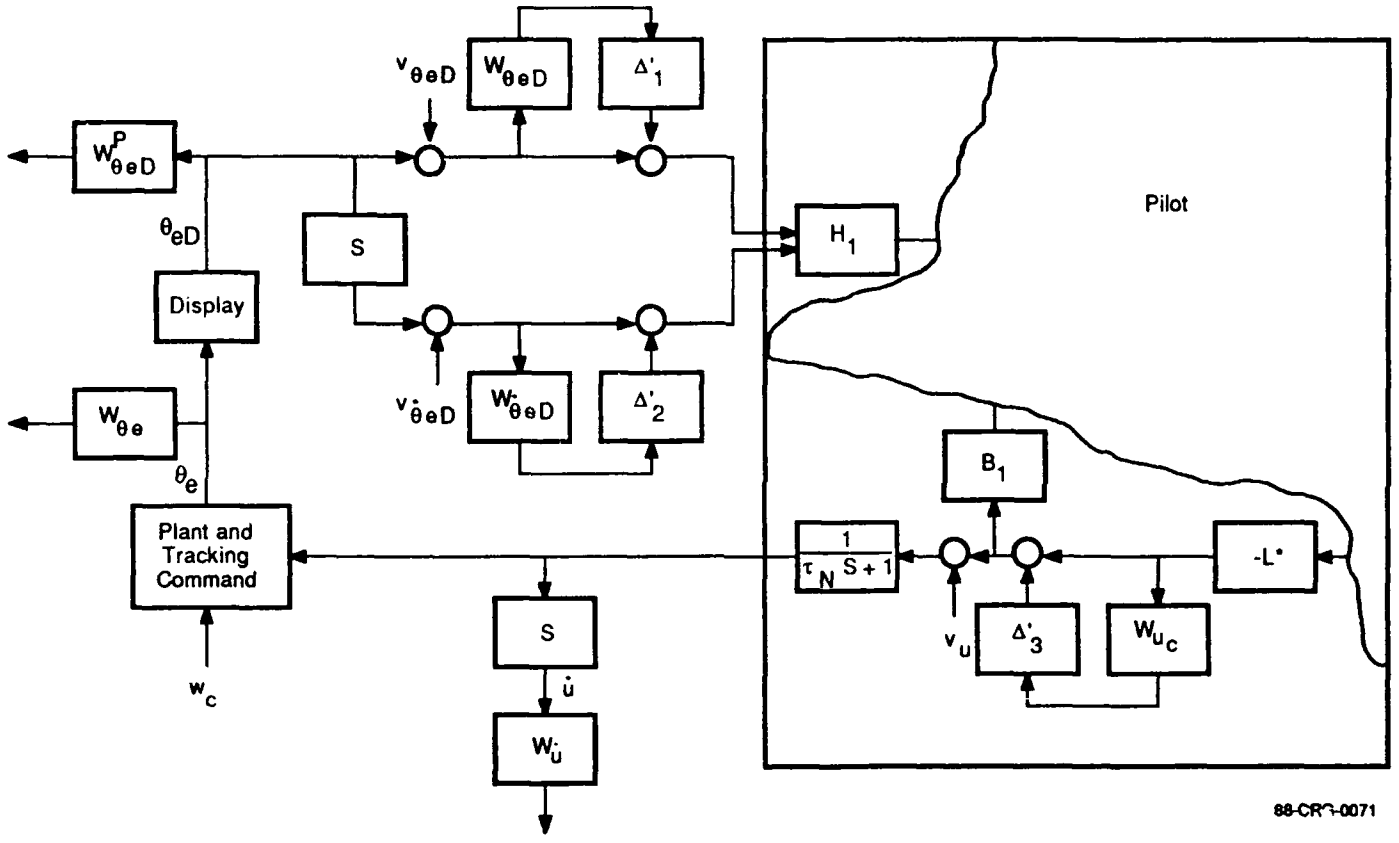

Figure 28. Block Diagram for Display Synthesis.

and $\dot{\theta}_{eD}$ are observed. The basic OCM model assumes that a certain level of error in observation occurs and models this as a white noise disturbance (e.g., $v_{\theta eD}$ and $v_{\dot{\theta}eD}$). However, because of environmental conditions or because of fatigue, this error may be greater than the nominal -20-dB noise-to-signal ratio usually assumed. Thus the uncertainties Δ'_1 and Δ'_2 have been included to model this effect.

The frequency-dependent weighting functions $W_{\theta eD}$ and $W_{\dot{\theta}eD}$ chosen for the observation uncertainty are the same, and are given as

$$W_{\theta_{eD}}(s) = W_{\dot{\theta}_{eD}}(s) = \frac{s + 0.005}{s + 0.5} \tag{45}$$

Figure 29 shows a magnitude plot of Equation 45. The rationale behind this choice is as follows. Qualitatively, it is assumed that a human can observe a low-frequency signal more accurately than a signal of higher frequency. (Consider the situation of trying to visually follow a slowly changing indicator versus following an indicator that is highly variable.) At the extremes, this is assumed to equate to a zero error at low frequency and a 100% error at high frequency. Based on experimental evidence (Reference 44), the transition from low to high frequency is assumed to occur somewhere around 0.5 rad/sec, which is reflected in Equation 45.

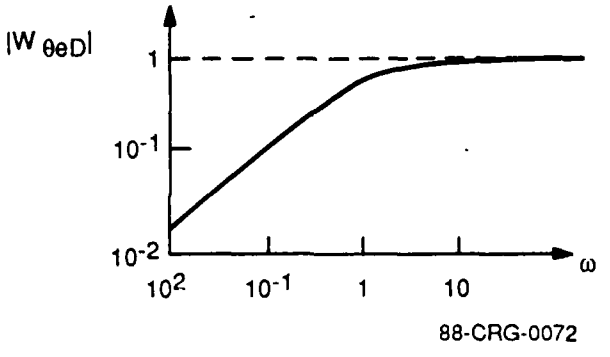

Figure 29. Weight on Displayed Error and Error Rate (magnitude).

The second type of uncertainty assumed is a variability in the pilot's control gains, which is shown in Figure 28 as Δ'_3. As with observation error, such a deviation might be prompted by pilot fatigue or stress. The weighting function that is used to characterize this uncertainty has the form of Equation 45, but with different parameter values, however:

$$W_{u_c}(s) = 0.5\left(\frac{s + 0.01}{s + 1}\right) \tag{46}$$

W_{uc} reflects an assumption that high-frequency control gain deviations will be within 50% of nominal. Also reflected is a different assumption regarding where the transition from low to high frequency occurs. Based on Reference 45, a transition near 1 rad/sec has been assumed. The selection of different break frequency values for the perceptual and motor uncertainties is an attempt to reflect actual differences that have been observed experimentally with respect to these behaviors.

Before turning to the selection of performance weights, the inclusion of motor and observation noises in the problem formulation should be discussed. This has been done because they are part of the nominal model of the pilot as derived from the OCM. They represent a significant set of excitation sources within the system that are influential in the SSV-based consideration of robustness qualities. The difficulty with their inclusion is that their intensities are, according to the OCM, determined by a noise-to-signal ratio. In the synthesis problem, where a new dynamic element is being introduced into the system, these ratios are not maintained. Instead, the noise intensities for $v_{\theta eD}$, $v_{\dot{\theta} eD}$, and v_u during μ-synthesis are fixed at the values that resulted from the previous OCM solution. In a convergent iteration process, this discrepancy will become insignificant, although disagreement at the outset may give intermediate display designs that are qualitatively different from final results.

ii) Performance Weights–The overriding performance criterion is that of achieving good flying qualities. Moreover, in view of the possible deviations in pilot behavior from nominal, achieving robust flying qualities is the actual desired performance result. Following on the analysis presented in Section II, it will be assumed that satisfactory

flying qualities are achieved by maintaining the RMS value of tracking error (θ_e) below a certain maximum and by maintaining the RMS value of control rate ($\dot{u}$) within a specified range.

Translating these time-domain performance goals into frequency domain weights is in general a nontrivial and inexact process. For the specific example under consideration, the process has proceeded as follows. With respect to tracking error, a line of reasoning similar to that suggested earlier in subsection 2 has been used. Relatively speaking, contributions to θ_e at low-frequency are assumed to be of more interest than high-frequency contributions. This is due to a combination of factors, such as known system bandwidth limitations and an assumption that high-frequency contributions to θ_e have a secondary impact on system performance. The form of the performance weight on θ_e chosen to reflect these assumptions is given as

$$W_{\theta_e}(s) = K \cdot \frac{(0.02s + 1)}{s + 1} \tag{47}$$

The value of K in Equation 47 is usually selected based on an independently defined performance specification that states the maximum permitted value of θ_e. One way of representing such a specification is to choose K such that

$$K \cdot |\theta_e|_{max} = 1 - \epsilon \tag{48}$$

where ϵ is the equivalent of a performance margin. For the problem at hand, however, there is no absolute specification on θ_e. Furthermore, there is only a loose correlation in general between RMS θ_e and $|\theta_e|_{max}$. Therefore, for present purposes K has been chosen as follows. First, the nominal transfer function between the vector of external inputs ($v_{\theta eD}$, $v_{\dot{\theta} eD}$, v_u, w_c) and θ_e has been determined. Then, for purposes of this problem, $|\theta_e|_{max}$ has been taken to be

$$|\theta_e|_{max} \triangleq \bar{\sigma}(M_{\theta_e, v}) \Big|_{|v| = 1} \tag{49}$$

where v is the vector of external inputs and $M_{o,i}$ denotes the nominal multivariable transfer function from i to o. Finally, ϵ is chosen to be 0.1, from which K can be calculated.

Essentially, this scheme assumes that nominal θ_e performance is satisfactory and includes a small margin of tolerance for (upward) deviations from it. It should be emphasized, however, that the scheme does not directly affect $\sigma_{\theta e}$, although higher weights on θ_e will tend to keep $| \theta_e |$ small.

Establishing a weighting function on control rate is similar to choosing $W_{\theta e}$. The situation in this case is more complex, however, because of the interval nature of the performance specification on $\sigma_{\dot{u}}$. Recall from the results in Section II that achieving satisfactory (Level 1) flying qualities seemed to require that workload (as quantified by $\sigma_{\tilde{u}}$) should fall within upper and lower bounds. The rough characterization of this interval made in Section II was that it spanned ± 50% of some central value. Carrying this over to the present case, it is then necessary to select a center value for $\sigma_{\dot{u}}$ and then choose $W_{\tilde{u}}$ such that $\sigma_{\dot{u}}$ after synthesis is within 50% of this value. Since a central value is not known a priori for this task situation (one of the issues discussed in Section II), one has been chosen based on an OCM analysis of the task situation where no display is assumed present. A value for $\sigma_{\tilde{u}}$ of 95 was obtained from this analysis. For present purposes, then, 100 will be chosen as the target value for $\sigma_{\tilde{u}}$. This means that if a μ-synthesized display, or any display for that matter, results in a model-based value for $\sigma_{\dot{u}}$ of 100 ± 50%, then the workload level will be declared satisfactory.

The above discussion still leaves unresolved the issue of what weighting function to choose to achieve the desired result for $\sigma_{\tilde{u}}$. The line of reasoning used to obtain a functional form for $W_{\theta e}$ is not applicable in this case. Moreover, since the constraint on $\sigma_{\tilde{u}}$ is two-sided (maximum and minimum), it is probably not appropriate to penalize only the magnitude of $\dot{u}$ (which achieves an upper bound). Nevertheless, lacking further qualitative information of a basic nature, the weighting function on $\dot{u}$ has been chosen as a pure gain, that is, $W_{\dot{u}}$ is of the form

$$W_{\dot{u}} = K \tag{50}$$

The value of K has been chosen using a procedure similar to that used for $W_{\theta e}$, except here ε has been set to 0.33. This reflects the tolerance for a 50% (upward) variation in

$\sigma_{\dot{u}}$ from the target value. Furthermore, it is also presumed that the nominal situation (which consists of the task situation, the previous display, and the new pilot model) has a calculated value of $\sigma_{\dot{u}}$ near 100.

A scheme for choosing $W_{\dot{u}}$ that takes into account the lower limit on $\sigma_{\dot{u}}$ might be the following. From an analysis of the nominal situation (or a situation that yields a $\sigma_{\dot{u}}$ near the target value), a power spectrum for $\dot{u}$ can be calculated. By approximating this spectrum with a rational transfer function and inverting it, a weighting function is obtained that biases $\dot{u}$ to have a spectrum that is known to be acceptable with respect to workload. This scheme has not been used in the present investigation, but its use of frequency domain information makes it a reasonable alternative. Its disadvantage, however, is that there are many frequency spectra that will yield a single RMS value. Biasing a signal to match only one of these spectra may be overly restrictive.

With the definition of performance weights in place, formulation of a μ-synthesis problem is now complete. Based on OCM analysis, a pilot model in state space form has been established with inputs θ_{eD} and $\dot{\theta}_{eD}$ (refer to Figure 27). Nominal observation errors for these quantities have been established in the form of additive white noises with intensities calculated from OCM analysis. Similarly, an additive motor noise has been included at the pilot output. Associated with the input observations is an uncertainty structure intended to represent likely pilot deviations from nominal. A similar uncertainty structure has been included at the pilot's output, where control gains are effected.

This entire model and perturbation structure has been interconnected to the model of the task situation. As part of this interconnection, performance signals θ_e and $\dot{u}$ have been tapped and weighted to achieve desired flying qualities. The only element of the interconnection structure undefined is that of the display, which is to be synthesized. As indicated earlier, the display element has been assumed to be single-input, single-output for simplicity, although the synthesis approach readily accommodates multivariable situations. This has required that an adjustment be made in the model interconnection structure to generate the signal $\dot{\theta}_{eD}$.

Finally, note that Figure 28 shows an additional performance weight on the signal θ_{eD}. While the actual tracking error θ_e is a principal indication of system performance, the signal θ_{eD} is the one actually observed by the pilot and the one that he is assumed to be minimizing in the OCM objective function. Not placing a penalty on θ_{eD} permits the synthesis process to produce a high gain display that magnifies already small tracking errors. When presented with what would appear to be large tracking errors, the pilot would have to effect a high gain compensation in order to reduce this perceived error. This could in turn make workload unacceptable. In fact, such an effect was observed in an earlier formulation of the synthesis problem that did not include observation and motor noises as additional excitation signals. To reduce this effect, a performance weight on θ_{eD} was added to regulate display gain. In the present formulation, however, such a weight has not been necessary and is not defined.

b. Synthesis Results

1) Initial Display Selected as Unity–In terms of the approach for deciding display dynamics depicted in Figure 24, the discussion above has established the task situation representation and the structure of the display synthesis formulation. To begin the iterative process, an initial OCM-based pilot model is needed. The following discussion describes a μ-synthesis result that was obtained using a pilot model derived under the assumption that the display was a unity gain element, i.e., a wire. Because this initial pilot biases the display design toward one that has no dynamics, the results for this case provide an indication of whether additional display dynamics are able to improve stability and performance robustness.

Using the wire pilot, the synthesis problem yielded the display dynamics shown in Figure 30, hereafter referred to as design M1 (for μ-based synthesis result 1) and expressed analytically as

$$D_{M1}(s) = 16.2 \frac{(s - 3.5)(s + 0.0342)}{(s + 0.125)(s + 0.865)(s + 19.8)} \qquad (51)$$

As discussed earlier, this result represents an intermediate step in the iterative process shown in Figure 24. The next step would be to substitute the new display for the old one

and obtain a new OCM-based pilot model for use in yet another synthesis problem, and so on until the displays obtained on successive iterations did not change substantially. At that point, consideration would turn to identifying key dynamic features of the display.

For a variety of reasons, the iterative process has not been carried on beyond the first synthesis result. This is partially due to the impact of program time and resource constraints. It is also partially a result of the experience gained in solving this first synthesis problem, and earlier preliminary formulations of it, which indicated that alternating between display and pilot may not be wholly satisfactory with respect to convergence.

Even though the result in Figure 30 is preliminary, it does suggest display compensation for the task situation. Therefore, it is still worthwhile to consider its key dynamic features. Moreover, previous experience with μ-based synthesis has indicated that a final design does not tend to differ substantially from the preliminary results. That is, though adjustments may be made in the design process to system elements and weighting functions, so long as they are relatively small, the major qualitative features of the design do not change.

With this in mind, there are two features of interest in $D_{M1}(s)$. The first is its limited bandwidth. Though it was in principle possible for the synthesis process to effectively return a wire display (especially when biased with a wire pilot model), M1 limits the high-frequency content of θ_{eD}. This is a direct result of the observation error uncertainties included in the formulation, and represents a mechanism for limiting the performance deviations that might be caused by these errors.

The second feature in M1 of interest is the apparent lead compensation provided to the pilot at middle frequencies. Lead, of course, is a standard display compensation mechanism; it is particularly interesting here that it should emerge as a result of a model-based optimization process that did not explicitly make provision for it. Once identified, these two features might be used to decide qualitative characteristics of display dynamics appropriate for this task situation.

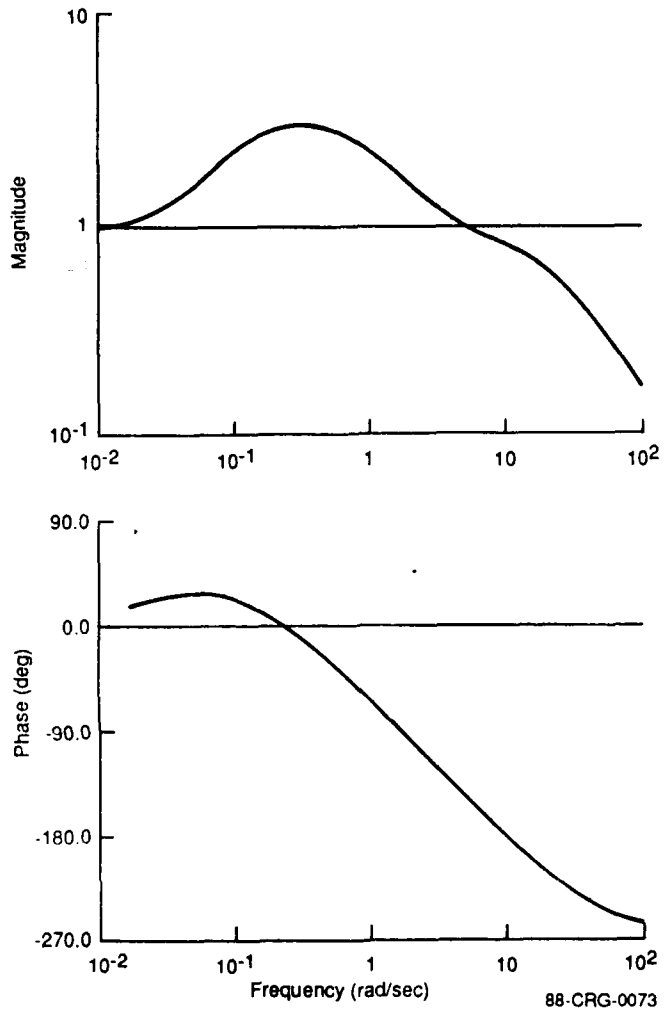

Figure 30. First μ-Synthesis Display Result (M1): $D_{M1}(s)$.

2) **Initial Pilot Selected by Prior Analysis**–One of the difficulties encountered in pursuing earlier formulations of the display synthesis problem, and which to a lesser extent is also present in M1, is that the workload indicator (RMS $\dot{u}$) is a sensitive performance measure. Coupled with the lack of a solid technique for choosing $W_{\dot{u}}$, it becomes a challenging design problem to maintain RMS $\dot{u}$ within a desired range. As a means of biasing the synthesis process to achieve this performance goal, one of the

dynamic features observed in the M1 design has been used to choose an initial pilot model.

Specifically, the limited bandwidth feature has been used to perform preliminary analysis with a family of first-order lag displays in order to obtain an OCM-based analysis result that has a workload value close to the target value for the current problem. Through this preliminary analysis, a first-order lag at 3 rad/sec was selected. Since this display transfer function will be of interest in the sequel, it is designated as $D_F(s)$, i.e.,

$$D_F(s) = \frac{3}{s+3} \tag{52}$$

Using the OCM-based pilot model devised assuming $D_F(s)$, the SSV-based synthesis result is shown in Figure 31, hereafter referred to as M2. The transfer function for M2 is given by

$$D_{M2}(s) = -\frac{0.33\ (s-12)}{s+4} \tag{53}$$

A comparison of D_{M1} and D_{M2} shows that the two have definite qualitative similarities and differences. Both have attenuation at high frequencies and are nonminimum phase. This latter property is perhaps more a result of the model reduction that has taken place on each design, as opposed to an inherent dynamic feature that is important for consideration. The nonminimum phase zeros do indicate the importance of phase in this problem, however, particularly in the region near crossover (5 to 8 rad), which is consistent with other analyses (e.g., References 4 and 5).

The displays differ in that M1 apparently provides some lead whereas M2 does not. Thus the biases introduced by the respective pilots do appear to have some effect. Whether or not continued iterations would eventually lead to the same display from these two starting points is not obvious at this point, although the display similarities do indicate that the task situation dynamics and performance and uncertainty weights may dominate the problem enough to effect convergence of the iterations between display synthesis and pilot model definition. This has not been pursued further here. Instead,

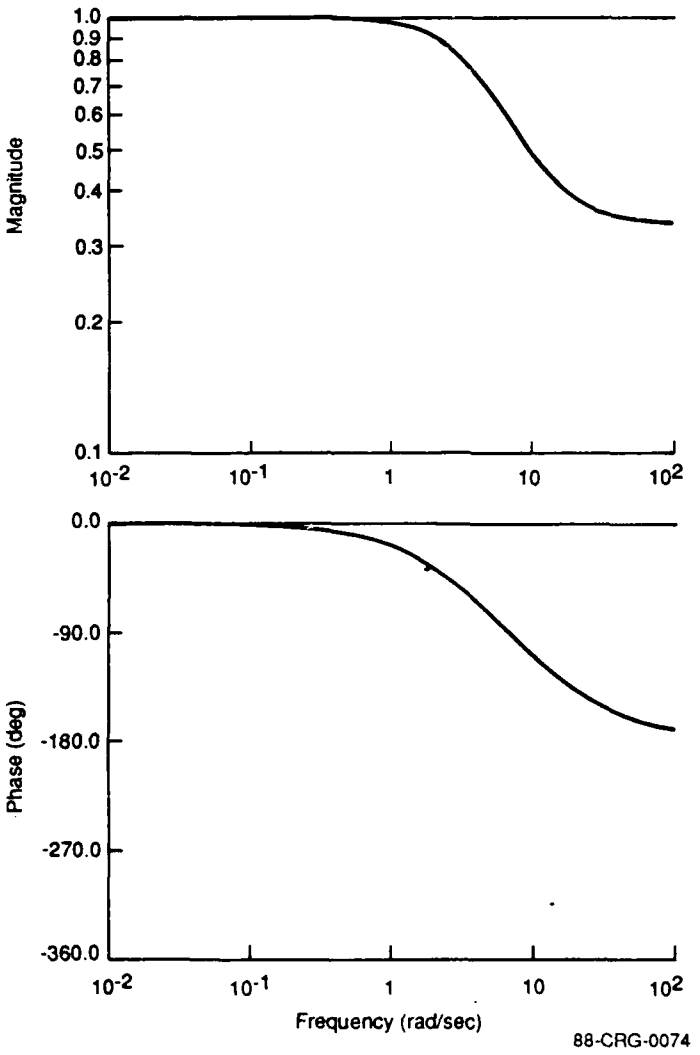

Figure 31. Second μ-Synthesis Display Design (M2): $D_{M2}(s)$.

effort has been devoted to a comparative analysis of several display candidates using SSV-based tests of robustness as described in the next subsection.

c. Comparative Analysis Using SSV Methods

Whatever the design for display dynamics and however it was obtained, SSV-based analysis methods can be applied to determine robustness properties. To illustrate the utility of these methods, the following presents such a comparative analysis of the four displays considered above. They are listed in Table 7, along with partial comparative results that will be considered in subsequent discussion.

The analysis was performed using the system structure shown in Figure 28. For each display transfer function D(s), a pilot model was generated using OCM analysis. Thus the analysis results obtained are for the situation where the pilot model does indeed match the display.

A first test of interest is whether the closed-loop system is robustly stable. To determine this, the test in Equation 37 was applied. For the wire display (W), the frequency-dependent μ-plot shown in Figure 32 was obtained. Since $\mu < 1$ for all frequencies, the system has robust stability with a wire display. This means that within the range of pilot behavior reflected in the uncertainty structure, no combination of permitted Δ' values will destabilize the system. A similar result was obtained for the F and M2 displays, as shown by the plots in Figures 34 and 35. However, the result for M1, as shown in Figure 33, indicates that there is a destabilizing combination of Δ'_i values.

A second SSV-based analysis test is that of nominal performance. Recall that this test, defined in Equation 38, indicates whether the nominal system will meet the performance specifications encoded into the weighting functions W_{θ_e} and $W_{\dot{u}}$. The nominal performance plot for the system with a wire display is shown in Figure 36. Since the results in this plot have essentially been used to select performance weights, it is not particularly interesting. However, it does point out an interesting feature of the problem, which is that the two performance objectives (one on θ_e and one on $\dot{u}$) are largely decoupled with respect to frequency. The weighting function on θ_e emphasizes low frequencies. The power spectrum of $\dot{u}$ tends to be spread evenly over the pilot's bandwidth, which means that $\dot{u}$ has a spectrum that emphasizes high frequencies.

TABLE 7. WORST CASE PERTURBATIONS FOR DISPLAYS

Display	D(s)	Δ' Complex		Δ' Real	
		Δ'	ω	Δ'	ω
Wire (W)	1	diag [(.333, -.504), (-.0787, .599), (.602, .0453)]	7.94	diag [1.00, -1.00, -.0142]	3.16
First Synthesis Design (M1)	$\frac{16.2\,(s-3.5)\,(s+0.0342)}{(s+0.125)\,(s+0.865)\,(s+19.8)}$	diag [(.262, -.552), (.461, .401) (.380, -.478)]	7.94	diag [.965, 1.00, -1.00]	3.55
First-Order Lag (F)	$\frac{3}{s+3}$	diag [(.0421, -.573), (.508, .269) (.424, -.389)]	6.31	diag [(.962, 1.00, -1.00]	3.55
Second Synthesis Result (M2)	$\frac{-0.33\,(s-12)}{s+4}$	diag [(.305, -.497), (.387, .437), (.506, -.290)]	7.94	diag [.206, 1.00 -1.00]	3.98

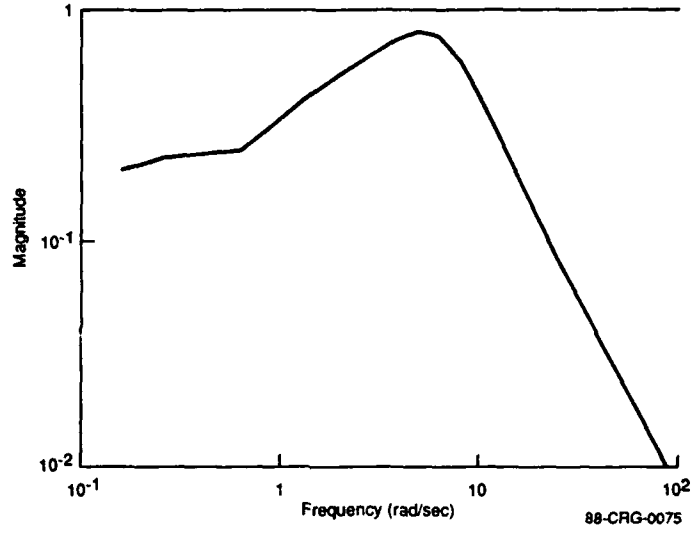

Figure 32. Robust Stability Test for W.

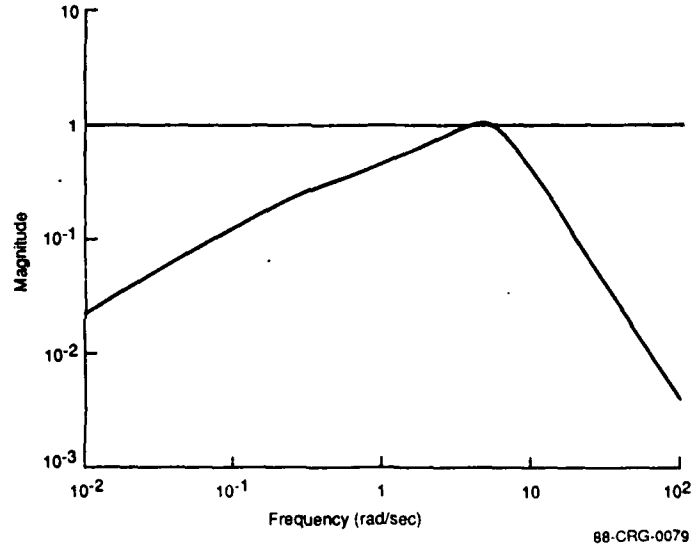

Figure 33. Robust Stability Test for M1.

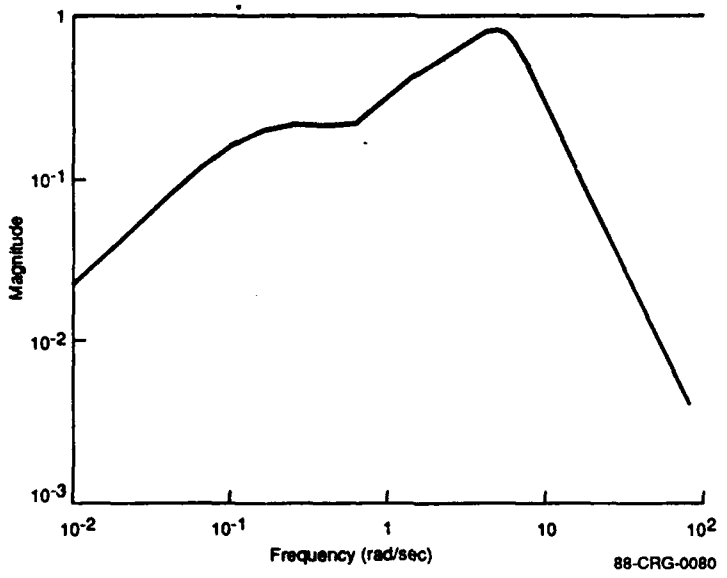

Figure 34. Robust Stability Test for F.

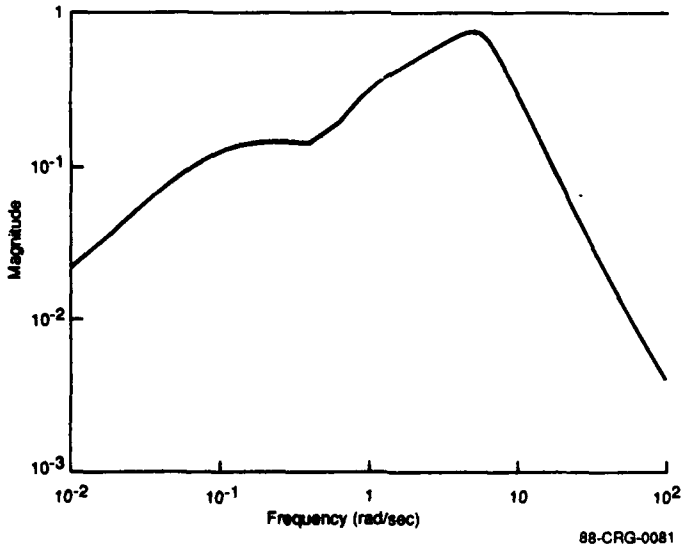

Figure 35. Robust Stability Test for M2.

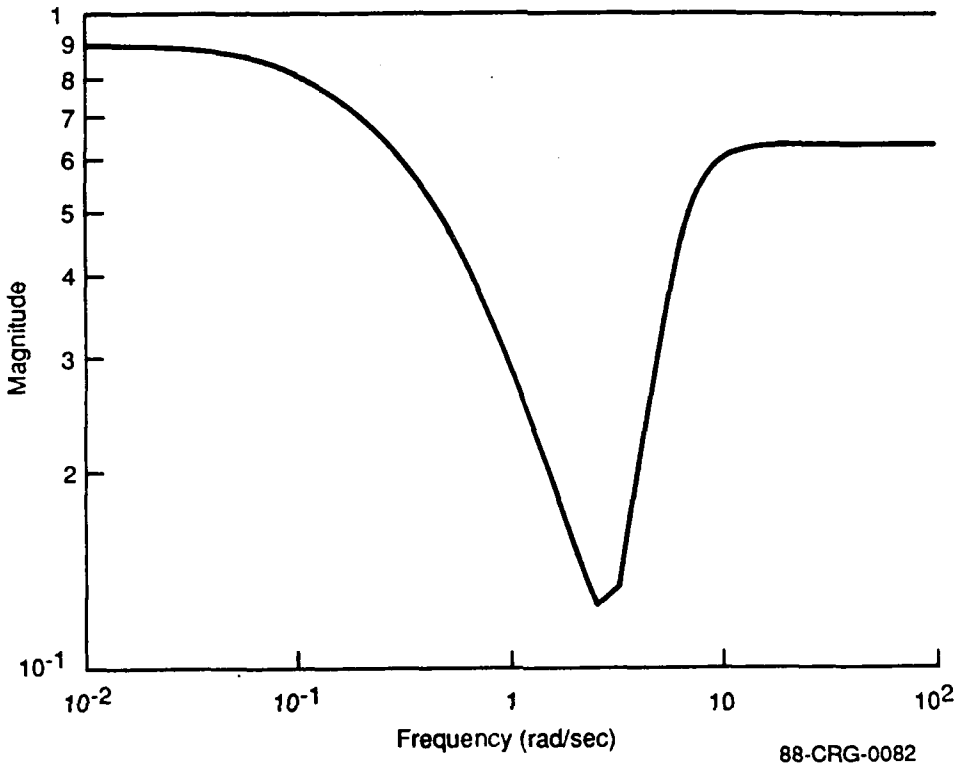

Figure 36. Nominal Performance Test for W.

Thus, in the nominal performance plot, $\bar{\sigma}(M_{\theta e,\, v})$ dominates low frequencies and $\bar{\sigma}(M_{\dot{u},\, v})$ dominates high frequencies. Because of this, the performance margins selected for each are evident in Figure 36, where the low-frequency maximum is 0.9 and the high-frequency maximum is 0.66. In addition, the decoupling, makes it possible to readily infer which performance objective is violated if a nominal or robust performance plot exceeds 1 at some frequency.

Consider now the question of robust performance. The appropriate SSV indicator functions (Equation 39) for this quantity are shown in Figures 37 to 40. In every case there is a region at high frequencies where μ exceeds 1. Since it is known that all of the displays (essentially) have robust stability, μ values greater than 1 here indicate that there

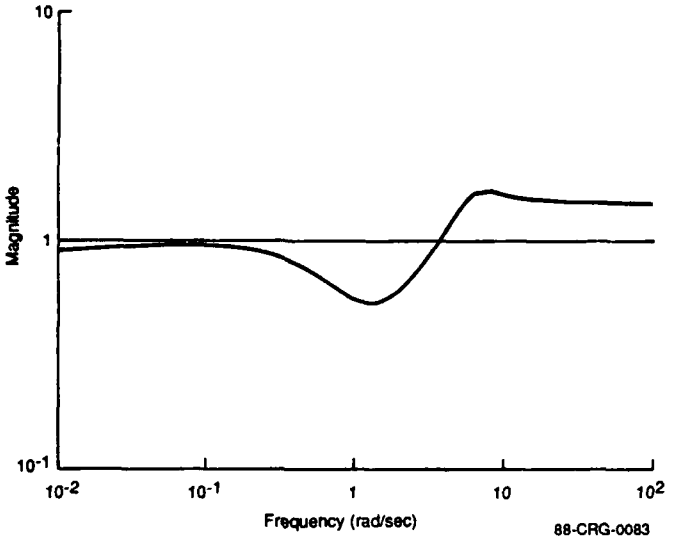

Figure 37. Robust Performance Test for W.

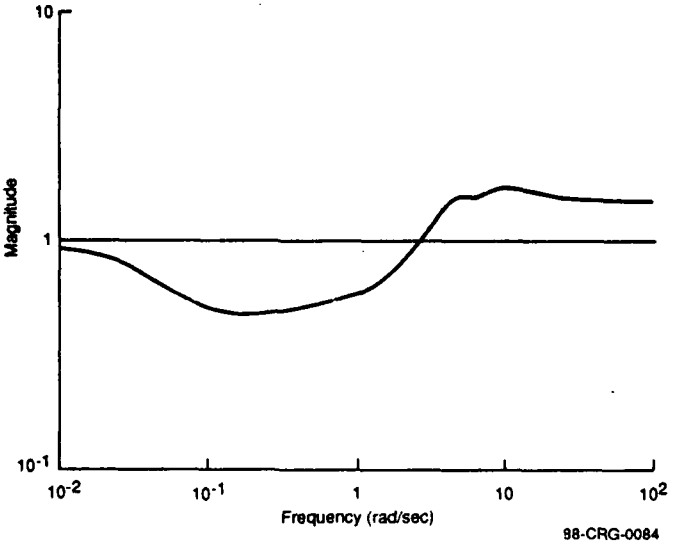

Figure 38. Robust Performance Test for M1.

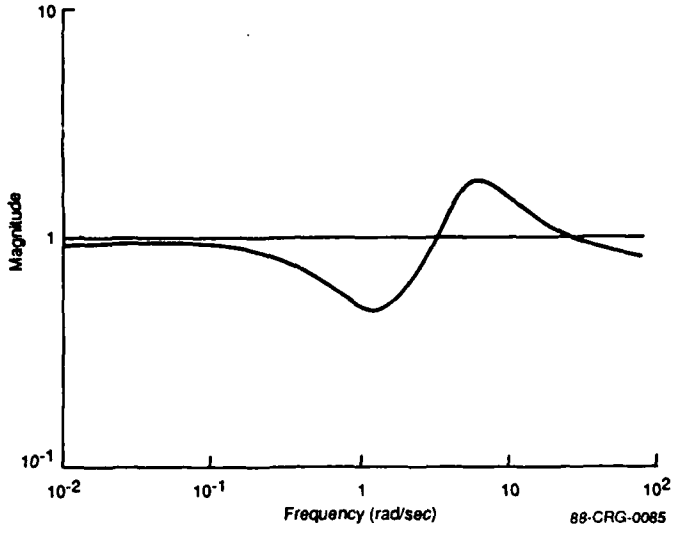

Figure 39. Robust Performance Test for F.

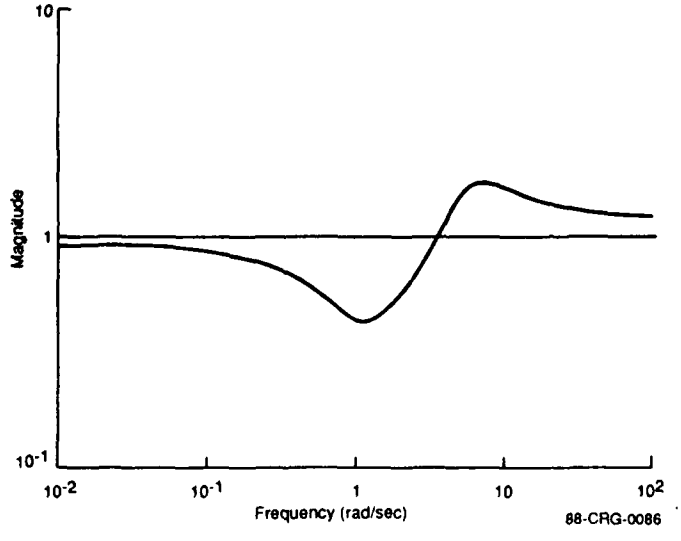

Figure 40. Robust Performance Test for M2.

is some combination of values for Δ' that will cause the performance objectives to be violated. In particular, since the μ violations occur at higher frequency, the expectation is that the workload objective will be the one violated. Though the robust performance plots are all similar in form, there are notable differences that tend to distinguish the displays. For example, while robust performance margins at low frequency for W, M2, and F are relatively small, the M1 design exhibits a substantial margin. Again, relying on the assumed dominance of tracking error at low frequencies, this might indicate that M1 is able to tolerate even wider variations in pilot behavior and still maintain performance and stability robustness, with respect to tracking error objectives. M1 does not offer much improvement over the wire, however, at high frequencies. Here the F and M2 designs offer some improvement, but all displays are subject to performance specification violations at high frequencies.

As a byproduct of the μ-analysis, the combination of Δ' values that produces the highest value of μ is available. These values have been recorded in Table 7 in the center columns, along with the frequency at which they occur. Recall that these worst case Δ' values are in general complex perturbations, which is evident in the table entries. From these values, it is often possible to gain insight as to how the various perturbations must interact in order to produce a deviation sufficiently large to fail robust performance or stability tests. In fact, it often happens that certain worst case combinations can be ruled out based on the physics of the problem. Other combinations of lesser impact, but perhaps more likely to occur, can then be considered. In the present case, however, all of the Δ's correspond to deviations in pilot behavior and there is little physical basis for discounting any one combination of Δ's as unlikely.

In principle it is possible to substitute the worst case Δ' combination back into the model structure and then calculate worst case RMS values of the performance signals θ_e and $\dot{u}$. This has not been done here, however, due to the additional complexity involved in integrating a complex scalar into the system state space structure. A qualitatively similar and computationally easier indication is offered by examining robust stability with Δ' restricted to real variations. Termed a real-mu or rmu test, an rmu plot of robust performance for the wire display case is shown in Figure 41. Note that when Δ' is

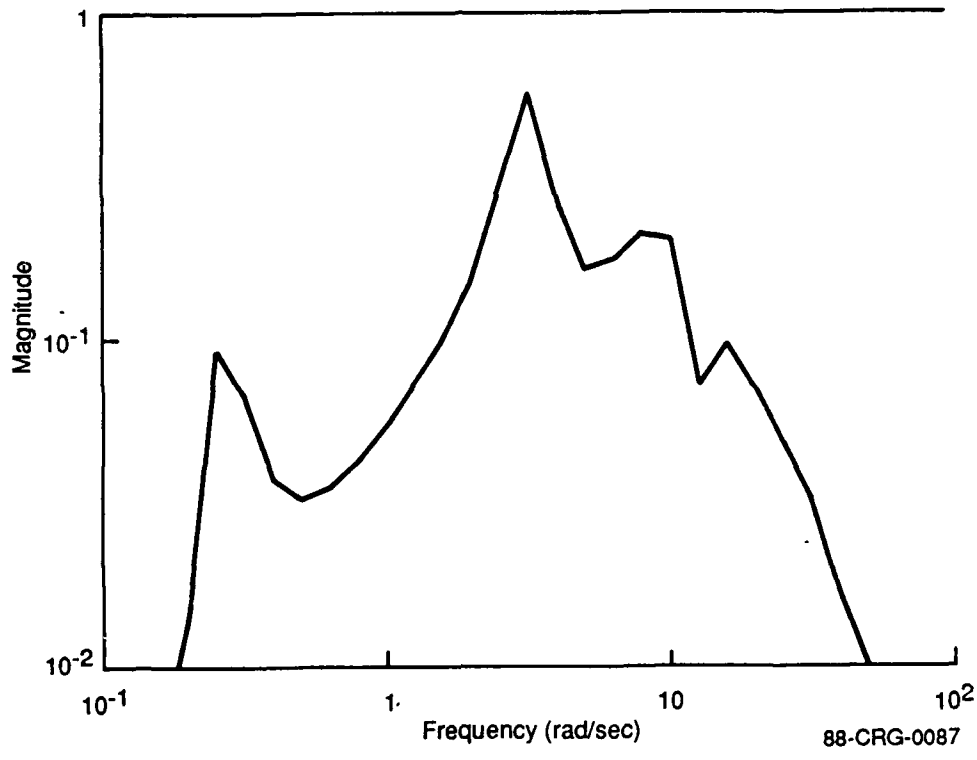

Figure 41. Real-μ Test of Robust Stability for W.

restricted to real variations, robust stability is maintained. A similar result was observed for the other displays.

The worst case real Δ' combinations and the frequencies at which they occur are shown in the right-hand columns of Table 7. Again, there is no basis for discounting any of these combinations on physical grounds, although it is interesting to note that in a couple of cases the relationship of observation error perturbations for θ_{eD} and $\dot{\theta}_{eD}$ is opposite in sign, while in another it is equal in sign, suggesting that the displays might be providing qualitatively similar compensation in some cases and qualitatively different in others.

Taking the worst case Δ' values and substituting them into the model structure, an RMS analysis has been performed. The results of this analysis are plotted in Figure 42, along with the results obtained for the nominal situation (i.e., $\Delta' \equiv 0$) and one other situation to be described shortly. Normalized workload, as quantified by the RMS value of $\dot{u}$, is plotted on the abscissa, where the normalization is with respect to the target value for $\sigma_{\dot{u}}$ of 100. Normalized tracking error performance, as quantified by RMS θ_e, is plotted on the ordinate, where the normalization is with respect to the nominal wire display case ($\sigma_{\theta e} = 0.0212$).

Consider first the RMS performance and workload values for the nominal cases. Recall that the performance goals for this problem were to keep RMS θ_e small and to maintain

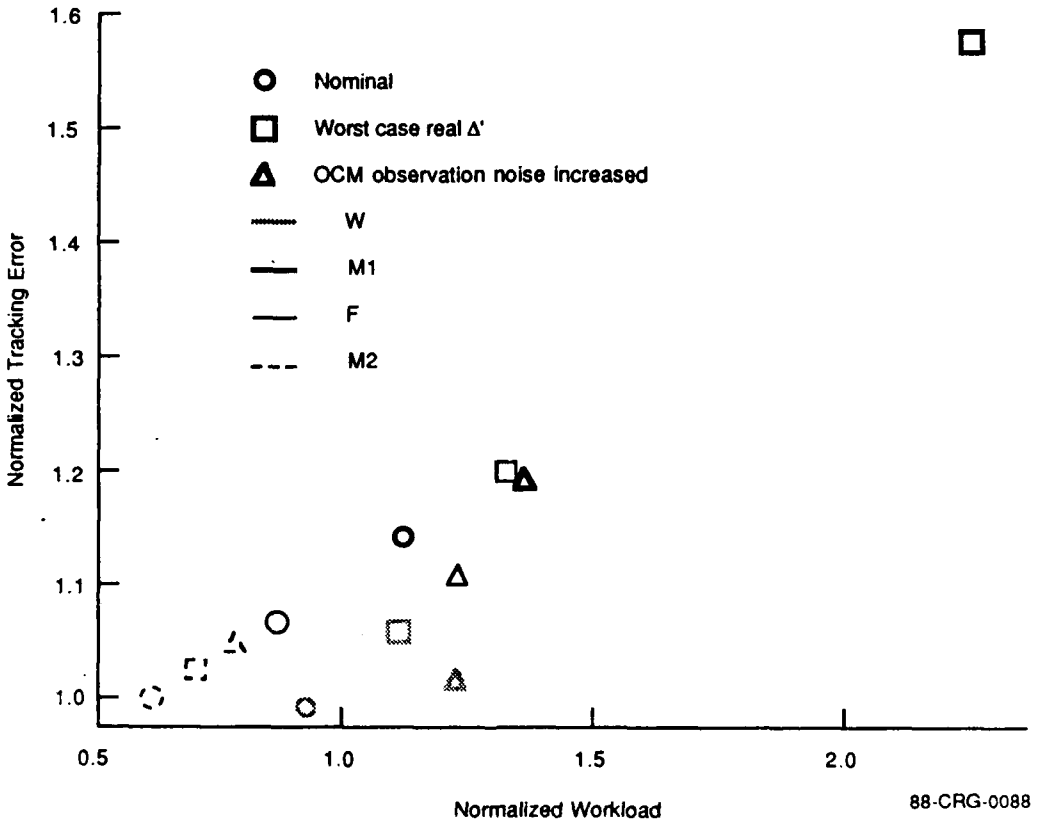

Figure 42. Comparison of Displays in Performance/Workload Plane.

RMS $\dot{u}$ within ±50% of 100. From Figure 42, it is evident that a modest degree of success was achieved in regulating RMS values using frequency domain weighting functions. Both of the synthesized displays have nominal RMS θ_e and $\dot{u}$ values that satisfy performance goals. It is interesting to note, however, that the effort to bias the synthesis problem toward realizing the target workload value was less than completely successful. While the first-order lag has nominal RMS θ_e and $\dot{u}$ quite close to those of the wire, which presumably leads to an OCM-based pilot model that biases the synthesis process toward these values, the actual synthesis result has a nominal RMS $\dot{u}$ that is considerably less (though still within the rather arbitrary acceptable limits of deviation from the target value).

Now consider the effect of permitting the worst case real values of Δ' to perturb the system. RMS values obtained under this condition for the four displays are shown in Figure 42. These results tend to point up a weakness in using only rmu for evaluation purposes and to reinforce that the process of representing time domain performance specifications in terms of frequency domain weighting functions is still imprecise. The results also provide support for the μ-based synthesis and analysis approach for discriminating between displays.

With respect to the use of rmu, recall that all of the displays exhibited robust stability when Δ' was restricted to real variations. Yet there exist complex Δ' combinations that will not yield robust performance, or in one case, will not yield robust stability. RMS values for these combinations will presumably be much more divergent from performance goals than what is exhibited in Figure 42. Since it is not necessarily true that worst case real variations are indicative of worst case complex variations, extending any conclusions made on the basis of Figure 42 to the general case is somewhat tenuous.

On the positive side, the relative positions of nominal and perturbed points for M2 and W indicate that the SSV-based synthesis approach can result in displays that achieve a beneficial degree of robust compensation. Again, within the class of real variations in Δ', it is evident in the figure that while the nominal operating point for the wire case is superior to the M2 design (better tracking performance, workload closer to target value),

comparison of the perturbed operating points indicates that the M2 display is less sensitive to pilot variability. Tracking performance does not degrade as much and workload does not deviate as much from nominal. Based on these observations, it might be concluded that the M2 display, while compromising on performance under nominal (e.g., optimal) conditions, is a desirable addition to the system because it provides a degree of tolerance for pilot variability.

As a final consideration of how best to represent human behavioral variability in SSV-compatible terms, a comparison was made of the results just discussed with results obtained from a variation in OCM parameters. Specifically, the observation noise-to-signal ratio was changed from its nominal value of -20 dB to a value of -17 dB. This roughly doubles the observation noise intensity, which was thought to be compatible with the transfer function selected for $W_{\theta eD}$ and $W_{\dot{\theta}eD}$. To obtain model-based RMS results for these cases, the internal pilot model structure was left unchanged (including filter and control gains), all Δ' values were assumed to be zero, and noise intensities were adjusted to achieve equilibrium with respect to the new noise-to-signal ratio. The normalized RMS tracking error and RMS $\dot{u}$ that resulted are plotted in Figure 42. Based on the positions of these points relative to the respective nominal and worst case (real) Δ' operating points, a certain degree of consistency is evident between OCM parameter variations and the uncertainties constructed in SSV terms to be similar to them. Thus, it does seem possible that pilot variations that are well understood in OCM terms can be systematically reflected in SSV terms.

d. Experimental Test of SSV-Based Analysis Results

From the discussion in the previous subsection, it was tentatively concluded that the M2 display might exhibit a greater tolerance to pilot variability than a wire display. This subsection considers how one might verify experimentally that this is the case.

Recall that the potential variations in pilot behavior considered in the synthesis formulation were of two types. The first was an increase in observation error and the second was a variability in the pilot's control gains. An experimental test that seeks to

compare robustness properties of displays must systematically manipulate these two effects. This could be done as follows.

To increase the observation error, a defocusing lens could be placed in front of the pilot. This defocusing lens would blur the pilot's vision, thus interfering with his ability to accurately perceive the display. The degree of perceptual degradation can be manipulated by varying the refractive power of the lens. To increase the pilot's control action variability, a random vibrator can be secured to the cockpit and attached to the pilot's forearm. The effect of the vibrator will be to introduce noise in motor performance while not influencing the pilot's ability to perceive or interpret the display. The motion of the vibrator must be made random, however, so that the pilot cannot compensate for its interference by anticipatory muscle control. If this were not the case, the pilot would not only compensate for the interference, thereby maintaining a reduced rate of motor variability, but would also allocate a large amount of attention to the task of motor compensation, thereby reducing his perceptual attention and increasing his observation error rate. The degree of motor degradation can be manipulated by varying the mean frequency of the vibrator motion.

To accurately observe the effects of perceptual and motor variations, an experiment should be performed in two phases. The first phase would consist of pretesting, and the second phase would consist of the experimental sessions. The same subjects would be used in both phases of the experiment, and all subjects should receive extensive practice on the tracking task for all displays prior to pretesting. Pretesting would ensure that the independent variables chosen to manipulate perceptual and motor error rates are adequate, i.e., they achieve the desired effects on perceptual and motor performance. It would also be used to adjust the manipulation ranges of refractive power and vibrator frequency to match the range of variation assumed in the SSV analysis.

Once the experiment was performed, results for RMS tracking error, RMS $\dot{u}$, and subjective difficulty rating could be compared with those predicted from the SSV analysis. For the case where the M2 and W displays are under test, the predicted result would be that the wire display is better under optimal conditions, but that it becomes

worse than the M2 display when the pilot's perceptual and motor performance is degraded.

5. ISSUES FOR FURTHER STUDY

Based on the example presented, the tentative conclusion is that an SSV-based approach to deciding display dynamics requirements is reasonable. The example problem has surfaced a number of issues that require further investigation, however, in order to make such an approach well-understood and reliable. First, there is a need for considerable work in the area of representing variations in human behavior in SSV-compatible terms. This involves the selection of a nominal block diagram structure for a pilot model and then specifying potential behavioral variations as Δ blocks within that structure. Deciding frequency domain weights that adequately reflect these phenomena is also a nontrivial task that needs further study. Two approaches are possible in pursuing this development. One is to attempt to duplicate the effects of OCM parameter variations. Another, more fundamental, approach is to consider relevant human behavioral phenomena and then attempt a direct translation into SSV-compatible terms.

A second major area for further study is related to the first. It is the examination of how to represent performance specifications and goals in SSV-compatible terms. The analysis in Section II has indicated that RMS values of a performance and workload signal are indicative of flying qualities. However, translating specifications on RMS values into frequency-dependent weighting functions has proven to be an uncertain process. Although a modest amount of success was achieved in regulating RMS values, it is evident that further consideration is needed in this area.

Finally, the use of an iterative scheme to converge on SSV-based display design needs to be further explored. At issue is the viability of the procedure whereby pilot and display are alternately modified, with the expected result that their respective dynamic characteristics will settle into an optimal combination that matches the task situation dynamics. Exploration of alternatives that simultaneously consider task situation, pilot, and display dynamics is warranted here, with the goal being to develop an SSV-based scheme that is similar to the Cooperative Synthesis scheme considered in Section IV.

SECTION VI

SUMMARY

The underlying theme of this research effort has beer the development of a model-based, multivariable methodology for deciding display dynamics requirements to ensure good flying qualities. Each topic considered in the research fits within this theme and has resulted in a contribution toward the goal of having such a methodology. A depiction of how the research effort was organized is shown in Figure 43. Areas of investigation are shown vertically in the center, with key data and other inputs shown on either side.

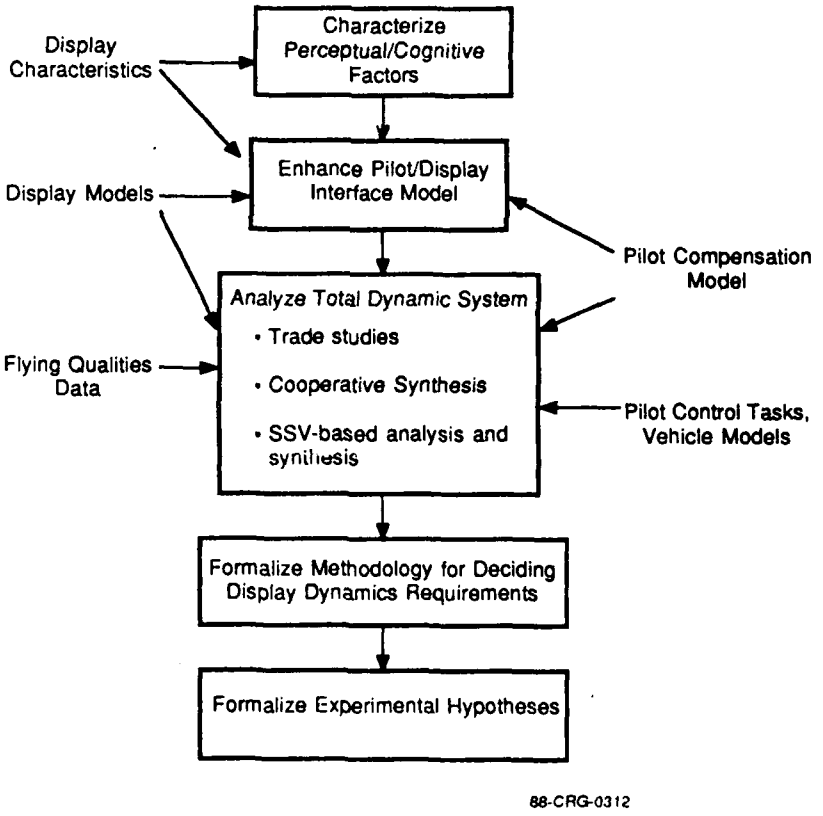

Figure 43. Display Dynamics Program Flow.

An implicit assumption made in this effort is that the OCM is likely to be an essential feature of any model-based display dynamics methodology. Thus the pilot compensation model referred to in Figure 43 is the OCM. This choice has prompted one particular area of analysis of the total dynamic system, which is to further establish the link between flying qualities ratings and OCM-based quantities. This was of particular interest with respect to the anticipated consideration of multivariable situations. To this end, a two-dimensional, OCM-based system performance and pilot workload space has been found that gives a reasonable grouping of flying qualities according to data obtained from the Neal-Smith and LAHOS studies.

Using the OCM as a display dynamics methodology element has also prompted a reconsideration of how best to represent complex pilot/display interaction phenomena in terms of lumped OCM pilot parameters. In its fully developed form, a display dynamics design and analysis methodology should have a set of guidelines for selecting OCM parameters to reflect the variety of human behavioral phenomena that are affected by a particular display design. A first step toward this end has been taken here with a review of relevant research in human perception and cognition, along with a preliminary indication of how such basic psychophysical effects map into OCM parameters. These results were obtained from the first two areas of investigation shown in Figure 43.

In conjunction with the analysis of the total dynamic system, a topic of consideration has been the investigation of display dynamics effects in a realistic situation. In particular, a STOL aircraft in an approach-to-landing configuration has been considered, with the pilot assumed to be executing the approach using a HUD. Moreover, a processing and formatting delay has been included in the HUD. OCM-based analysis of this situation has indicated both the potential value of having the additional information that a HUD presents and the high cost of HUD delay with respect to realizing the full value of this information. Using the OCM-based Cooperative Synthesis approach, compensating display dynamics in the form of a flight director have been designed that substantially overcome the losses due to HUD delay. This case study indicates the potential negative impact of display dynamics effects in a realistic setting and reinforces the observation that these effects cannot be neglected in a closed-loop analysis that includes the pilot.

Moreover, this example shows how a systematic model-based approach can be used to specify display dynamics.

Finally, SSV-based analysis and synthesis methods have been used to consider the problem of display dynamics design requirements. As a result of this investigation, a methodology has been suggested for determining these requirements. Building on the other elements of research performed in this study, the methodology also addresses the important issue of ensuring that any display dynamics introduced into the system do not make the system overly sensitive to variability in pilot behavior. Moreover, the methodology incorporates a systematic means for deciding display dynamics that are tolerant to these possible variations. Though it is in a preliminary state of development, an example has been constructed that exercises its principle features and points to its viability as an approach for deciding display dynamics requirements to ensure good flying qualities. In particular, the example has been constructed around an existing experimental paradigm. Analysis results in this context lead directly to hypotheses that can be tested using this paradigm.

REFERENCES

1. D.L. Kleinman, S. Baron, and W.H. Levison, "An Optimal Control Model of Human Response," *Automatica,* Vol. 6, 1970, pp. 357-383.

2. W.H. Levison, S. Baron, and D.L. Kleinman, "A Model for Human Controller Remnant," *IEEE Trans. on Man-Machine Systems,* Vol. MMS-10, No. 4, 1969, pp. 101-108.

3. R.E. Curry, W.C. Hoffman, and L.R. Young, "Pilot Modeling for Manned Simulation," AFFDL-TR-76-124, Flight Dynamics Laboratory, Wright-Patterson Air Force Base, Ohio, 1976.

4. B.J. Bacon and D.K. Schmidt, "An Optimal Control Approach to Pilot/Vehicle Analysis and the Neal-Smith Criteria," *Journal of Guidance and Control,* Vol. 6, No. 5, 1983.

5. M.R. Anderson and D.K. Schmidt, "Closed-Loop Pilot Vehicle Analysis of the Approach and Landing Task," *Journal of Guidance,* Vol. 10, No. 2, 1987, pp. 187-194.

6. W.W. Weirwille and S.A. Conner, "Evaluation of 20 Workload Measures using a Psychomotor Task in a Moving-Base Aircraft Simulator," *Human Factors,* Vol. 25, 1983, pp. 1-16.

7. T.P. Neal and R.E. Smith, "An In-Flight Investigation to Develop Control System Design Criteria for Fighter Airplanes," AFFDL-TR-70-74, Vol. I, Flight Dynamics Laboratory, Wright-Patterson Air Force Base, Ohio, 1970.

8. R.E. Smith, "Effects of Control System Dynamics on Fighter Approach and Landing Longitudinal Flying Qualities," AFFDL-TR-78-122, Flight Dynamics Laboratory, Wright-Patterson Air Force Base, Ohio, 1978.

9. S. Baron and W.H. Levison, "An Optimal Control Methodology for Analyzing the Effects of Display Parameters on Performance and Workload in Manual Flight Control," *IEEE Trans. on Systems, Man, and Cybernetics,* Vol. SMC-5, No. 4, 1975, pp. 423-430.

10. D.L. Kleinman and S. Baron, "A Control Theoretic Model for Piloted Approach to Landing," *Automatica,* Vol. 9, 1973, pp. 339-347.

11. S. Baron and W.H. Levison, "Display Analysis with the Optimal Control Model of the Human Operator," *Human Factors,* Vol. 19, No. 5, 1973, pp. 437-457.

12. R. Curry, D.L. Kleinman, and W.C. Hoffman, "A Design Procedure for Control/Display Systems," *Human Factors*, Vol. 19, No. 5, 1977, pp. 421-436.

13. R. Hess, "Analytical Display Design for Flight Tasks Conducted under Instrument Meteorological Conditions," *IEEE Trans. on Systems, Man, and Cybernetics*, Vol. SMC-7, No. 6, 1977, pp. 453-462.

14. J. Korn, S. Gully, and D.L. Kleinman, "Modeling, Design, and Validation of an Advanced Cockpit Display System," *Proceedings AIAA Workshop on Flight Testing to Identify Pilot Workload and Pilot Dynamics*, Edwards Air Force Base, California, January 1982.

15. J.J. Gibson, *Perception of the Visual World*, Houghton Mifflin, Boston, Massachusetts, 1950.

16. S. Baron and J. Berliner, "Manmod 1975: Human Internal Models and Scene-Perception Models," RD-CR-76-3, U.S. Army Missile Command, Redstone Arsenal, Alabama, 1975.

17. W.G. Matheny et al., "An Investigation of Visual, Aural, Motion, and Control Movement Cues," Naval Training Devices Center, Report NAVTRADEVCEN 69-C-0304-1, April 1971.

18. J.M. Naish, "Control Information in Visual Flight," *Proceedings Seventh Annual Conference on Manual Control*, Los Angeles, California, 1971 (also NASA SP-281, 1972).

19. P.H. Wewerinke, "A Theoretical and Experimental Analysis of the Outside World Perception Process," *Proceedings Fourteenth Annual Conference on Manual Control*, Los Angeles, California, pp. 535-555.

20. A.J. Grunwald and S.J. Merhav, "Vehicular Control by Visual Field Cues–An Analytical Model and Experimental Validation," *IEEE Trans. on Systems, Man, and Cybernetics*, Vol. SMC-6, No. 12, 1976, pp. 835-845.

21. A.J. Grunwald and S.J. Merhav, "Effectiveness of Basic Display Augmentation in Vehicular Control by Visual Field Cues," *IEEE Trans. on Systems, Man, and Cybernetics*, Vol. SMC-8, No. 9, 1978, pp. 679-690.

22. R.A. Hess and K.K. Chan, "A Model of the Human's Use of Visual Field Cues in Nap-of-the-Earth Flight," AIAA Paper 86-2252, 1986.

23. G.L. Zacharias and A.K. Caglayan, "A Visual Cueing Model for Terrain-Following Applications," *Journal of Guidance*, Vol. 8, No. 2, 1985, pp. 201-207.

24. J.A. Franklin et al., "Flight Evaluation of Augmented Controls for Approach and Landing of Powered-Lift Aircraft," *Journal of Guidance, Control, and Dynamics,* Vol. 9, No. 5, September-October 1986.

25. S. Garg, Ph.D. Thesis, School of Aeronautics and Astronautics, Purdue University, 1987.

26. Military Specification, "Flying Qualities of Piloted Airplanes," MIL-F-8785B (ASG), U.S. Air Force, Wright-Patterson Air Force Base, Ohio, 1969.

27. D. Moorehouse and B. Woodcock, "Background Information and User Guide to MIL-F-8785C Military Specification–Flying Qualities of Piloted Airplanes," AFWAL-TR-81-3109, Air Force Wright Aeronautical Laboratory, Wright-Patterson Air Force Base, Ohio, July 1982.

28. W.C. Hoffman, D.L. Kleinman, and L.R. Young, "Display/Control Requirements for Automated VTOL Aircraft," NASA CR-158905, ASI-TR-76-39, October 1976.

29. S. Garg and D.K. Schmidt, "Model-Based Analysis of Display-Dynamics Effects in Pursuit Tracking," *Proceedings 21st Annual Conference on Manual Control,* Dayton, Ohio, 1986.

30. W.H. Levison, "The Effects of Display Gain and Signal Bandwidth on Human Controller Remnant," Wright-Patterson Air Force Base, Ohio, Aerospace Medical Research Laboratory, AMRL-TR-70-93, March 1971.

31. R.E. Bailey, "Effect of Head-Up Display Dynamics on Fighter Flying Qualities," AIAA paper 86-2206, Guidance, Navigation and Control Conference, Williamsburg, Virginia, August 1986.

32. G.P. Pavassilopoulos, J.V. Medanic, and J.B. Cruz, Jr., "On the Existence of Nash Strategies and Solutions to Coupled Ricatti Equations in Linear-Quadratic Games," *Journal of Optimization Theory and Applications,* Vol. 28, No. 1, May 1979.

33. R.H. Hoh, R.H. Klein, and W.A. Johnson, "Development of an Integrated Configuration Management/Flight Director System for Piloted STOL Approaches," NASA TR-1015-4, August 1977.

34. J.A. Franklin, R.C. Innis, and G.H. Hardy, "Flight Evaluation of Stabilization and Command Augmentation System Concepts and Cockpit Displays during Approach and Landing of a Powered Lift STOL Aircraft," NASA TP-1551, 1980.

35. M.K. Sankrithi and W.F. Bryant, "7J7 Manual Flight Control Functions," AIAA Paper 87-2454, Guidance, Navigation and Control Conference, Monterey, California, August 1987.

36. J.C. Doyle, "Analysis of Feedback Systems with Structured Uncertainties," *Proceedings IEEE,* Vol. 129, Pt. D, No. 6, 1982, pp. 242-250.

37. J.C. Doyle, J.E. Wall, and G. Stein, "Performance and Robustness Analysis for Structured Uncertainty," *Proceedings 21st IEEE Conference on Decision and Control,* 1982, pp. 629-636.

38. J.C. Doyle, "Lecture Notes," 1984 ONR/Honeywell Workshop on Advances in Multivariable Control, Minneapolis, Minnesota, 1984.

39. J.C. Doyle, "Structured Uncertainty in Control System Design," *Proceedings IEEE Conference on Decision and Control,* 1985.

40. L.B. McCormack, M.J. Detroit, and D.N. See, "Improving Pilot-Vehicle Integration using Cockpit Display Dynamics," *Proceedings National Aerospace Electronics Conference,* Dayton, Ohio, pp. 530-536.

41. Lt. Mark Detroit, personal communication.

42. K. Glover, "All Optimal Hankel-Norm Approximations of Linear Multivariable Systems and Their L^{∞}-Error Bounds," *International Journal of Control,* Vol. 39, No. 6, 1984, pp. 1115-1193.

43. A. Phatak, H. Weinert, I. Segall, and C.N. Day, "Identification of a Modified Optimal Control Model for the Human Operator," *Automatica,* Vol. 12, 1976, pp. 31-41.

44. J.F. Elkind, "Characteristics of Simple Manual Control Systems," Technical Report 111, MIT Lincoln Laboratory, Lexington, Massachusetts, 1956.

45. M. Noble, P.M. Fitts, and C.E. Warren, "The Frequency Response of Skilled Subjects in a Pursuit Tracking Task," *Journal of Experimental Psychology,* Vol. 49, 1955, pp. 249-256.

APPENDIX A

ON CHOOSING OCM PILOT PARAMETERS TO MODEL COMPLEX DISPLAY INTERFACE SITUATIONS

Contents

Contents (concluded)

APPENDIX A

ON CHOOSING OCM PILOT PARAMETERS TO MODEL COMPLEX DISPLAY INTERFACE SITUATIONS

This appendix summarizes basic research in human perception and cognition relevant to the consideration of display dynamics and the pilot/display interface. Written as a stand-alone report, it is intended as a first step in the development of guidelines for representing complex pilot/display interaction phenomena in terms of the lumped parameters in the Optimal Control Model. As such, for each display, pilot and environmental factor discussed, an indication is given as to how that factor impacts OCM pilot parameters in direction and degree.

1.0 INTRODUCTION

Cockpit displays in modern aircraft play an increasingly critical role in determining the ability of the aircraft to meet mission requirements. Accordingly, display design is of crucial concern to aircraft system designers. Current efforts to improve display design focus on the development of quantitative rather than qualitative design and evaluation techniques. One such effort is the use of the optimal control model to analyze the effects of display and pilot parameters on pilot workload and overall closed-loop performance. The optimal control model has frequently been used to analyze closed-loop compensatory tracking or state regulation performance, where the goal of the operator is to minimize some observed system error (see, for example, Kleinman, Baron, and Levison, 1970).

The pilot component of the optimal control model (OCM) assumes that constraints on the pilot's performance can be described by three parameters associated with each displayed variable: his or her observation or indifference threshold, delay in observation, and observation noise. The observation threshold in the optimal control model is the minimum absolute change in a displayed variable, expressed in units of that variable, that can be detected by the pilot's perceptual system. An alternative to the observation threshold used in some implementations of

the OCM is the indifference threshold, which is the minimum change in the displayed variable that the pilot observes before the pilot's intolerance level is reached and a corrective response is made.

The observation noise parameter in the optimal control model represents the inherent randomness in human response, including random errors, variations in response characteristics, and variations in response time. Observation noise is that component of pilot response variability which is not accounted for by the remaining OCM parameters.

Finally, the OCM parameter of pilot observation delay reflects the combined delays in pilot response to a displayed variable due to sensory, perceptual, and cognitive neural processing. In other words, this delay reflects the amount of time it takes the pilot to see the displayed variable, to interpret and attach meaning to the information that is conveyed, and to reach a decision on what to do about that information.

The OCM's pilot parameters of observation or indifference threshold, observation noise, and pilot delay are based on the assumption that the pilot perceives a flawed, noisy, and delayed version of each displayed variable. Apart from these inherent constraints, pilot performance is assumed to be optimal. The purpose of this report is to attempt to explicate how the amount of this degradation, noise, and delay depends on the cockpit display design.

Unfortunately, however, the nature of the inherent pilot constraints in perceiving and interpreting displayed variables, as well as their impact of display design on pilot performance, are not well understood. That is, given a specific displayed variable, it is difficult to predict, prior to experimental measurement, its associated observation or indifference threshold, observation noise, and pilot delay. Previous applications of the optimal control model have set parameter values to those measured in a small number of studies, in which the display and task conditions were not necessarily similar to those in which the model was being applied (e.g., Levison, Baron, and Kleinman, 1969; Kleinman and Baron, 1971). To the authors' knowledge, no comprehensive studies of the relations between the variables of display design and optimal control model parameters have been undertaken.

This report will partially fill that gap by summarizing basic research in human perception and cognition to provide a framework for estimating the direction and degree to which pilot parameters in the optimal control model are affected by variations in display design, pilot, and environmental conditions. The object of this review is to show how pilot parameters in the optimal control model may be more precisely tuned to reflect the impact of particular cockpit conditions without the need for costly experimentation.

This report will be limited in scope to the following areas. This report will consider the effect of stimulus variables which are determined by display design and environmental conditions on optimal control model pilot parameters. This report will also consider the effect of some pilot variables on these model parameters. The stimulus variables to be considered include luminance, color, display location relative to the fixation point, display indicator size and shape, display clutter, layout, motion, and variability. The pilot variables which will be considered include pilot pupil size, effects of eye movements, and pilot attention to the displayed variable. These stimulus and pilot variables will be considered in terms of their effects on observation threshold and pilot delay.

The parameters of indifference threshold and observation noise will not be considered in this review because these variables are not measured in basic psychological experiments. Psychological research is geared toward discovering the absolute limits of the perceptual, cognitive, and motor systems, i.e., observation thresholds, rather than the amounts of change that are detected before the observer "decides" to respond, i.e., indifference thresholds. Moreover, psychological research is aimed at determining whether or not well-controlled variables have significant effects on observer performance, and is not concerned with how much of the observer's response variance is unaccounted for. From the perspective of the optimal control model, however, it is particularly important to accurately characterize observation noise, because this variable has a large impact on model results. At the present time, tuning of the observation noise parameter may be performed on the basis of the assumption that the stimulus and pilot variables discussed below have the same qualitative effect on observation noise as on observation delay and threshold. The discussion below may thus be used to make inferences rather than direct conclusions about the effect of relevant stimulus and pilot variables on observation noise.

The next section of this report will give a brief overview of the nature of human visual and cognitive processes. This overview is included to give both a general introduction to the problem of display interpretation and to indicate some of the theoretical sources of pilot constraints. The following sections of the report contain a summary of basic research for each of the stimulus and pilot variables considered. In these sections, the examples related to cockpit displays will be used to illustrate the implications of basic research results.

2.0 OVERVIEW OF PILOT PROCESSES

The ability of the pilot to see, interpret, and react to a cockpit display is the result of an extremely complex and poorly understood interaction between the external environment and the pilot's internal systems. Through his or her visual and cognitive processes, a pilot is able to efficiently monitor and react to complex cockpit displays. Although pilot performance in this respect is impressive, inherent constraints in vision and cognition produce limitations. This section will give a brief overview of visual and cognitive processes and their corresponding limitations.

The construction of the perceived version of a cockpit display is the result of a sequence of processing stages. In the first stage, an image of the display is formed at the back of the eye. The image of the display is centered at the direction of gaze or fixation. The imaging process is schematized in Figure A-1. Each point on the display surface either reflects or transmits light, some of which travels in the direction of the pilot's pupil. Light which passes through the pupil is focused at the cornea and lens and passes through other ocular media of the eye to form a slightly blurred, two-dimensional image of the display on the retina. Blurring of the retinal image, caused by optical imperfections of the eye in addition to light scattering, places an absolute limit on the pilot's ability to resolve fine spatial and temporal detail.

In the second stage of the perceptual process, light in the retinal image is absorbed by photoreceptors contained in the retina. These photoreceptors transform light energy into neural impulses. There are two types of photoreceptors, each mediating a functionally different mode of vision. Rods are photoreceptors which mediate night vision. They are extremely sensitive to light, and are color blind. Cones are the class of photoreceptors which mediate vision under high levels of illumination. Cones are less sensitive to light, and are responsible for color vision. Rod-mediated vision is referred to as scotopic or night-time vision; photopic or day-time vision is vision mediated by cones. Under medium illumination, both rods and cones may operate. Vision in this condition is called mesopic.

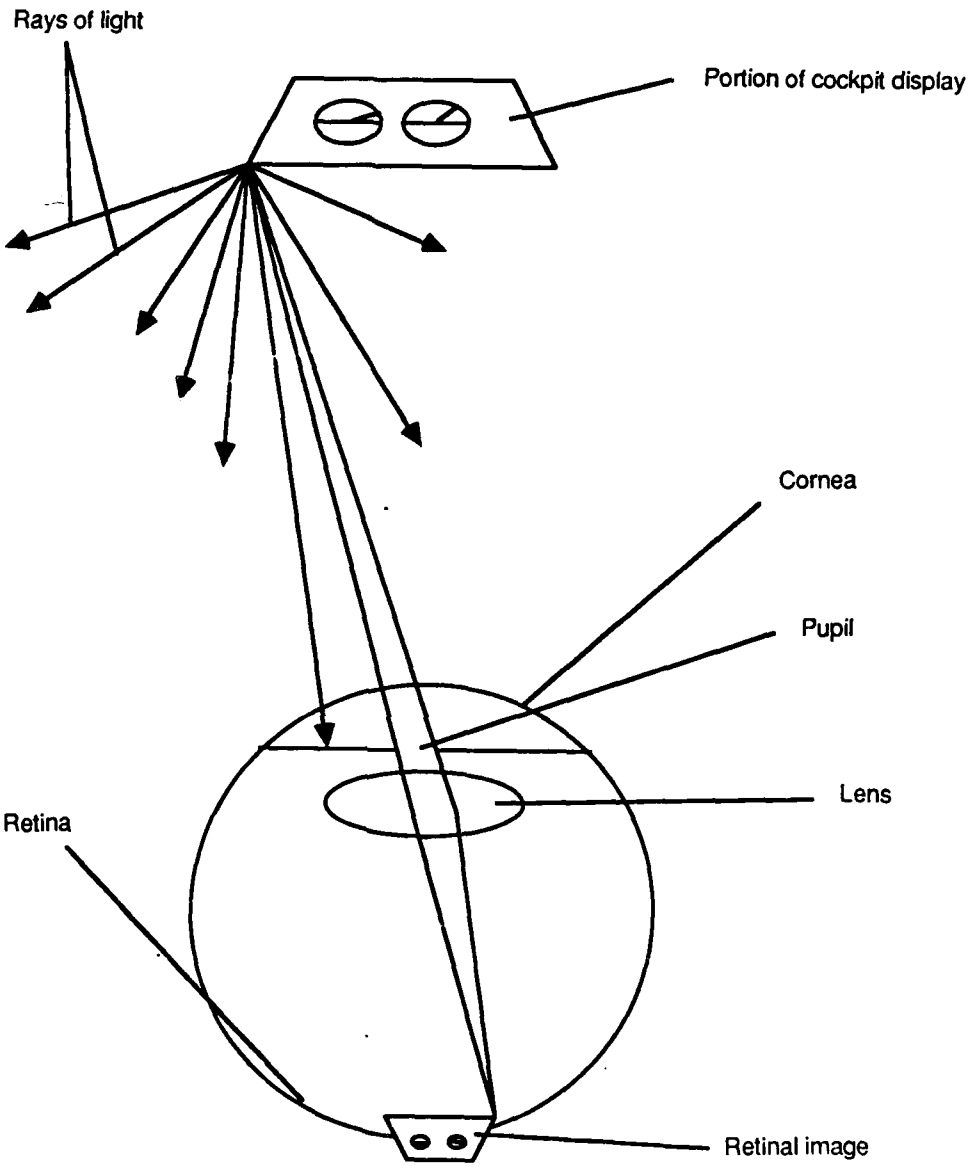

Figure A-1. Schematic Diagram of the Process by which the Cockpit Display Is Imaged onto the Retina of the Eye

The ability of the visual system to respond to information in the retinal image is limited by the absolute sensitivity of the rods and cones to the presence of light. Photopic and scotopic sensitivity depends largely on the average level of luminance in the visual field, as well as on the color or wavelength of the light. The average level of display luminance determines the stage of photoreceptor adaptation. Photoreceptors are maximally sensitive to light under conditions of low average luminance, and their sensitivity decreases monotonically with increases in background luminance. The process of adaptation allows the photoreceptors to respond to a large range of luminance information over time. However, at any one time the range of luminance information to which photoreceptors can respond is relatively small. As a result, larger absolute differences in luminance between the display background and a critical display element are required for detection at high background luminances than at low background luminances.

In addition to background luminance, photoreceptor sensitivity depends on the wavelength composition of light in the retinal image. Photoreceptors are not equally sensitive to all wavelengths of light, as diagrammed in Figure A-2 for scotopic and photopic vision. The region of spectral sensitivity is from about 400 to 750 nm, with peak scotopic and photopic sensitivities at about 555 and 505 nm, respectively. As a result of the variation in photoreceptor sensitivity as a function of stimulus wavelength, some display colors are detected more easily or are perceived as brighter than other display colors which have the same luminance.

Another limitation of pilot vision at the photoreceptor stage results from the distribution of photoreceptors across the retina. Rods and cones have quite different distributions, as can be seen from Figure A-3. The retina contains about 120 million rods, compared to only 7 million cones. Most of the cones are concentrated at the fovea, which is the intersection of the retina with the line of sight. The fovea is the region of the retina which processes information in the area of the display which is being fixated, or "looked at." The size of the region of the cockpit display which can be processed by the fovea at any one time is circular, with a radius of only two degrees visual angle (see Figure A-4). Due to the high concentration of cones in the fovea, vision at the region of fixation is characterized by a high degree of spatial resolution and good color vision.

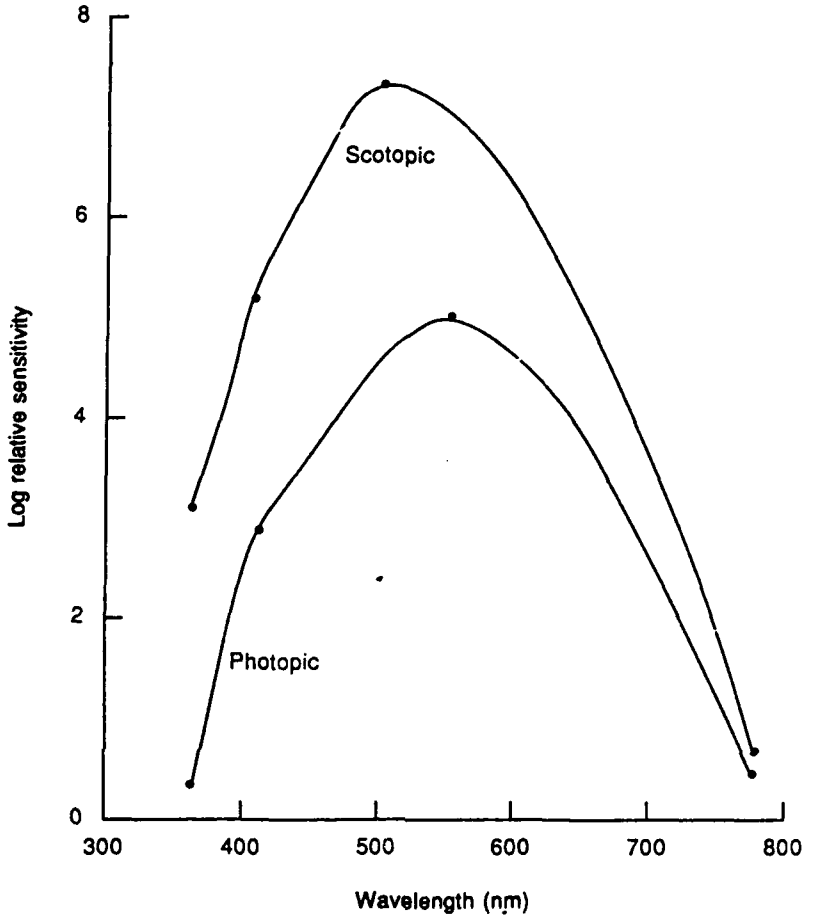

Figure A-2. Photopic (cone) and Scotopic (rod) Sensitivity to Light as a Function of Wavelength

Away from the fovea, the density of cones falls off rapidly, with very few cones present beyond 10 degrees into the periphery of the retina. However, the density of rods is much higher in the periphery than in the fovea. From no rods at the center of the fovea, density increases to about 16 degrees on both sides of the fovea, with density slowly decreasing from 16 degrees out to the edge of the retina at about 100 degrees. Due to the sparse photoreceptor distribution in the periphery of the eye, vision away from the point of fixation is characterized by increasingly poor

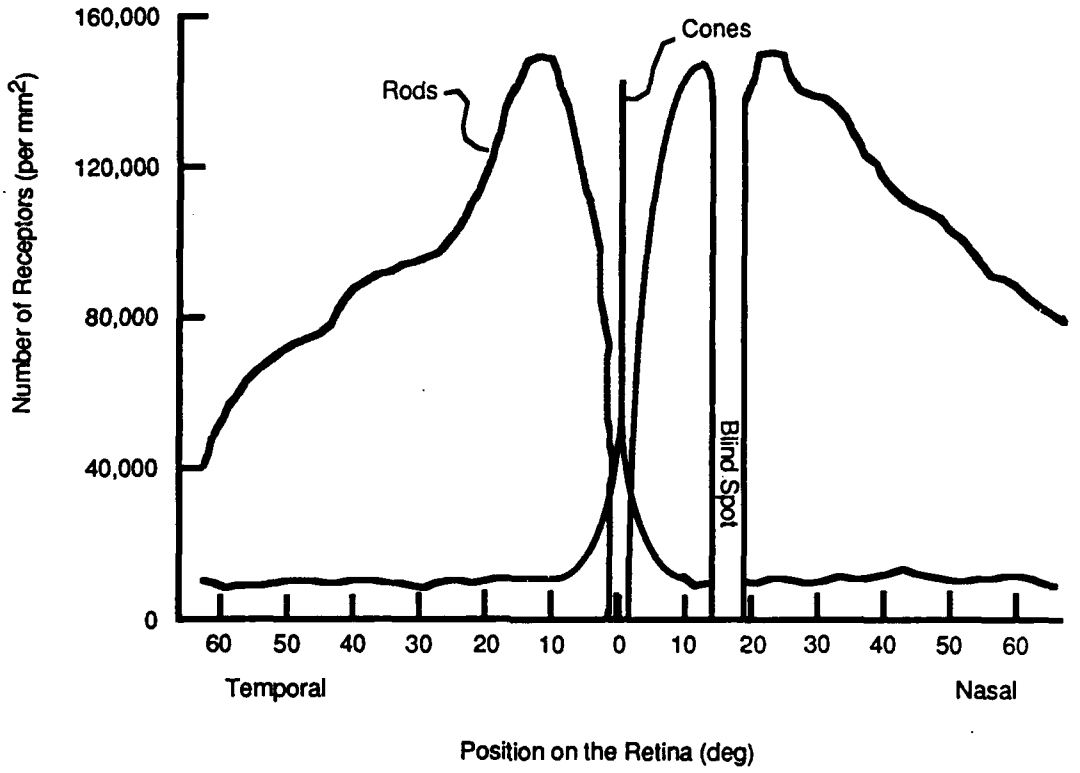

Figure A-3. Distribution of Rods and Cones across the Horizontal Meridian of the Retina

spatial resolution and color vision, but a relatively high sensitivity to the presence of light under conditions of low illumination. Loss of spatial acuity and color vision for portions of the display away from the point of fixation constitutes a major limitation in the ability to monitor cockpit displays.

To compensate for the concentration of visual resources in the small region of the visual field that is fixated, eye movements are used to change the point of fixation around the visual field. Through this mechanism, the entire visual field may be processed in fine detail over a period of time. The major limitation associated with eye movements is the amount of time they take to initiate and complete. A second limitation associated with eye movements is saccadic

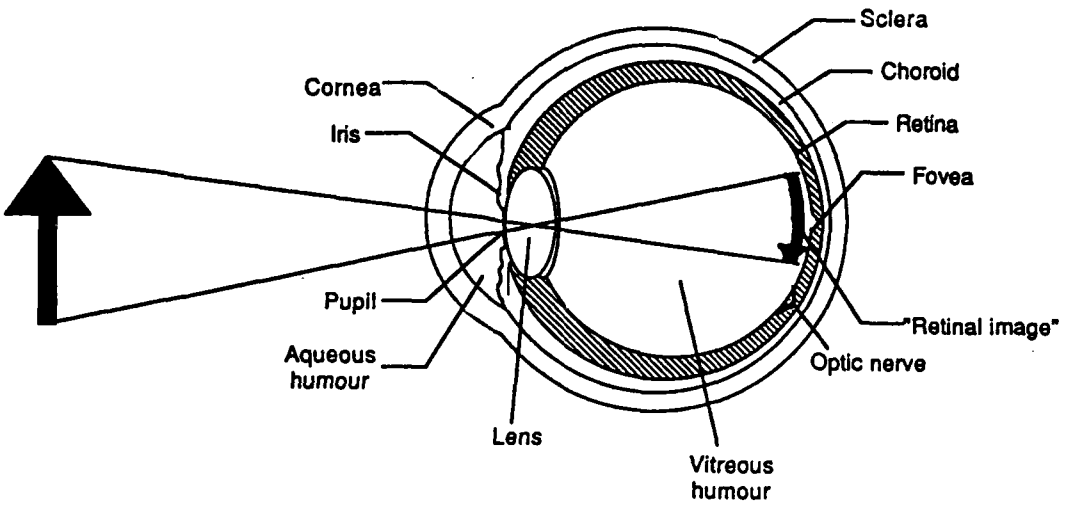

Figure A-4. Schematic Drawing of the Eye (arrow imaged onto the fovea) (The visual angle subtended by the fovea of the eye is approximately 2 deg in diameter. The visual angle subtended by an object of height, h, and at distance, d, is equal to $\tan^{-1}$ (h/d).)

suppression. Saccadic suppression refers to a phenomena associated with saccadic eye movements in which visual sensitivity decreases significantly prior to and during a saccade. A saccadic eye movement, or saccade, is the fast, jerky eye movement used to quickly change thelocation of the point of fixation to different parts of a display.

Before light information in the retinal image is transformed into a perceived visual scene, it goes through several stages of neural analysis, from the photoreceptors and other layers in the retina to regions in the cerebral cortex and midbrain. The result of this neural analysis is the perception of a cockpit display along the dimensions of spatial layout, brightness, color, depth, and motion.

One important constraint associated with this neural processing is the presence of a limit on the amount of information that can be processed at one time. Moreover, the visual system is limited in its ability to filter the desired subset of the information for further processing. In general, the more cluttered the display, the more difficult it is to extract a specific subset of information.

This is evident in two respects. First, the more cluttered the visual field, the more difficult it is for the pilot to locate or fixate on the display region of interest. Second, even when the pilot is fixated on the desired display location, he or she is slower and less accurate in responding to that information in the presence of surrounding information. Both the difficulty in locating and in responding to a subset of information in the visual field depends on the visual similarity of that information to surrounding information, the proximity of surrounding information, and the amount of surrounding information in the display. All of these clutter factors are pertinent to display design.

Ease of interpretation of a cockpit display depends not only on the ability of the pilot to extract the relevant information, but on the degree of cognitive processing that is required to respond to that information. The pilot's perceptual tasks may be classified according to whether they require information detection, discrimination, or recognition. The simplest visual task to perform is detection, where the pilot decides simply whether or not any visual stimulus is present. An example of a monitoring task performed on the basis of stimulus detection is one in which the pilot must make a response in the presence of a blinking light, and no response when the light is not blinking. A discrimination task is somewhat more difficult, and is one in which the observer must decide whether a stimulus that has been detected is the same or different from another stimulus which may or may not be present. An example of a discrimination task is one in which the pilot must decide whether a detected gap between the horizon and aircraft symbols on an attitude indicator are formed by the presence of the aircraft symbol above or below the horizon symbol. In a recognition task, the observer must not only detect information and be able to discriminate it from other information, but must also be able to identify or give meaning to that information through the use of memory. For example, memorial processes are required to recognize or identify numeric symbology on a HUD.

In the following sections, stimulus variables associated with display design and environmental conditions will be discussed in terms of the impact they have on the efficiency of pilot performance. In particular, the effects of these variables will be discussed in relation to the optimal control model parameters of observation threshold and pilot delay. Distinctions will be made between four different types of observation thresholds which are defined by the pilot's monitoring task.

The term observation threshold in the pilot model of the OCM is misleading, in that it implies that there is a single type of threshold that determines whether or not a change in a displayed variable can be seen. In fact, the psychological literature distinguishes between several types of thresholds, depending on the observer's task. In the reviews to follow, the impact of display, environmental, and pilot conditions will be considered in terms of four different types of observation thresholds: the incremental threshold, the acuity threshold, the displacement threshold, and the rate threshold. To determine the appropriate value of the observation threshold for an optimal control model application, it is necessary not only to consider the display, environmental, and pilot variables, but also to determine which type of observation threshold limits pilot performance. The type of observation threshold of interest depends on the pilot's task.

If the pilot's task is to detect a change in display luminance, then his or her performance is constrained by the incremental threshold. The incremental threshold is defined as the minimum change in luminance that can be detected. In a cockpit display, the incremental threshold is the minimum difference between the luminance of a display element and the surrounding display luminance that must be present before the display element can be seen. The incremental threshold is relevant for modeling purposes when the pilot's performance is limited by his or her ability to see elements of the display. This threshold may be relevant, for instance, when a pilot is monitoring HUD symbology overlayed on a bright, out-of-cockpit scene, or when the interior displays are brightly illuminated by the sun or other sources of glare.

If the pilot's task is to detect or discriminate fine spatial detail in a region of the display, then the pilot's performance is constrained by his or her acuity threshold. The acuity threshold is defined as the reciprocal of the minimum visual angle in minutes that can be resolved (see Figure A-5). High visual acuity is required to discriminate among stimuli which differ in spatial detail, such as in the discrimination of alphanumeric characters or the detection of a gap between two solid lines. In monitoring a cockpit display, a frequent visual acuity task is detection of indicator displacement. Visual acuity also plays a role in other cockpit monitoring tasks, such as in correctly identifying symbology.

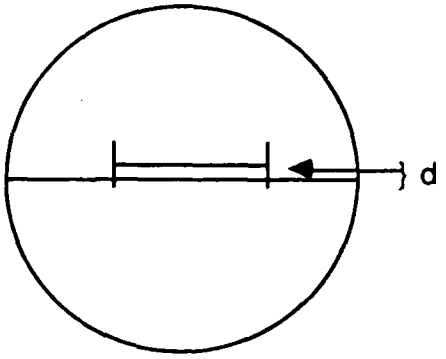

Figure A-5. Visual Acuity (Visual acuity is the reciprocal of the minimum gap, d, that can be detected, where d is measured in minutes of visual angle (1 degree = 60 minutes). For example, if the minimum discriminable gap is one minute of visual angle, then visual acuity = 1.0.)

When the pilot's task is to resolve fine spatial differences between elements that are moving relative to each other, as opposed to elements which remain fixed in relation to each other, the observation threshold in question is the displacement threshold. The displacement threshold is defined as the minimum discriminable extent of movement. The value of the displacement threshold is always equal to or better than the value of the acuity threshold. That is, the ability to detect a gap is at least as good when the elements forming the gap are in relative motion than when they are stationary. That is because the presence of motion provides a second cue to the presence of a gap in addition to the spatial distance between the elements. Pilot's are frequently tasked with the detection of indicator displacements when monitoring cockpit displays, such as the detection of a gap between the aircraft and the horizon symbols in a pitch tracking task.

If the pilot's task is not only to determine the position or makeup of a display indicator, but to determine the velocity of indicator movement, then the observation threshold which constrains his or her performance is the rate threshold. The rate threshold is defined as the minimum rate of movement that can be detected.

3.0 LUMINANCE

Luminance has a major impact on the speed and accuracy with which a pilot perceives a cockpit display. There are several aspects of display luminance to consider. The first aspect to consider is the luminance of the display indicator that is monitored by the pilot. As a general rule, the brighter the indicator, the faster and more accurately it is perceived. The luminance of the background of the display surrounding the indicator also affects pilot performance. Background luminance is the second aspect of display luminance to be considered. As a general rule, the lower the background luminance, the better the display indicator is perceived. The ratio of the luminance of a display indicator and its background defines the indicator's luminance contrast. In general, it is not absolute brightness of the display indicator or of the background that determines the pilot's speed and accuracy of interpretation, but the ratio of these luminances. For that reason, effects of luminance on observation thresholds and delays are frequently reported in terms of indicator or stimulus contrast.

A third aspect of display luminance is external illumination. Bright sources of light in the environment, such as the sun or a laser flash, can significantly increase the luminance of the cockpit display. Light from external sources increases the luminance of both the display indicator monitored by the pilot as well as the background luminance. Thus, environmental illuminance degrades pilot performance by decreasing display indicator contrast.

Luminance is defined as the intensity of light which is reflected from a surface. Luminance is distinguished from illuminance, the intensity of light that impinges on a surface, or the intensity of a light source, and reflectance, which is the proportion of illuminance which is absorbed by a surface. The typical units of luminance include the millilambert (mL), footlambert (ftL), and candles per square meter (c/m2) [1 mL = 0.929 ftL = 3.182 cm2]. Figure A-6 lists typical visual stimuli over the normal range of brightnesses and their corresponding luminances.

The following subsections report on the relation between display luminance contrast or display luminance and pilot observation thresholds and observation delay.

Visual stimulus	Luminance (mL)	
Sun's surface at noon	10^{10}	Damaging
	10^{9}	
	10^{8}	
Tungsten filament	10^{7}	
	10^{6}	
	10^{5}	
White paper in sunlight	10^{4}	Photopic
	10^{3}	
	10^{2}	
Comfortable reading	10	
	1	Mesopic
	10^{-1}	
White paper in moonlight	10^{-2}	
	10^{-3}	Scotopic
White paper in starlight	10^{-4}	
	10^{-5}	
Lowest amount of light that can be detected	10^{-6}	

Figure A-6. Luminance Values for Common Levels of Brightness (based on Riggs, 1965)

3.1 EFFECT OF LUMINANCE ON OBSERVATION THRESHOLDS

Display luminance, or indicator contrast, has a significant effect on all four types of observation thresholds.

3.1.1 Incremental Threshold

As is true for all psychological parameters, the incremental threshold is not a constant, but varies as a function of stimulus conditions. Display luminance is one stimulus variable that determines the value of the incremental threshold, i.e., the minimum change in luminance that is required before a target can be seen against its background.

The incremental threshold is highly dependent on the background display luminance; the higher the luminance the greater the increase (or decrease) in indicator luminance required for indicator detection. It is convenient to express the incremental threshold in terms of the contrast required for indicator detection. The contrast is defined in terms of the Weber ratio, $\Delta L/L$, where L is the background luminance and ΔL is the increase in luminance required for indicator detection. Figure A-7 shows the relation between the incremental threshold, plotted as a Weber ratio, and background luminance (based on Konig and Brodhun, 1889, reported by Hecht, 1934). At low luminance levels, less than -1 log mL, the Weber ratio for the incremental threshold decreases at an accelerating rate with increasing background luminance. However, at photopic luminance levels, i.e., greater than 0 log mL, the Weber ratio is approximately a constant whose value is less than 0.1. Thus at luminance levels equivalent to those obtained under daylight conditions, the eyes are extremely sensitive to the presence of light. Under these conditions a change in luminance of less than 1 percent of the background luminance can be detected.

According to the above results, for relatively bright displays, the ability to detect an indicator which differs in luminance from its background by some constant will generally not limit the pilot's ability to monitor that display, as long as the luminance difference between the display indicator and background is greater than 1 percent. However, the ratio between indicator and background luminance may be reduced below threshold in the presence of strong external illumination. Under dim cockpit conditions, the ratio of indicator and background luminances must be greater than 1 percent to be above threshold.

3.1.2 Acuity Threshold

Visual acuity refers to the ability to resolve fine spatial detail within a detected object. The visual acuity threshold, like the incremental threshold, is greatly dependent on the luminance of the object to be resolved. The dependence of the visual acuity threshold on luminance derives from the fact that in order to resolve fine spatial detail, that detail must first be seen.

The relationship between the visual acuity threshold and luminance has been the subject of considerable research. Representative data are shown in Figure A-8 (based on Hecht, 1934). In this figure, visual acuity is shown as a function of luminance measured in trolands. A troland is

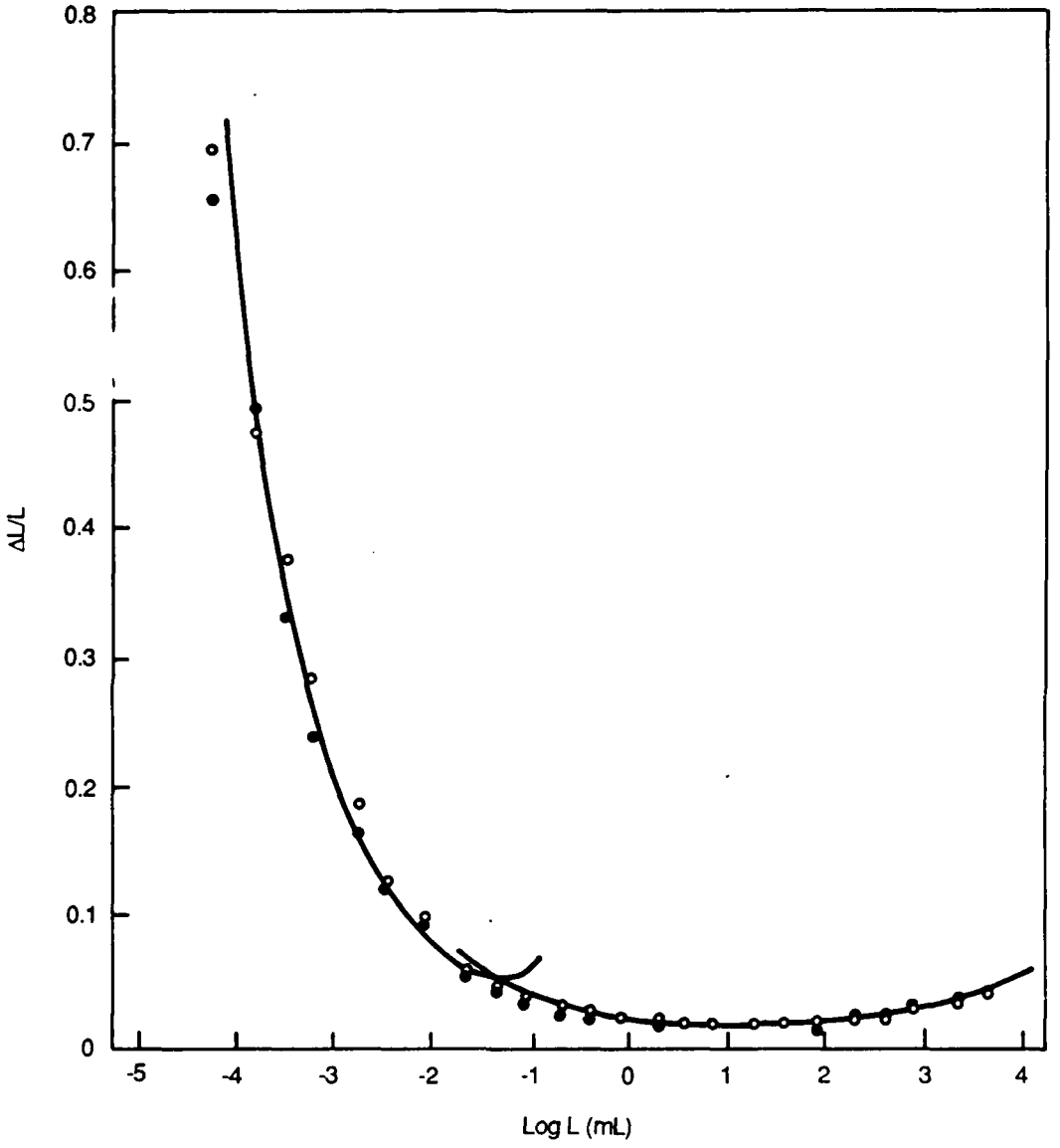

Figure A-7. Relation between Incremental Threshold and Background Luminance (based on Konig and Brodhun, 1889, reported in Hecht, 1934)

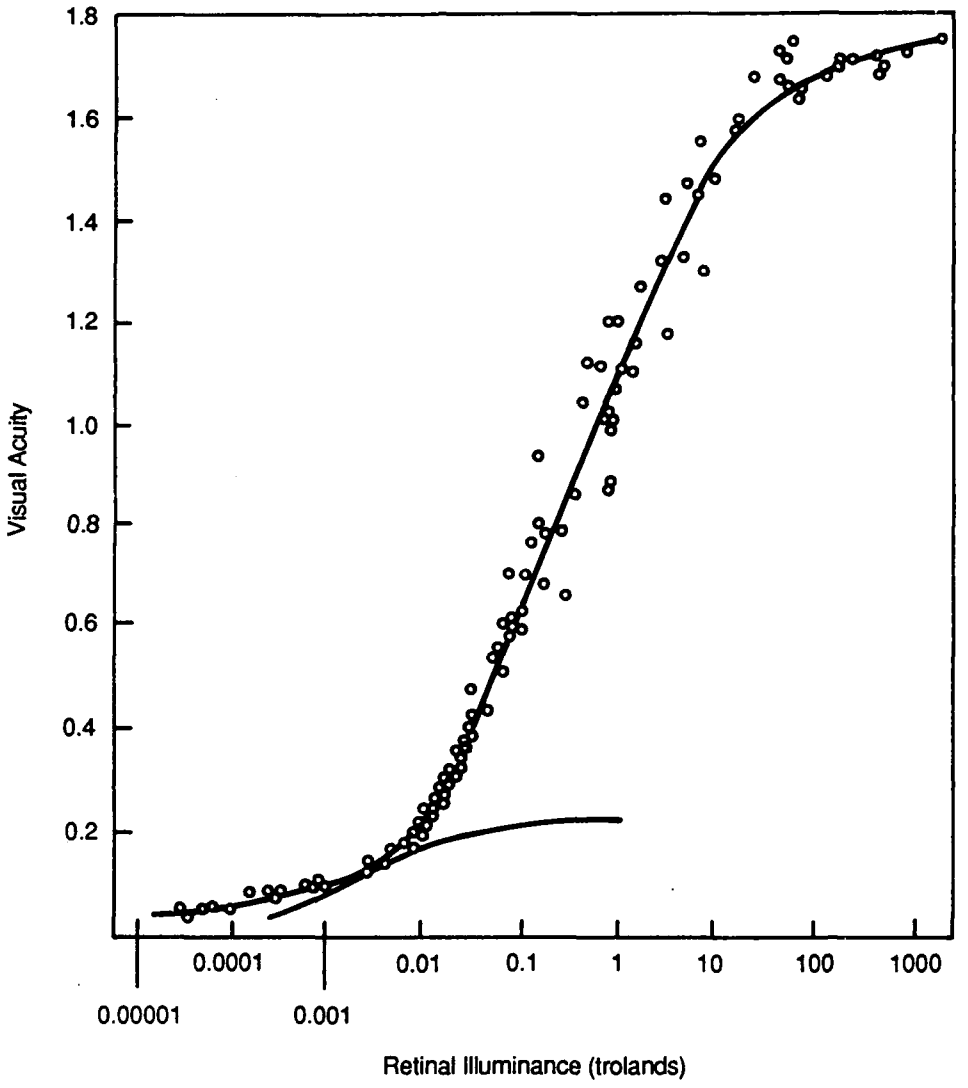

Figure A-8. Relation between Visual Acuity and Luminance (based on Hecht, 1934)

the unit used to express the amount of light that illuminates the retina. The troland is computed by taking the product of the stimulus luminance, measured in units of candles per square meter, and the pupil area, in units of square millimeters. These data were collected under near-optimal conditions to obtain the best possible visual acuity. At high luminances, under bright photopic conditions, visual acuity approaches 1.8, corresponding to resolutions of around 50 seconds of

visual angle. Over a wide, intermediate range of luminances of -2 to 2 log mL, visual acuity increases linearly with log luminance. At luminances less than -2 log mL, visual acuity approaches zero.

According to these results, visual acuity varies considerably as a function of display luminance. Because visual acuity is so high under optimal conditions, however, the visual acuity threshold will generally not limit pilot performance, even under medium-level luminances. On the other hand, many pilot monitoring tasks do require fine spatial resolution, such as the identification of alphanumeric characters. When display luminance may vary, it is important to consider the possibility that critical display regions may at times be too dim or have too low of a contrast for accurate spatial resolution.

3.1.3 Displacement Threshold

The displacement threshold is defined as the minimum extent of movement that can be detected. This section considers the effects of luminance on the displacement threshold. Because the displacement and acuity thresholds are very similar in definition, it may be assumed that luminance has the same effect on the displacement threshold as on the acuity threshold. The question of interest is whether or when the displacement threshold is less than, i.e., better than, the acuity threshold.

Gordon (1947) found that displacement and acuity thresholds are similar under scotopic or low levels of illumination. However, under photopic or daylight levels of illumination, displacement thresholds have been found to be on the order of 20 seconds of visual angle (Basler, 1906), a value that is considerably less than the corresponding visual acuity threshold. On the basis of these results it may be assumed that displacement thresholds are generally lower than acuity thresholds, at least when luminance is relatively high, but that the displacement threshold shows the same pattern of change with respect to luminance as the visual acuity threshold.

Based on this assumption, it may be assumed that the observation threshold for detection of a gap in a moving indicator is superior to the observation threshold for detection of spatial differences among nonmoving display elements, but only for relatively bright displays.

3.1.4 Rate Threshold

The rate thresholds are affected by display luminance in the same way as the other types of thresholds; in general, brighter displays produce lower rate thresholds. Thus, for example, perception of the velocity of an attitude indicator is generally faster when the luminance of that indicator is increased.

Leibowitz (1955) measured the relationship between the rate threshold and luminance for various exposure durations; these data are summarized in Figure A-9. These data illustrate that for a constant duration of exposure, the rate threshold decreases, i.e., improves, with increasing luminance. The decrease in threshold is rapid at low luminances and slows until an asymptote is reached at high luminances. The value of the rate threshold at high luminances depends on the duration of exposure. For exposures greater than 1 second, optimal rate thresholds are less than 1 minute of arc/second. Following an 1/8-second exposure, the shortest duration investigated, the optimal threshold was approximately 4 minutes of visual angle per second.

3.2 EFFECTS OF LUMINANCE ON PILOT OBSERVATION DELAY

Observation delay also is affected by the luminance of the display; in general, displays are processed more rapidly when luminance is increased.

A large amount of data regarding the effect of luminance on perceptual delay was presented by Roufs (1963). These experiments measured the time taken by observers to perceive the presentation of small white stimuli presented foveally in a otherwise dark stimulus field. The relation between stimulus luminance and perceptual delay fit a common equation for luminances of 10 to 1000 trolands: $D = t - to = -T \log E/Eo$. In this equation, D is the delay associated with the perception of and reaction to the stimulus, t and to are the perceptual delays for stimuli having intensities of E and Eo trolands, and T is a constant of 10 milliseconds. Thus the difference in response times to stimuli having two different luminances, is a linear function of the log ratio of their luminances, such that the brightest stimuli in these experiments were observed about 50 msec faster than the dimmest stimuli.

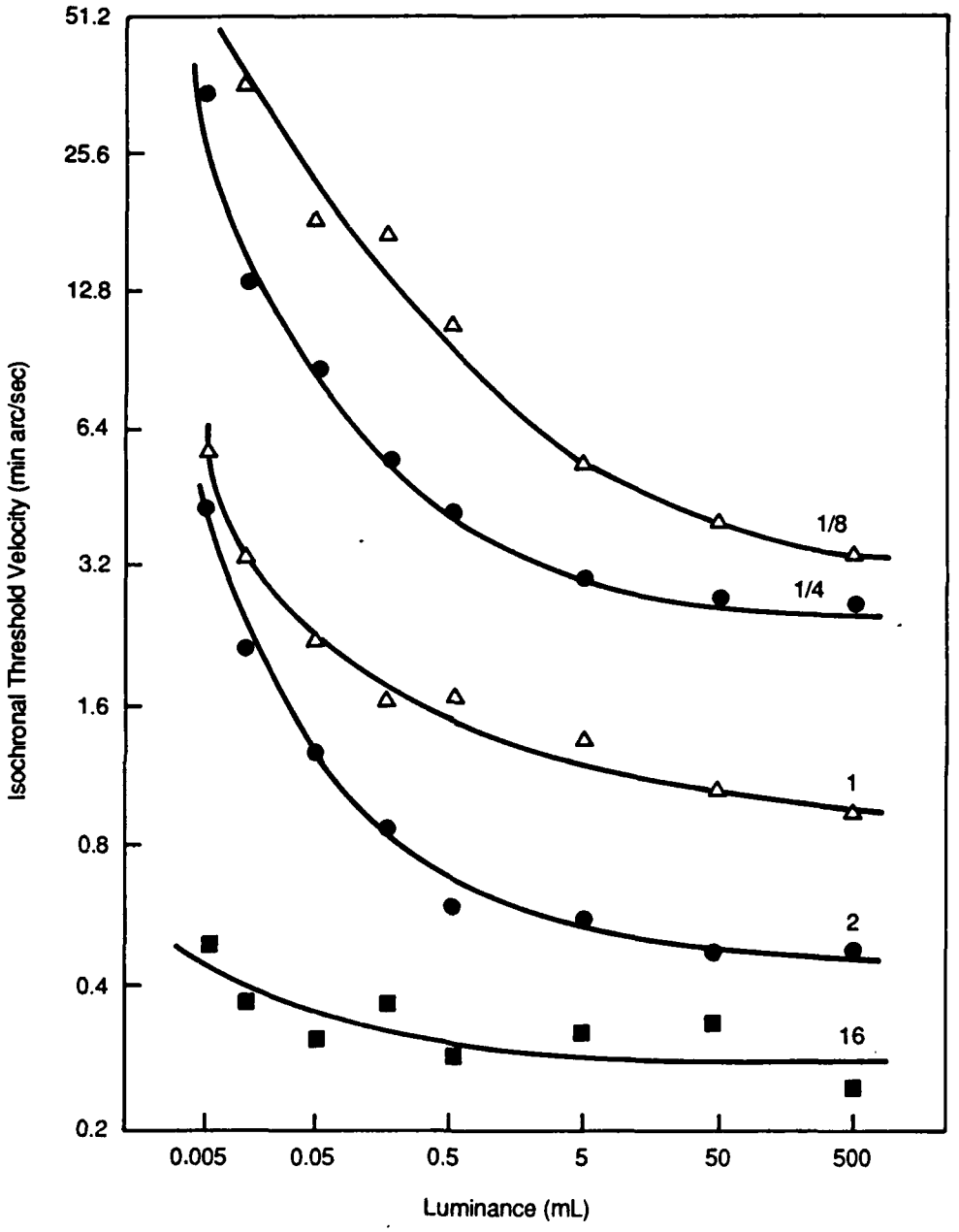

Figure A-9. Relation between the Rate Threshold and Background Luminance for Various Exposure Durations (based on Leibowitz, 1955)

It appears that observation delay depends on the luminance of the portion of the display which is being monitored, but only to a small extent on the display background. Wilson and Lit (1971) empirically investigated the effect of surrounding, background luminance on the time taken to respond to a target stimulus. They found the effect of background luminance on response time was of minor importance compared to the effect of target luminance.

From these data it may be concluded that the brightness of the monitored display indicator, but not overall display brightness, influences the speed with which pilots process the displayed information. Over a considerable range of luminances, the greater the luminance of the display indicator, the faster the pilot will respond.

4.0 COLOR

As noted above, the photoreceptors of the eye are not equally sensitive to all wavelengths of light. The wavelength composition of a display indicator determines its perceived color. The result of the wavelength dependence of photon absorption is that the effective luminance of light varies for display indicators having equal luminances but different colors. The wavelength composition of the display thus affects the minimum luminance required for stimulus detection, i.e., the observation threshold, and the time taken to perceive the stimulus, i.e., observation delay.

4.1 EFFECT OF COLOR ON OBSERVATION THRESHOLDS

Because the visual system is not equally sensitive to all wavelengths of light, the observation threshold associated with a display indicator depends on its color. The observation threshold will depend directly on the sensitivity of the eye to the wavelengths associated with the display indicator. This was verified by Wald (1945), who measured the luminance required to detect a small circular patch centered either in the fovea or 8 degrees in the periphery of the eye for several stimulus wavelengths. The obtained observation thresholds parallcled the known spectral sensitivity of the eye as a function of wavelength, shown in Figure A-2.

The relationship between observation threshold and stimulus wavelength, observed by Wald (1945), is shown in Figure A-10. Observation thresholds are plotted in terms of log units of light energy relative to the optimal threshold obtained from the most readily absorbed wavelength presented in the fovea. The results are plotted in terms of light sensitivity, defined as the reciprocal of the observation threshold. The relationship is inverse-U-shaped, with a peak sensitivity at 500 nm for peripheral viewing, and at about 560 nm for foveal viewing. Note that, in general, less luminance is required to detect a stimulus presented at the periphery of the eye than in the fovea, due to the fact that rods are more sensitive to the presence of light than cones. However, the difference between foveal and peripheral sensitivity is minimal at long wavelengths.

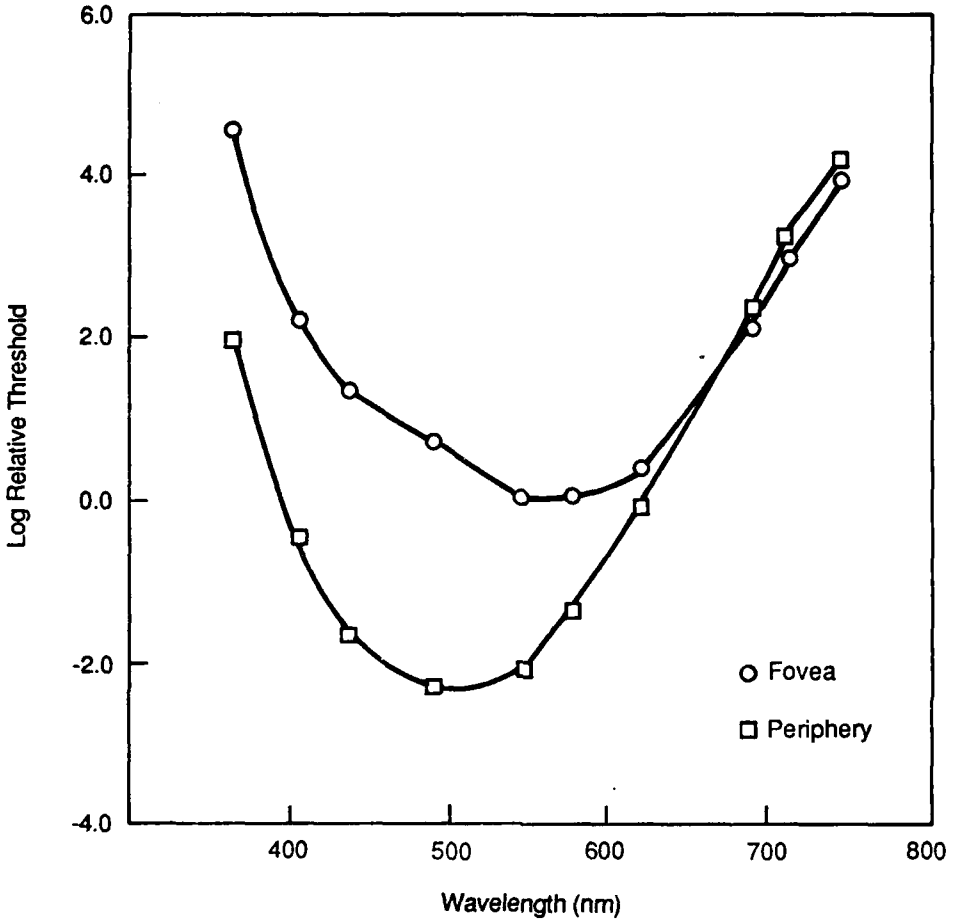

Figure A-10. Changes in the Absolute Sensitivity of the Eye as a Function of Stimulus Wavelength and Foveal versus Peripheral View (based on Wald, 1945)

These data show the relative differences in observation thresholds for light of various wavelengths presented in the fovea and periphery. However, the task used by Wald (1945) to obtain these results was an absolute detection task, where the dependent variable was the minimum energy required to detect the presence of a stimulus in an otherwise dark field. This task is not representative of a pilot's responsibilities in monitoring a cockpit display. Nonetheless, these data may be used directly to infer the effects of wavelength composition on

incremental, acuity, displacement, and rate thresholds. All of these thresholds depend directly on the amount of light absorbed by the photoreceptors of the eye, which in turn is dependent on stimulus wavelength. All types of observation thresholds will be highest for display indicators whose wavelength compositions correspond to the region of peak photoreceptor sensitivity.

4.2 EFFECT OF COLOR ON OBSERVATION DELAY

The wavelength composition of a display indicator influences to some extent the speed at which that indicator is processed. Wavelengths to which the photoreceptors are less sensitive produce longer observation delays than wavelengths in the region of high photoreceptor sensitivity. For example, a blue indicator is processed slightly more slowly than a green indicator when both indicators have the same luminance.

Observation delays associated with nonwhite display indicators may be determined from the equation of Roufs (1963), described above, multiplied by a luminance efficiency coefficient to account for the effective luminance of the indicator wavelength. According to Roufs' (1963) formulation, the relation between stimulus luminances and relative perceptual delays may be described by a simple logarithmic function of the display indicator luminances. Luminance efficiency coefficients as a function of wavelength are shown in Figure A-11 (based on Wagner and Boynton, 1972). These coefficients represent the amount of light which is actually absorbed by the photoreceptors relative to the most optimal wavelength.

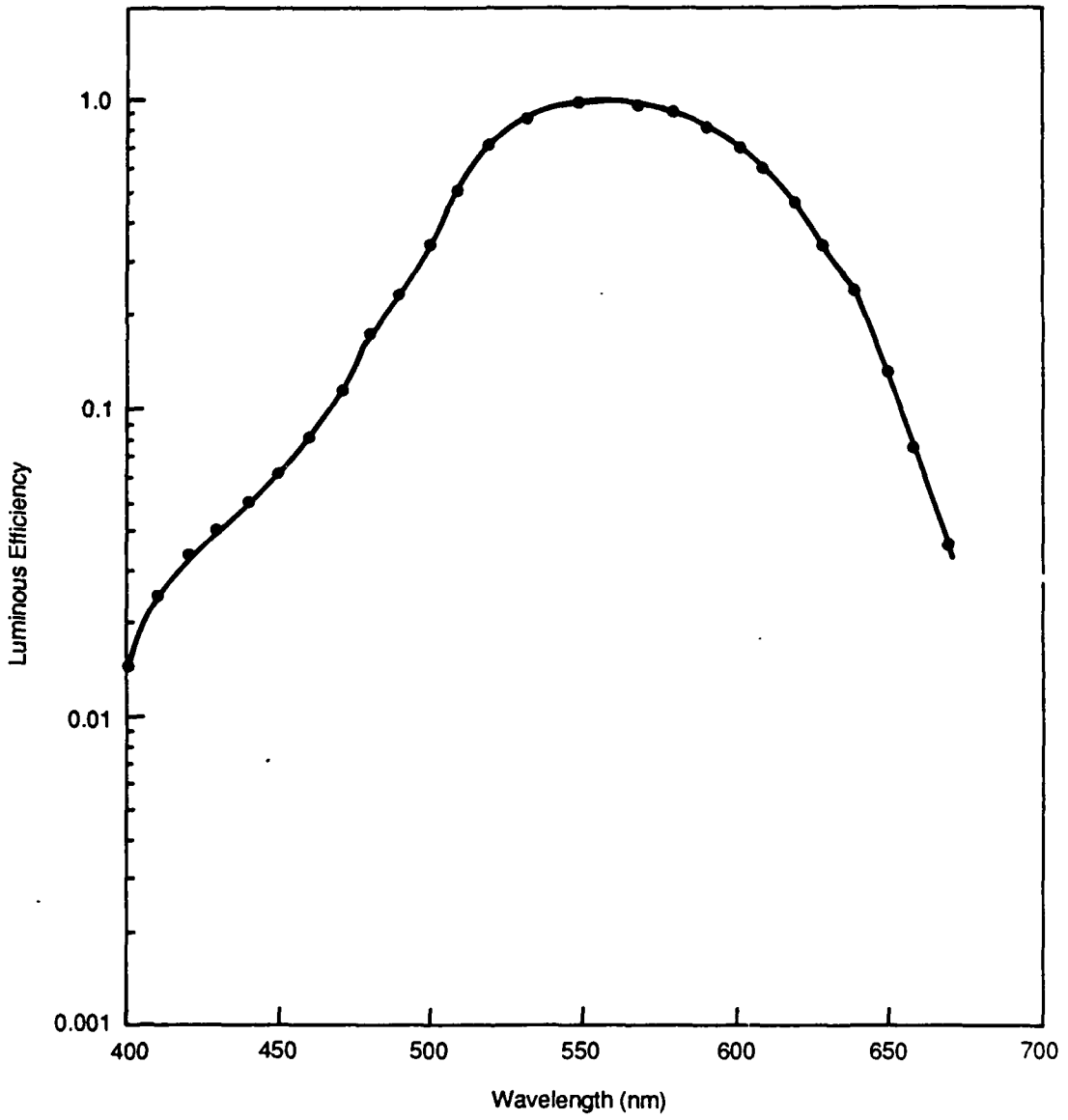

Figure A-11. Luminance Efficiency Coefficients as a Function of Wavelength (based on Wagner and Boynton, 1972)

5.0 ANGLE OF VIEW

The region of the retina in which a display indicator is processed has a large effect on the pilot's level of performance. As discussed above, and as shown in Figure A-3, different regions of the retina have quite different photoreceptor compositions. The fovea and the periphery of the retina also differ greatly in their types and degrees of subsequent neural processing. Although the fovea may yield the best observation thresholds and fastest response times, it is frequently the case that a pilot must look away from a monitored display indicator to perform another task. This section will describe the effect of moving the point of fixation away from the monitored indicator on the corresponding observation threshold and delay.

5.1 EFFECT OF VIEWING ANGLE ON OBSERVATION THRESHOLDS

All four types of thresholds to be discussed are lower when the display indicator is fixated than when seen through peripheral vision. The magnitude of the effect of retinal location on observation threshold, however, depends on the type of observation threshold that is required. Because rods are more sensitive to the presence of light than cones, absolute sensitivity of light is greater in the periphery of the eye than in the fovea. Nonetheless, the incremental threshold, or the ability to detect a change in luminance is better in the fovea of the eye than in the fovea. And because foveal processing is associated with much greater spatial resolution than peripheral processing, acuity, displacement, and rate thresholds are much better at than away from the point of fixation.

5.1.1 Incremental Threshold

The incremental threshold is defined as the minimum change in luminance required for stimulus detection. In the absence of background luminance, the incremental threshold is higher in the periphery of the eye than in the fovea. Changes in the absolute threshold as a function of angle of view are shown in Figure A-12 (based on Crozier and Holway, 1939). In this figure, DIo is defined as the smallest increase in luminance that can be detected against a constant dark background. In Crozier and Holway's experiments, the stimuli for detection were brief, 200 msec, flashes of 4.8 minutes visual angle in size.

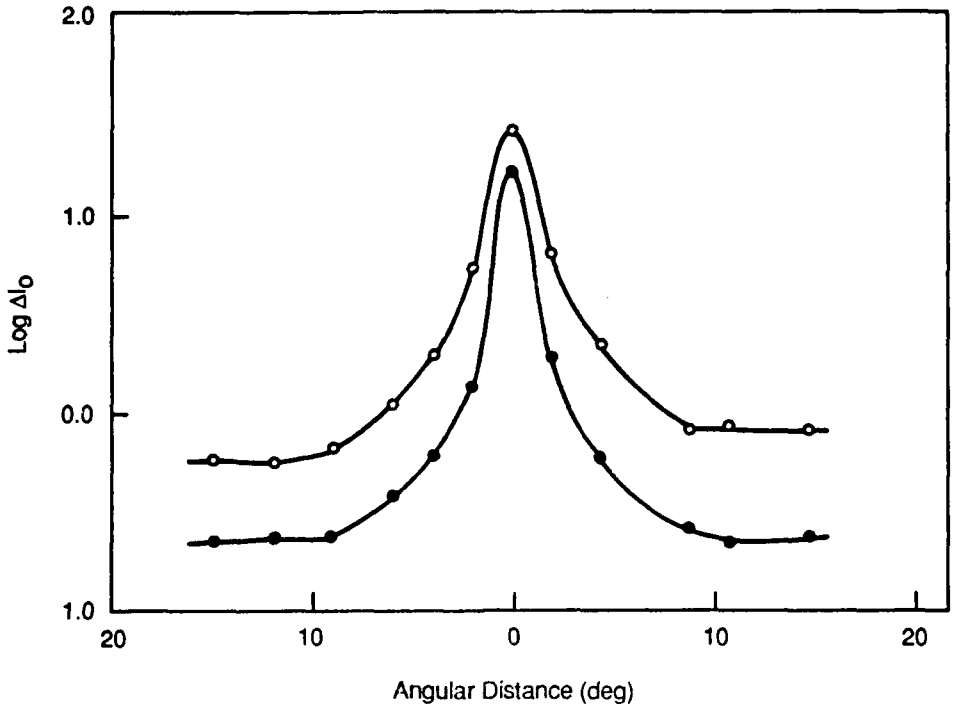

Figure A-12. Changes in the Absolute Threshold as a Function of Angle of View (based on Crozier and Hoiway, 1939)

However, in cockpit situations, the average level of luminance in the field of view is relatively high. Under these conditions, the incremental threshold is lowest in the fovea. Sloan (1961) measured incremental thresholds at various retinal distances, for stimuli of various sizes. The rate of increase in the luminance threshold was found to be more rapid for small objects than for large objects. Large stimuli showed only a moderate increase in the incremental threshold from 20 to 50 away from the fovea, whereas small stimuli showed a large increase. These data show that the detectability of indicators decreases monotonically with increases in the angle of view. Moreover, small indicators are more difficult to see from a peripheral angle of view than large indicators.

5.1.2 Acuity Threshold

The region of the retina in which processing occurs has a major impact on the amount of spatial detail that is resolved. Much greater spatial detail is seen at the point of fixation than at regions

in the visual periphery. The significant effect of retinal region on visual acuity is related directly to the spatial distribution of the photoreceptors, as reviewed earlier. Visual acuity is limited largely by the distribution of cones, which are highly concentrated in the center of the fovea, and drop off rapidly with distance into the periphery. Relative visual acuities at various short distances from the center of the fovea are shown in Figure A-13 (based on Jones and Higgins, 1947). From a relative acuity of 100 percent at the center of the fovea, visual acuity drops off rapidly to only 40 percent at one degree visual angle away.

Visual acuity data from Sloan (1968) over a larger range of viewing angles and for a range of display luminances is shown in Figure A-14. At very low luminances, i.e., less than -1 log mL,

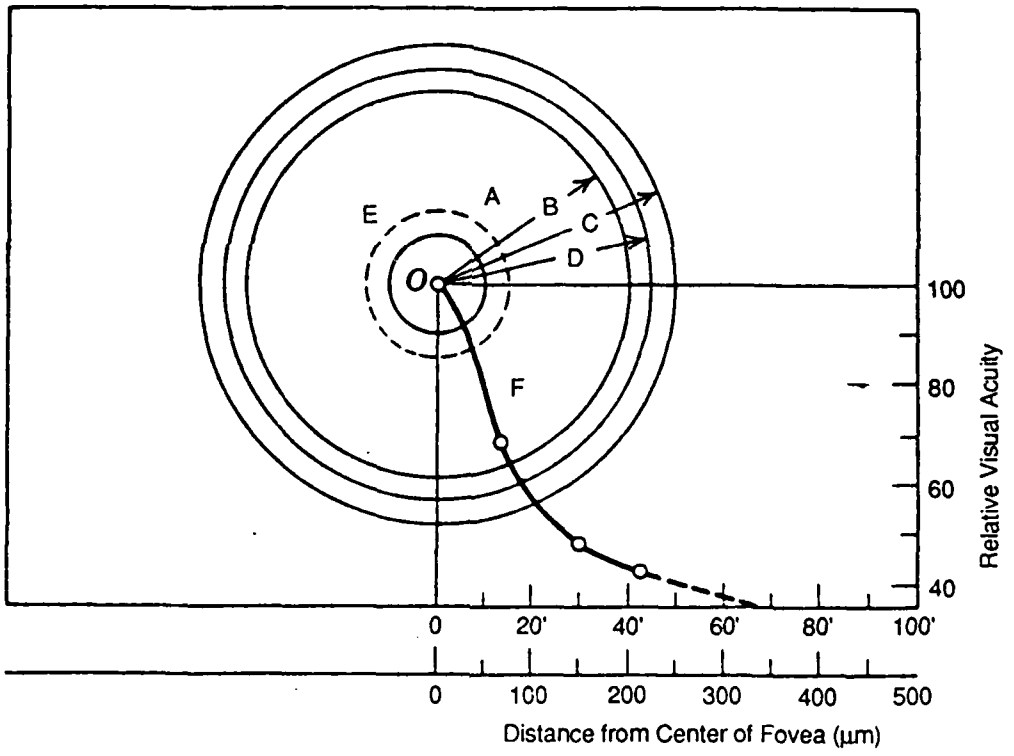

Figure A-13. Sharp Drop in Acuity at Short Distances from the Fovea (based on Jones and Higgins, 1947)

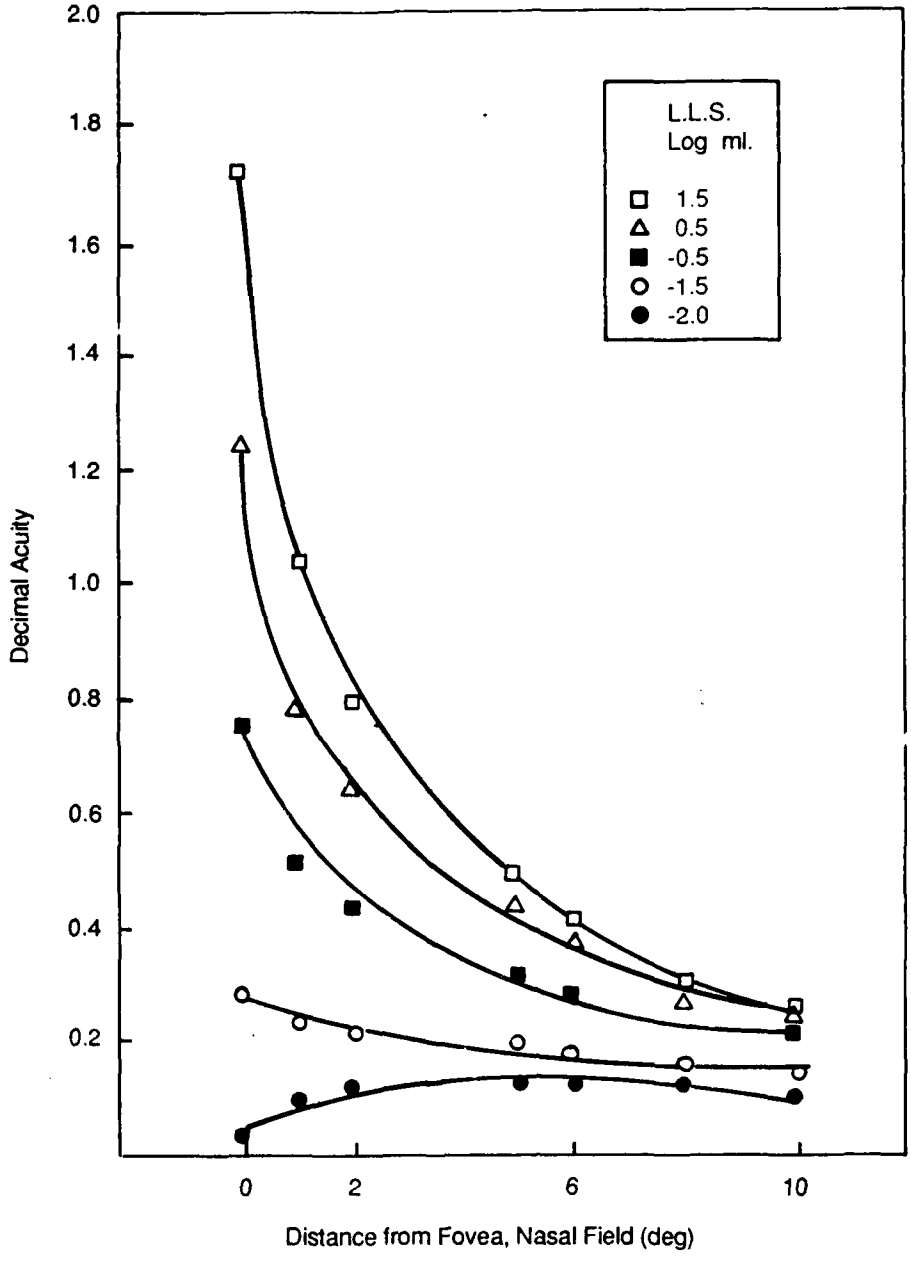

Figure A-14. **Relation between Visual Acuity and Angle of View for Several Background Luminances (based on Sloan, 1968)**

visual acuity is low for all retinal locations. Retinal location has a large effect on visual acuity at higher luminances. At 1.5 log mL, visual acuity varied from 1.8 when the target was fixated at the center of the fovea, to 0.3 when the target was viewed 10 degrees in the periphery.

It is clear from these data that the ability to perceive fine spatial detail in a display indicator depends greatly on whether or not it is fixated. Much less spatial resolution can be obtained from a monitored indicator when a pilot is looking in even a slightly different direction. Because pilots must often perform multiple tasks at once, it is critical to design displays such that elements that must be resolved in critical display regions are larger in size than the acuity thresholds for regions of the retina away from the fovea.

5.1.3 Displacement Threshold

It is reasonable to assume that the displacement threshold depends on viewing angle in the same manner and degree as the visual acuity threshold. This was verified in part by Basler (1906), who demonstrated that the displacement threshold is lower for foveal than for peripheral processing, and by Gordon (1947), who demonstrated that the displacement threshold increases systematically with increases in peripheral angle of view under scotopic luminance conditions.

5.1.4 Rate Threshold

The visual system's sensitivity to motion also depends on the angle of view or the region of retinal processing. As with sensitivity to increments of luminance and fine spatial detail, sensitivity to motion decreases with distance from the fovea. Aubert (1886) found that sensitivity to motion in the presence of a stationary background was between 1 and 2 minutes visual angle/second when viewed foveally, but was only 18 minutes/second when viewed 9 degrees to the side of fixation. Data from McColgin (1960) indicates that the decrease in rate threshold with distance from the fovea is monotonic.

As for the other types of perceptual tasks, it is important to consider the angle of view when modeling a pilot's ability to perceive rate of indicator motion. Pilots are very sensitive to rate of movement when fixated on a moving indicator, but their sensitivity drops off as their eyes move away from the indicator.

5.2 EFFECT OF VIEWING ANGLE ON OBSERVATION DELAYS

The amount of time taken to perceive or respond to a display indicator also depends on the retinal location in which the display indicator is processed. Hansteen (1971) found that latencies to respond to peripherally located information were on the order of 20 to 30 msec longer than foveal latencies. Pease and Sticht (1965) also found shorter reaction times to stimuli presented in the fovea than the periphery. For high luminances, reaction times were approximately 200 msec for foveal target presentations, while peripheral presentations produced average reaction times of around 230 msec, a difference of 30 msec.

In the absence of more comprehensive data, it may be assumed that the time taken to respond to a displayed stimulus is 30 msec longer when the monitored indicator is viewed at a peripheral angle than when the indicator is located at the point of fixation.

6.0 PILOT PUPIL SIZE

Pupil size is a pilot variable that influences the efficiency of perceptual processing by contracting to limit the amount of light that enters the retina, or expanding to increase it. Pupil size tends to fluctuate from moment to moment around a mean value that depends on the average luminance in the field of view. In general, the higher the average luminance, the smaller the pupil size. Pupil size also contracts and expands in a complex manner with emotional and cognitive changes. Whether the pupil expands or contracts as a function of stress and other emotional and cognitive variables varies from individual to individual, as does the degree of change in pupil size. The normal range of pupil sizes is approximately 2 to 8 mm in diameter.

Pupil size can affect the perceptual processing of a cockpit display in two ways. First, pupil size determines the amount of light that enters into the eye. Increasing or decreasing the size of the pupil increases or decreases the amount of display luminance that falls on the retina. Because changes in pupil size affect the absolute amount of light which enters the eyes, but not the relative luminance of display indicators to each other or to their background, the effect on efficiency of perceptual processing is minimal.

Second, pupil size can affect the amount of blur contained in the retinal image. The retinal image of the cockpit display is always blurred to some extent, but the amount of blur in the image depends on the size of the pupil. When the pupil is large, the retinal image of the display contains a relatively large amount of blur due to optical aberrations in the media of the eye, such as scratches in the cornea. When the pupil is small, blur associated with optical aberrations is minimized. On the other hand, the retinal image is also blurred by diffraction of light at the sides of the pupil. The proportion of light that is diffracted, and therefore the proportion of blur, is greatest when the pupil size is small. Because of the effect of pupil size on image blur, pupil size may be expected to have a significant effect on acuity and displacement thresholds, but little effect on the incremental or rate thresholds. Little or no relation is expected between pupil size and observation delay.

In order to determine the effect of pupil size on observation thresholds or delays, it is necessary to convert luminance measurements into units of trolands. As mentioned earlier, a troland is the unit used to express the amount of light which illuminates the retina. The retinal illuminance is not readily measured. Instead, the amount of retinal illuminance is computed by taking the product of the stimulus luminance, in units of candles per square meter, and the pupil area, in units of square millimeters.

6.1 EFFECT OF PUPIL SIZE ON OBSERVATION THRESHOLDS

Pupil size has a small effect on those observation thresholds that require fine spatial resolution, including the acuity and displacement thresholds, as well as those which require luminance discrimination, including all four types of thresholds.

6.1.1 Incremental Threshold

The incremental threshold is defined as the minimum change in luminance required before a luminance difference is detected. Changes in pupil size have two general effects: increasing or decreasing the amount of light which enters the eye, and increasing or decreasing the amount of blur in the retinal image. Because changes in retinal illumination equally affect the brightness of the retinal image of a display indicator as well as the image of the display background, changes in pupil size affect indicator contrast. Changes in pupil size thus affect the incremental threshold by decreasing or increasing an indicator's effective contrast. However, because adjustments in pupil size tend to optimize sensitivity to luminance contrast, the effect of these changes on the incremental threshold may be assumed to be negligible.

Because detection of a luminance difference does not involve detection of fine spatial detail, changes in pupil size that result in increases or decreases retinal blur as have little or no effect on the incremental threshold.

6.1.2 Acuity Threshold

The acuity threshold, on the other hand, reflects the ability of an observer to detect very fine differences in spatial detail, and therefore varies as a function of the observer's pupil size. Visual

acuity is highest with intermediate pupil sizes, between approximately 2.5 and 6 mm in radius. At smaller pupil sizes, acuity is decreased as a result of retinal blur associated with diffraction of light at the edges of the pupil. At larger pupil sizes, the retinal image becomes more blurred as a result of optical aberrations. The degradation in visual acuity for small pupil sizes is shown in Figure A-15 (based on Riggs, 1966).

6.1.3 Displacement Thresholds

Because of the close relationship between displacement and acuity thresholds, it may be assumed that pupil size has the same effect on the displacement threshold as shown in Figure A-15.

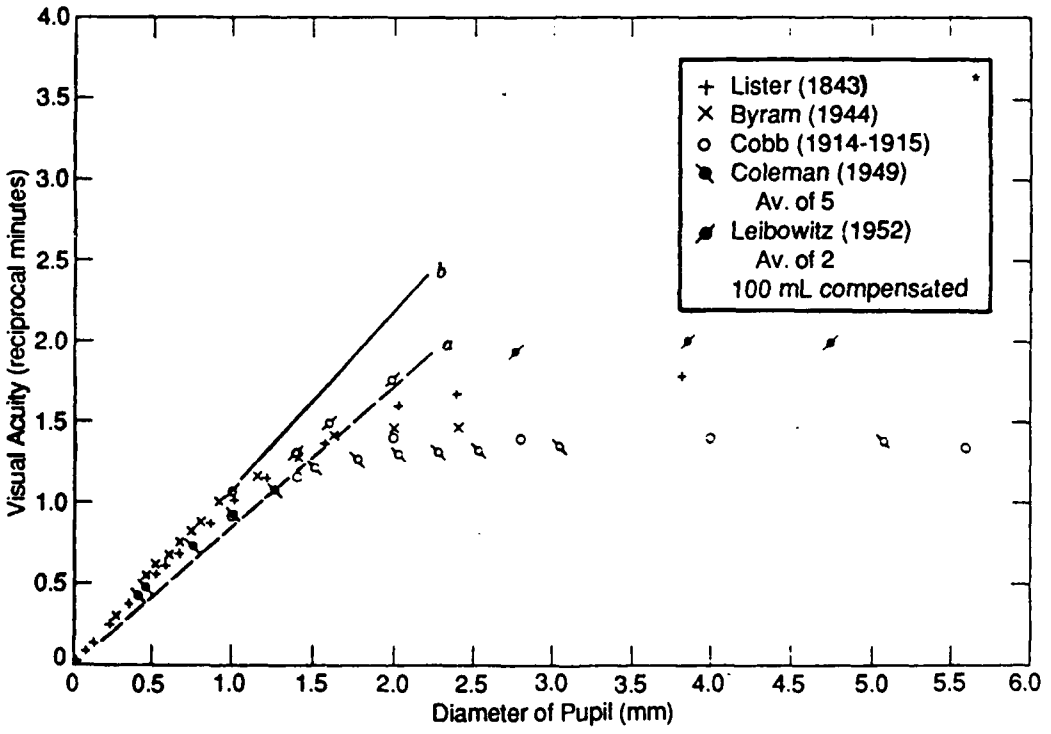

*Points are data from several published investigations.

Figure A-15. Effect of Pupil Diameter on Visual Acuity (based on Riggs, 1966)

6.1.4 Rate Threshold

The perception of very slow movement requires the ability to perceive the object in motion as well as a stationary background. Neither of these requirements, however, depends on fine spatial resolution. Therefore, it may be assumed that pupil size has a negligible effect on the rate threshold.

6.2 EFFECT OF PUPIL SIZE ON OBSERVATION DELAYS

Pupil size has a small but assumedly negligible effect on observation delay. Decreases in pupil radius limit the amount of light which enters the retina, thereby decreasing the retinal illuminance from the cockpit display. Section 3 shows that observation delays depend on indicator luminance, and it follows that they are also affected by changes in retinal illuminance that are independent of actual luminance. Effects of pupil change on the observation delay may be computed by conversion of the results measured in luminance units into units of trolands. However, given the small range of normal pupil sizes and the relatively small affect of luminance on observation delay, it may be assumed that pupil size is an unimportant variable with respect to observation delay.

7.0 DISPLAY INDICATOR SIZE AND SHAPE

Display indicators vary considerably in their size and shape. The design of a display indicator in terms of its size and shape is determined by many factors. One important design consideration should be the effects of size and shape on the efficiency with which an indicator can be processed by the pilot's visual system. This section will consider how the observation thresholds and observation delay for perception of a display indicator at the point of fixation is affected by its size and shape.

7.1 EFFECT OF DISPLAY SIZE AND SHAPE ON OBSERVATION THRESHOLDS

A relatively large amount of data has shown that the size and, to a lesser extent, the shape of an object determines the amount of luminance required before that object can be seen. The main import of this research is that very small objects must be very bright to be perceived, and objects which are asymmetrical in shape are more difficult to perceive than symmetrical objects.

Under some conditions the incremental threshold is affected by the size of the display indicator. In particular, the incremental threshold is increased when the display indicator is small. When the size of the indicator is relatively large, further increases in indicator size no longer have an effect on the incremental threshold. Several experiments have been performed to determine the quantitative relationship between the incremental threshold and indicator size (e.g., Blackwell, 1946; Crozier and Holway, 1939; Graham and Bartlett, 1940; Holway and Hurvich, 1938). These experiments have demonstrated that for small sizes, increases in indicator luminance are required for detection of indicators of decreasing size. Moreover, for small sized indicators, the product of the indicator area and the added luminance required for detection of that indicator is approximately a constant. The results of these experiments have demonstrated that the transition between incremental threshold size-dependence and size-independence is a gradual one. Figure A-16 presents illustrative data (based on Graham and Bartlett, 1940) showing the log incremental threshold as a function of stimulus intensity for circular stimuli whose diameters varied from 2.0 to 28.0 minutes visual angle.

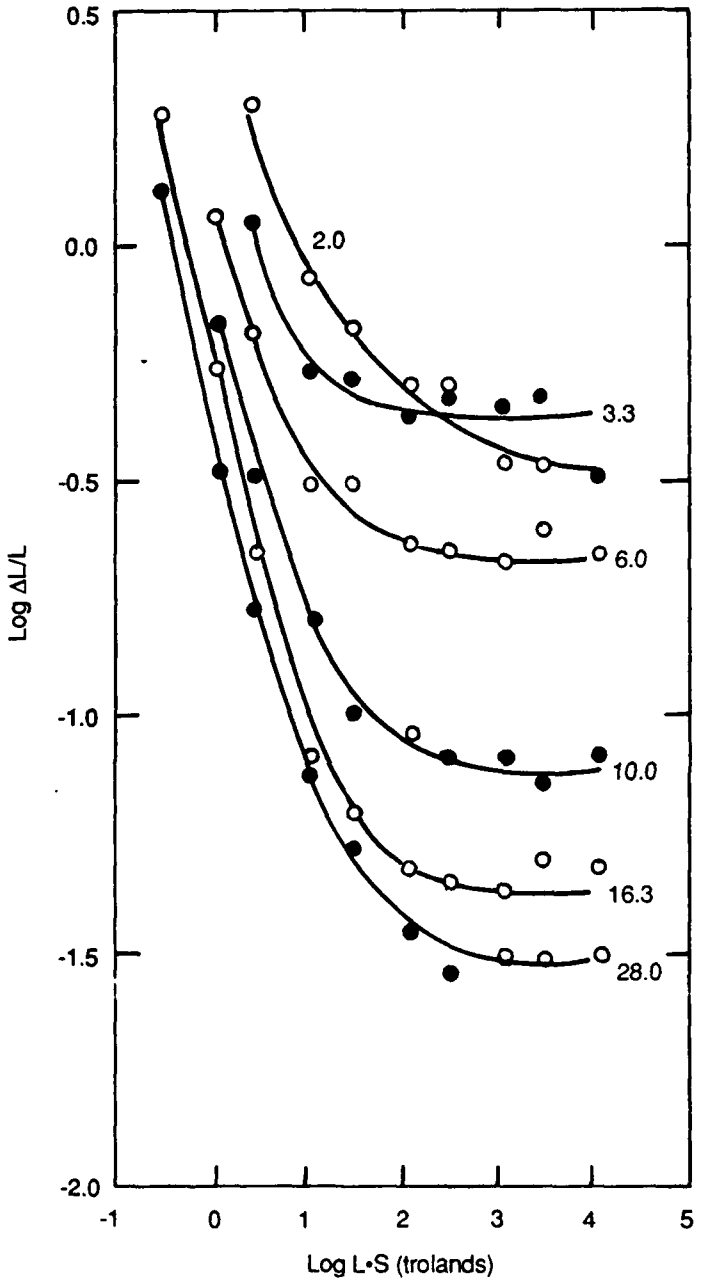

Figure A-16. **Effect of Stimulus Diameter on the Incremental Threshold for Various Background Luminances (based on Graham and Bartlett, 1940)**

The shape of the visual region to be discriminated also has been shown to influence the incremental threshold. The effect of indicator shape on this threshold was investigated by Lamar, Hecht, Shlaer, and Hendley (1947), who measured the incremental threshold for rectangles that varied in area from 0.5 to 800 square minutes of visual angle, and which varied from 2 to 200 square minutes of visual angle in their length/width ratio. The results are presented in Figures A-17 and A-18. Incremental thresholds shown in Figure A-17 were obtained under photopic levels of background luminance; threshold values in Figure A-18 were obtained under scotopic luminance conditions. These results show that increases in the length/width ratio of the luminous target result in increases in the incremental threshold. That is, the larger the length/width ratio, the harder the target was to detect. In addition, this effect is more profound with increasing asymmetry of rectangle length and width.

According to the above results, the amount of indicator luminance or contrast required to detect that indicator's presence is a function of its size and shape. Very small or very narrow indicators are difficult to perceive, and require a greater luminance for detection. How does indicator size

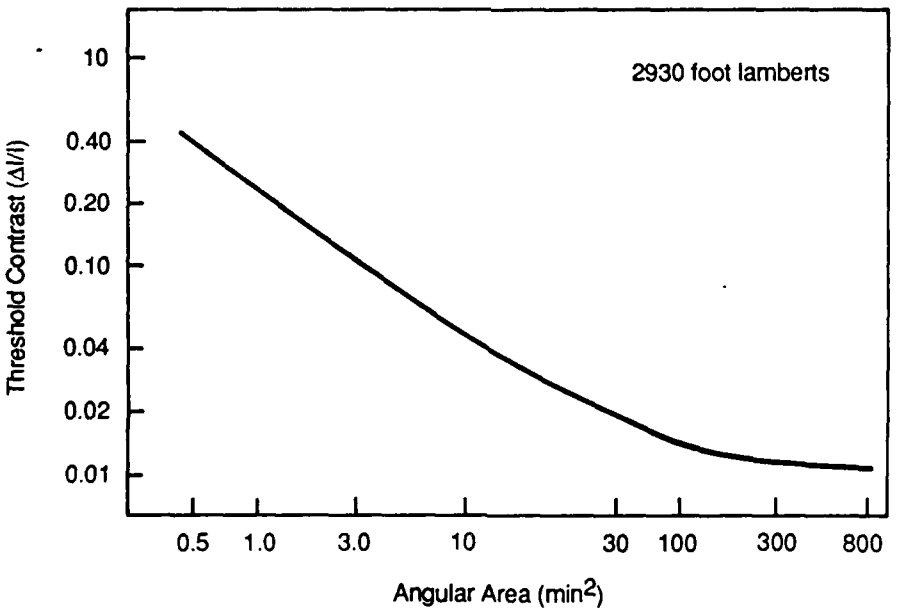

Figure A-17. Effect of Rectangle Length/Width Ratio on the Incremental Threshold under Photopic Conditions (based on Lamar et al., 1947)

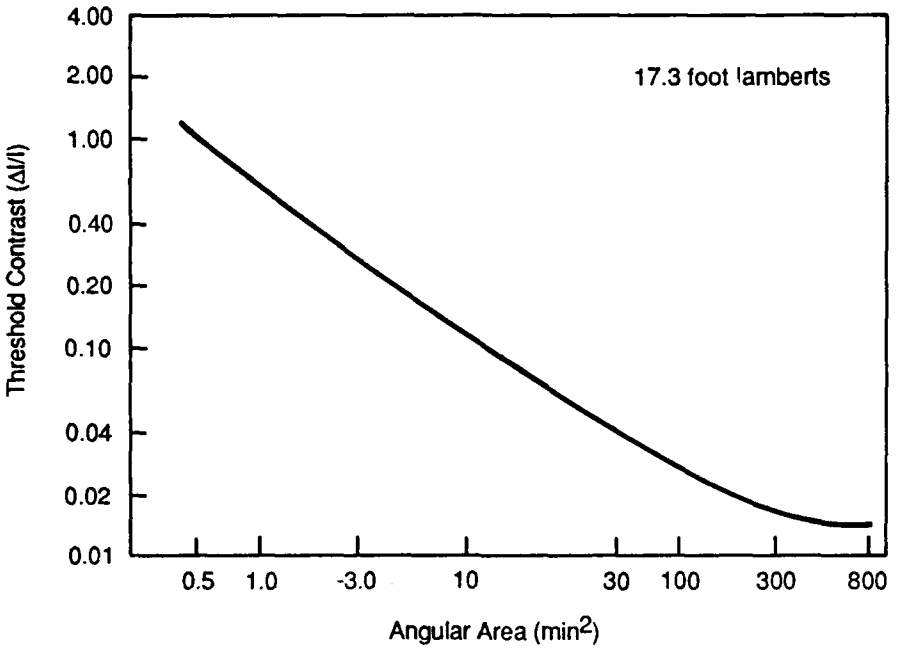

Figure A-18. Effect of Rectangle Length/Width Ratio on the Incremental Threshold under Scotopic Conditions (based on Lamar et al., 1947)

and shape affect acuity, displacement, and rate thresholds? It may be assumed that size and shape do not influence these thresholds, as long as the indicator luminance is well above the incremental threshold. That is, as long as the indicator is seen, spatial resolution and motion perception should be unaffected.

7.2 EFFECT OF INDICATOR SIZE AND SHAPE ON OBSERVATION DELAYS

To the authors' knowledge, there is no published data to suggest that observation delays are affected by stimulus sizes or shapes. An effect of size or shape on observation delay may be expected however, if an indicator is so small or so narrow as to be difficult to perceive. That is, normal indicator luminances may be near the incremental thresholds for extreme sizes and shape asymmetries. In these cases longer observation delays will be obtained, reflecting the pilot's difficulty in perceiving or located an indicator. Presumably, the process of cockpit design rules out such choices for indicator size and shape. For the range of indicator sizes and shapes likely to be found in cockpit applications, indicator luminances will be well above the incremental threshold, and no significant differences in associated observation delays can be expected.

8.0 DISPLAY CLUTTER

Display clutter may be defined in terms of the number of elements contained in a fixed region of the display, the proximity of multiple display elements to each other, and the visual similarity of the elements. Increases in the number of display elements, increases in their proximity, and increases in their visual similarity add to display clutter. Display clutter may also be created by the environment when display indicators are overlayed on an out-the-window view. Whatever its origin, increased display clutter may cause significant reductions in pilot performance. Because of the unavailability of data reflecting the impact of display clutter on observation thresholds, effects of display clutter will be considered only with respect to observation delays.

The latency to respond to a display indicator depends on the total number of elements within the region of the display that contains the indicator. It is often the case that observation delay is a linear function of the number of elements in the region to be searched, where the amount of time taken to process each item is on the order of 10 to 30 msec, although much longer processing times have been observed if the elements are visually similar (e.g., Atkinson, Holmgren, and Juola, 1969; Estes, 1972; Kaplan and Carvellas, 1965).

If the pilot must search a region of the display to locate the indicator of interest, a processing delay is introduced in the time taken to examine other display elements until the indicator has been located. The amount of time taken to process each additional display element is largely a function of the visual similarity of the additional elements to the display indicator of interest. Not surprisingly, when display elements look alike, the amount of time taken to find the desired element is longer than if the desired element looks different. Because visual similarity is extremely difficult to quantify, it is possible to specify the relationship between observation delays and the similarity of a display indicator to other elements of the display only in qualitative form: Displays containing physically similar elements will be associated with longer observation delays than displays containing elements which are easily discriminable (Farmer and Taylor, 1980).

9.0 DISPLAY LAYOUT

Display layout has a critical impact on visual performance in terms of the eye movements required to view required display information. If information is required by the pilot that is located on the display away from the current eye position, then the pilot may need to move his or her eyes to acquire that information. This will result in a significant reduction in performance associated with the eye movement, as discussed in Section 11. Display layout has a smaller effect in terms of the configuration of a display indicator. The display indicator design may have a significant effect on observation threshold, particularly on rate and displacement thresholds. This effect is briefly discussed below.

The minimum rate of movement that can be detected depends largely on the background in which the motion occurs. In an otherwise blank field, observers can detect motion of a luminous dot as slow as 10 to 20 minutes of visual angle per second. However, when the blank field is replaced by a visible and textured background, the rate threshold is on the order of 1 or 2 minutes of visual angle per second (Aubert, 1886). Rate thresholds are much lower in the presence of stationary reference lines because of the presence of positional cues in addition to velocity cues for motion detection. Presumably, the effect of a stationary reference on the rate threshold depends on the distance between it and the target. When a stationary reference point is close to the moving target, it should provide a strong cue for the presence of very slow movement. Movement of the target relative to a stationary background is more difficult when the reference points are distant.

Similarly, the presence and position of reference lines has a significant effect on the displacement threshold. In the absence of reference points, it is extremely difficult to determine whether an indicator has been displaced from its previous position. From the above results it may be assumed that the displacement threshold is optimal when the indicator and reference points are contiguous, and that the threshold increases with increasing distance between the indicator and reference.

10.0 DISPLAY MOTION

This section will consider the effects of display motion on pilot observation thresholds and delay. Display motion will be considered in two respects: motion of the entire region of the display fixated, and motion of a moving display indicator relative to its background. In the first case motion is unrelated to the displayed signal, and in the second case, motion of the indicator is the intended signal.

It is frequently the case that the position of display indicators are not fixed, but are subject to jitter or other types of movement. To maintain fixation on a moving indicator, the pilot must track the indicator using eye movements. If the direction of indicator movement is unpredictable, the pilot must use saccadic eye movements to maintain the point of fixation on the desired indicator. The effect of saccadic eye movements on observation thresholds and delays is discussed in Section 11. However, if the direction of indicator movement is predictable, or follows a relatively smooth course, fixation can be maintained with the use of pursuit eye movements. Pursuit eye movements are the slow, smooth changes in eye position used to maintain fixation on moving objects, and do significantly reduce visual sensitivity. Although visual sensitivity is not significantly reduced during this type of eye movement, tracking of moving objects is not perfect. As a result, any motion of the display indicator can have a deleterious effect on the pilot's perceptual performance. At extremely high velocities, the eyes can no longer track a moving object. At these speeds, objects first appear blurred or even invisible.

The second aspect of display motion to be considered is motion of an indicator with respect to the indicator's reference points. In this case, the position of the indicator varies as a function of some displayed system variable. This aspect of display motion has a different effect on pilot performance. In this case, increases in indicator motion can improve the accuracy and speed of indicator perception.

10.1 EFFECT OF DISPLAY MOTION ON OBSERVATION THRESHOLDS

Motion or jitter of the entire region of the display that is monitored generally increases the observation threshold. This effect is particularly significant for thresholds involving fine spatial discrimination, including acuity and displacement thresholds. The other aspect of display motion that can affect pilot performance is the velocity of moving indicators with respect to a stationary reference. In this case, increased indicator velocity can improve pilot performance. In particular, the displacement threshold improves as the rate of indicator motion increases, short of rates causing invisibility or blur. Perception of rate also depends on indicator velocity. The rate threshold, when defined as the minimum change in indicator velocity that can be detected, also depends on the baseline velocity.

10.1.1 Incremental Threshold

The incremental threshold is the threshold least affected by display motion, and it may be assumed for modeling purposes that motion has a negligible effect on the value of this threshold. This is because detection of a change in luminance between two regions of the display does not generally require fine spatial resolution. Blurring of relatively large regions having different luminances does not obscure the luminance change, and therefore does not significantly impair the perceptual task.

10.1.2 Acuity Threshold

Ludvigh (1948, 1949) investigated the effect of an object's motion on observer's ability to recognize the object, where object recognition required fine spatial resolution. The results indicated that, even when observers track a moving object with eye movements, visual acuity for identifying that object deteriorates rapidly with increasing velocity of the object. Ludvigh's results are plotted in Figure A-19. For relatively low velocities, i.e., velocities less than 100 degrees/second, the relationship between visual acuity and angular velocity in degrees/second, c, fit the following equation:

$$\text{Acuity} = 1 - 0.0088\ c.$$

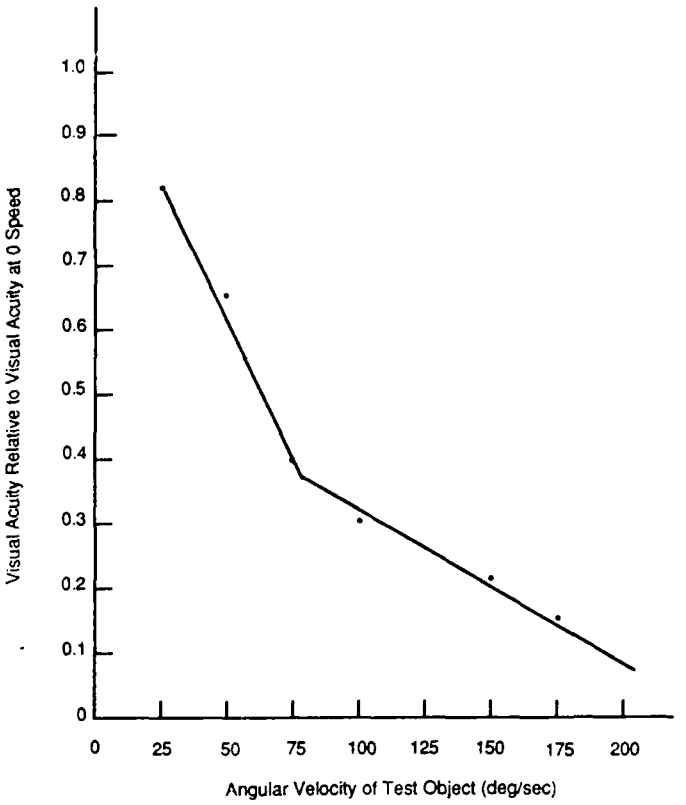

Figure A-19. Effect of Object Motion on Visual Acuity (based on Ludvigh, 1948)

For velocities greater than 100 degrees/second, the data could be fit by the following equation:

$$\text{Acuity} = 0.5 - 0.0021\ c.$$

Visual acuity approached zero, i.e., no spatial detail could be seen, when the angular velocity of the object approached 200 degrees visual angle/second.

Mackworth and Kaplan (1962) investigated the effect of pursuit eye movements on visual acuity for the perception of brief, stationary targets located at a point of fixation during the course of movement. Presumably, the eye movements decrease visual acuity by producing blur in the retinal image. The velocity of the pursuit eye movements varied between 0 and 120 degrees visual angles per second. They observed that for very bright targets of 60 candelas/square meter,

visual acuity was not reduced by pursuit eye movements at any speed. However, for dimmer targets, either 0.07 or 0.28 candelas/square meter, visual acuity was reduced with increases in the speed of the pursuit eye movement. These results are shown in Figure A-20. According to these results, the effect of motion on visual acuity depends on the luminance of the display. At low display luminances, significant effects of motion or jitter can be expected. At high display luminances, little or no effects may be present.

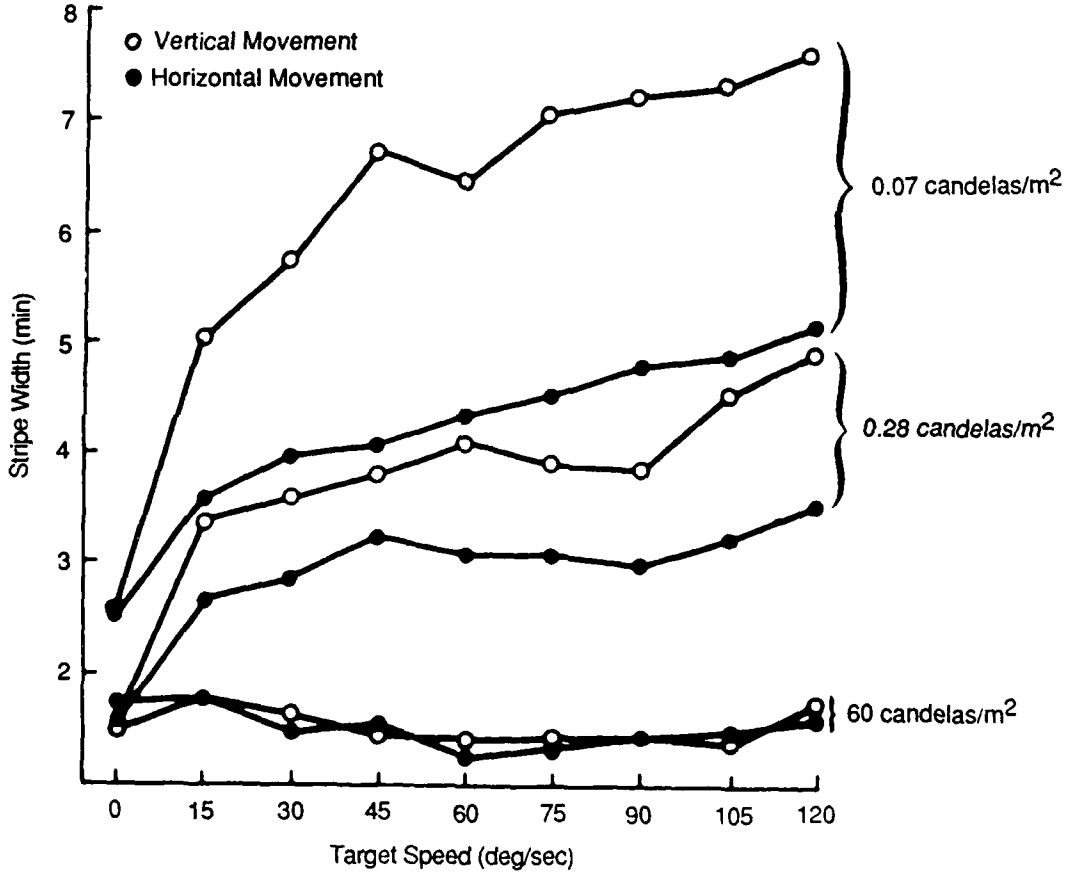

Figure A-20. Effect of Speed of Pursuit Eye Movements on Visual Acuity (based on Mackworth and Kaplan, 1962)

10.1.3 Displacement Threshold

Motion or jitter of an indicator that is not related to the indicator's signal may be expected to have the same deleterious effect on the displacement threshold as on the acuity threshold. However, with moving indicators, another issue is the effect of indicator velocity on the displacement threshold.

Basler (1906) reported that the displacement threshold varies as a function of the rate of indicator velocity. The displacement threshold is lowest for high rates of relative motion (falling short of rates beyond 200 degrees/second which cause blur or invisibility) and increases as rate decreases (Basler, 1906). Unfortunately, Basler's experiments were not sufficiently comprehensive to report quantitative results. However, on the basis of his results it may be concluded that at relatively slow speeds, displacement thresholds are equal to acuity thresholds. At higher angular velocities, displacement thresholds are slightly better than corresponding acuity thresholds.

10.1.4 Rate Threshold

Hick (1950) measured thresholds for instantaneous increases and decreases in velocity for a moving target. Notterman and Page (1957) performed a similar experiment that measured only increases in velocity. The results of both experiments are shown in Figure A-21, which shows the minimum amount of velocity change required for velocity discrimination, as a function of baseline velocity. The rate discrimination threshold is expressed in terms of the ratio of the minimum discriminable change in velocity and the baseline velocity, $\Delta v/v$. These results indicate that observers are most sensitive to velocity changes for baseline velocities of about 1 to 2 degrees/second, and are increasingly less sensitive to velocity differences with further increases in the baseline velocity.

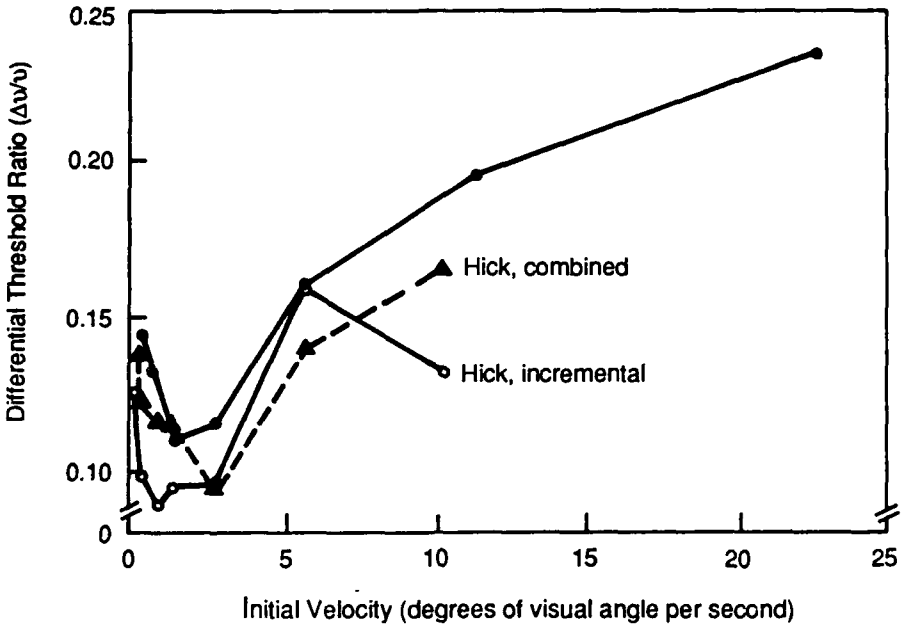

Figure A-21. **Difference Thresholds for Instantaneous Changes in Velocity as a Function of Basic Initial Velocity (based on data from Hick, 1950, and Notterman and Page, 1957)**

11.0 SACCADIC EYE MOVEMENTS

A saccadic eye movement is a sudden, jerky, parallel change in the position of the fixation point of both eyes from one point in space to another. Saccades are the principle type of eye movement used to change the direction of the eye's focus, and they occur with a maximum frequency of about three to four per second. When a saccadic eye movement occurs, there is a drastic increase in all types of observation thresholds for the duration of the movement. Observation delays for visual information presented at display locations away from the point of focus are increased by the duration of the saccade if an eye movement is initiated in order to look directly at that visual information.

11.1 EFFECT OF EYE MOVEMENTS ON OBSERVATION THRESHOLDS

Immediately prior to and during a saccadic eye movement, visual sensitivity is significantly reduced, presumably in order to avoid the perception of streaking or blur that might otherwise occur. Volkman (1962) found that, although vision is never totally lost during a saccade, visual thresholds during an eye movement are about three times higher than when the eye is not moving. The time course of the loss of sensitivity during a saccade was determined by Latour (1962) and later confirmed by Volkmann, Schick, and Riggs (1968). The percentage of light flashes observed at various time intervals before, during, and following a saccade are shown in Figure A-22. For the period beginning 50 ms before the start of an eye movement until 50 ms following the start of the eye movement, normally visible flashes of light were detected less than 20 percent of the time. These data illustrate the effect of a saccade on the absolute detection of light, i.e., the ability to detect the mere presence of a spot of light. The effect of a saccade on incremental, acuity, displacement, and rate thresholds therefore has the same qualitative form as the effect on the absolute threshold For most modeling purposes, it is therefore adequate to assume that little or no useful visual information is acquired during a 100-msec duration surrounding the initiation of a saccade.

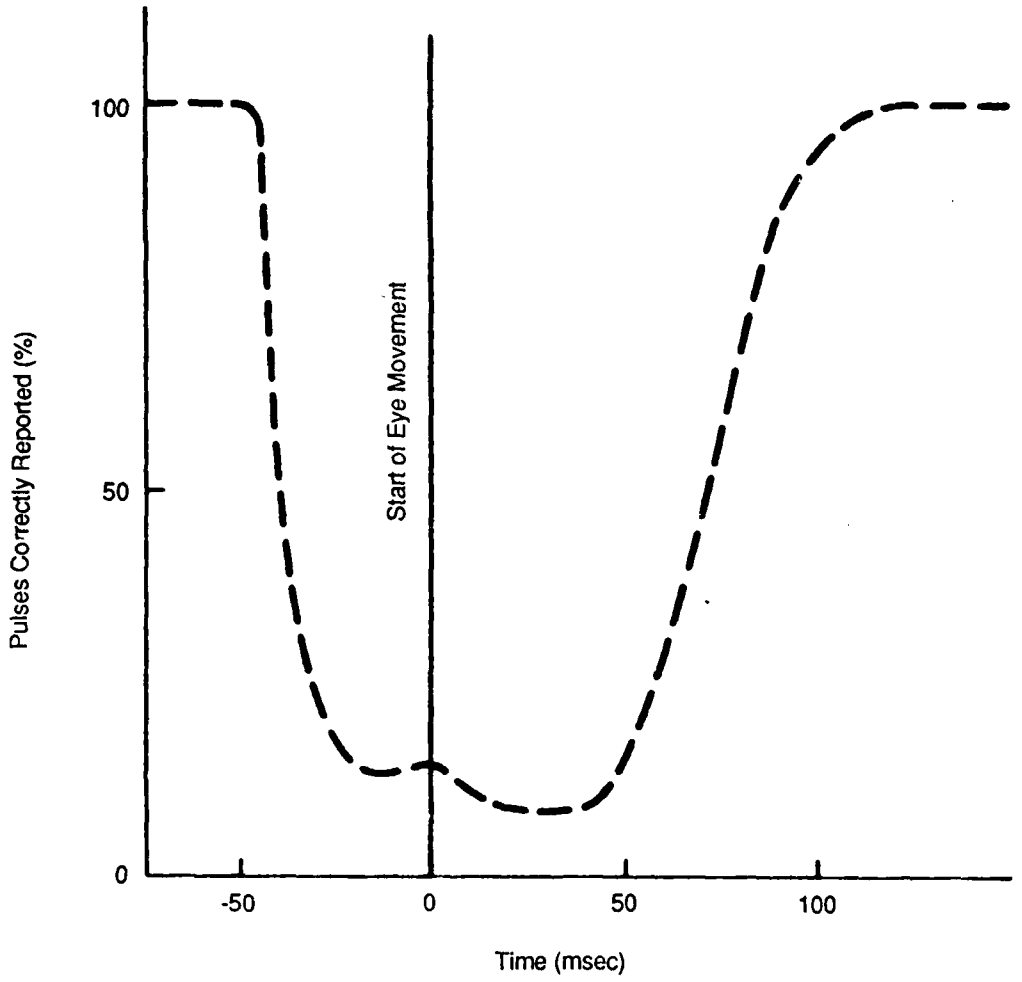

Figure A-22. Loss of Visual Sensitivity during a Saccadic Eye Movement (based on Latour, 1962)

11.2 EFFECT OF EYE MOVEMENTS ON OBSERVATION DELAY

If an eye movement is required in order to acquire the information of interest from a cockpit display indicator, the delay associated with the processing of that information will be increased by the amount of time taken to complete the eye movement. This delay depends on the amount of time required to determine the direction and amplitude of the eye movement, and on the amount of time the eyes are in actual motion.

Saccadic eye movements have an extremely high velocity, on the order of 400 to 1000 degrees visual angle/second (Alpern, 1971). The duration of a saccade is a linear function of the amplitude, increasing about 2 msec for each degree of movement. The peak velocity of the eye also increases with the amplitude of the movement, and for a 90-degree movement may become as large as 830 degrees/second (Alpern, 1971). Thus, for example, the amount of time in which the eye is in motion during a change in the point of fixation to 10 degrees visual angle to the right is approximately 20 msec.

However, before a saccade can be initiated, it must be programmed. Saccadic eye movements are ballistic in that their direction and amplitude are determined prior to their initiation. Once a saccade has begun, its path cannot be modified. The delay in processing associated with the programming stage of a saccade is approximately 200 ms (Westheimer, 1954; Wurtz, 1976). However, this delay is somewhat shorter when the desired path is known in advance, as is the case in most cockpit situations. When the location of interest is well known, the amount of time required to program the eye movement may be less than 180 ms (Saslow, 1967).

12.0 DISPLAY VARIABILITY

Display variability is related to the degree of predictability of displayed information. When display variability is low, the information conveyed is relatively predictable; when display variability is high, the displayed information is relatively unpredictable. It is frequently hypothesized that there is a close relation between observation thresholds and delays and display variability (e.g., Attneave, 1954). According to this hypothesis, increases in display variability will result in reductions in observer performance due to increases in observation thresholds and delays.

The concept of display variability may be formalized in terms of information theory, which is concerned with the statistical specification and measurement of information in input and output. According to information theory, the amount of information contained in a stimulus (or display) may be calculated given the number of display alternatives and their relative probabilities. In general, the greater the number of display alternatives, the greater the amount of information contained in a stimulus or display. For a given number of display alternatives, maximum stimulation information occurs when each alternative is equally likely. To translate the above hypothesis into information-theoretic terms, the greater the information contained in a stimulus or display indicator, the longer it will take to process that stimulus and the more difficult and error-prone it will be.

Unfortunately, attempts to relate observer performance to stimulus information or variability have resulted in ambiguous results. Some attempts at correlating observation thresholds or delays with the amount of information contained in a stimulus have been successful (e.g., Hyman, 1953, discussed below), while more often such attempts have failed (Corcoran, 1971).

Display variability or stimulus information has often failed to account for observer performance because of differences between the measured aspects of the stimulus and the aspects that are actually relevant to the human observer, and not because of an absence of a theoretical relationship between variability and performance. Stimulus information as measured using information theory may not correspond to psychologically relevant aspects of the stimulus. For

example, the amount of information conveyed by the position of a display indicator is measured in terms of the number of indicator positions and the frequency with which the indicator points to each position. However, this view of the stimulus may not be psychologically accurate. For example, the observer may "lump together" indicator positions to form coarser gradations, i.e., he or she may ignore fine differences in the indicator location. The number of observer-relevant indicator positions and their frequencies would thus be different from the objective ones.

Despite the difficulty of measuring of display variability or stimulus information, many attempts at relating this variable to observer performance have been successful, particularly with respect to the effect of display variability on observation delay. The following section will briefly review successful attempts at identifying the effect of stimulus variability on observation delay.

Donders (1868) was the first to measure a relation between observation delay and the number of stimulus alternatives. Observation delays to detect the presence of a single stimulus were compared to observation delays to detect one of five different stimuli, where each stimulus required a different response. He found that the average observation delay when there was only one possible stimulus was 197 msec, and the average observation delay when the observer had to decide which of 5 stimuli was present was 285 msec. These data demonstrated that the time to make a decision about what one sees can depend on the number of alternative stimuli and responses that can occur. The value of the observation delay obtained by Donders for the case in which there is only one stimulus alternative, approximately 200 msec, is fairly representative (Keele, 1973).

Many researchers have attempted to discover more precisely the form of the relationship between observation delay and the number of alternative values a stimulus can take (e.g., Hyman, 1953). According to the Hick-Hyman law, observation delay obeys the following function, where a and b are constants, and H is the amount of information conveyed according to principles of information theory:

$$D = a + bH.$$

Unfortunately, no fixed value could be obtained for decision time, or b. Undoubtedly, this is because different stimuli take varying amounts of time to process, as discussed in previous

sections. Moreover, the decision time depends largely on the relationship between the type of input and the form of the required response (e.g., Fitts and Seeger, 1953). As is well known, stimuli and responses may be compatible or incompatible. For example, consider a display in which the stimulus can appear on the left or on the right. A left motor response is compatible with the stimulus that appears on the left, but is incompatible with the stimulus that appears on the right. Stimuli and responses which are "compatible" have shorter associated decision times than stimuli and responses which are not.

Thus, to model the effects of stimulus information on observation delays, those aspects of the stimulus that are psychologically relevant to the observer must be measured, and the degree of compatibility between input and output must be considered. Because these variables are as yet extremely poorly defined, modeling of the effect of stimulus information must to a large extent be based on subjectively derived parameters.

13.0 SUMMARY

Figure A-23 lists the stimulus and pilot variables that have been discussed above, along with an indication of the magnitude of their effect on each type of observation threshold and observation delay. The variables whose effect on pilot performance have been reviewed include luminance, color, angle of view, pupil size, indicator size and shape, display clutter, display layout, display motion, eye movements, and display variability. These variables change dynamically as a function of environmental conditions, display design, and the state of the pilot. As is evident from the above discussion, although the effect of all of these variables may be significant, the magnitude of the effect varies considerably. Under normal conditions, display color and pilot pupil size have only a small effect on pilot performance; angle of view, display clutter, eye movements, and display variability have large effects; and the remaining variables have intermediate effects.

An issue that has been largely avoided in the above discussion is possible interactions between variables. Although it is convenient to assume that the effects of all of the above variables are additive, there are frequent instances in which they are not. For example, stimulus diameter has a large effect on the incremental threshold at high luminances, but has little or no effect at low luminances (see Figure A-16). Stimulus diameter has little effect at low luminances, no doubt, because at these luminances, the visual system is less sensitive to spatial detail (see Section 2.0). Nonlinearities at near-threshold conditions may frequently be described in terms of a "floor effect." That is, if visual performance is already reduced to extremely poor levels by one variable, the effect of a second variable on visual performance will in general be minimal. Exceptions to this rule of thumb are compensatory variables, where improved conditions in one variable can "compensate" for reduced conditions in another variable. A good example is compensation between stimulus intensity and duration. Over a considerable range of these variables, constant performance can be achieved with decreasing stimulus duration coupled with an increase in stimulus intensity.

To adequately model the effect of multiple variables at near-threshold conditions, it is sufficient to determine which of the variables has the greatest detrimental effect on performance and to consider whether other variables are sufficiently optimal to compensate for the detrimental effect

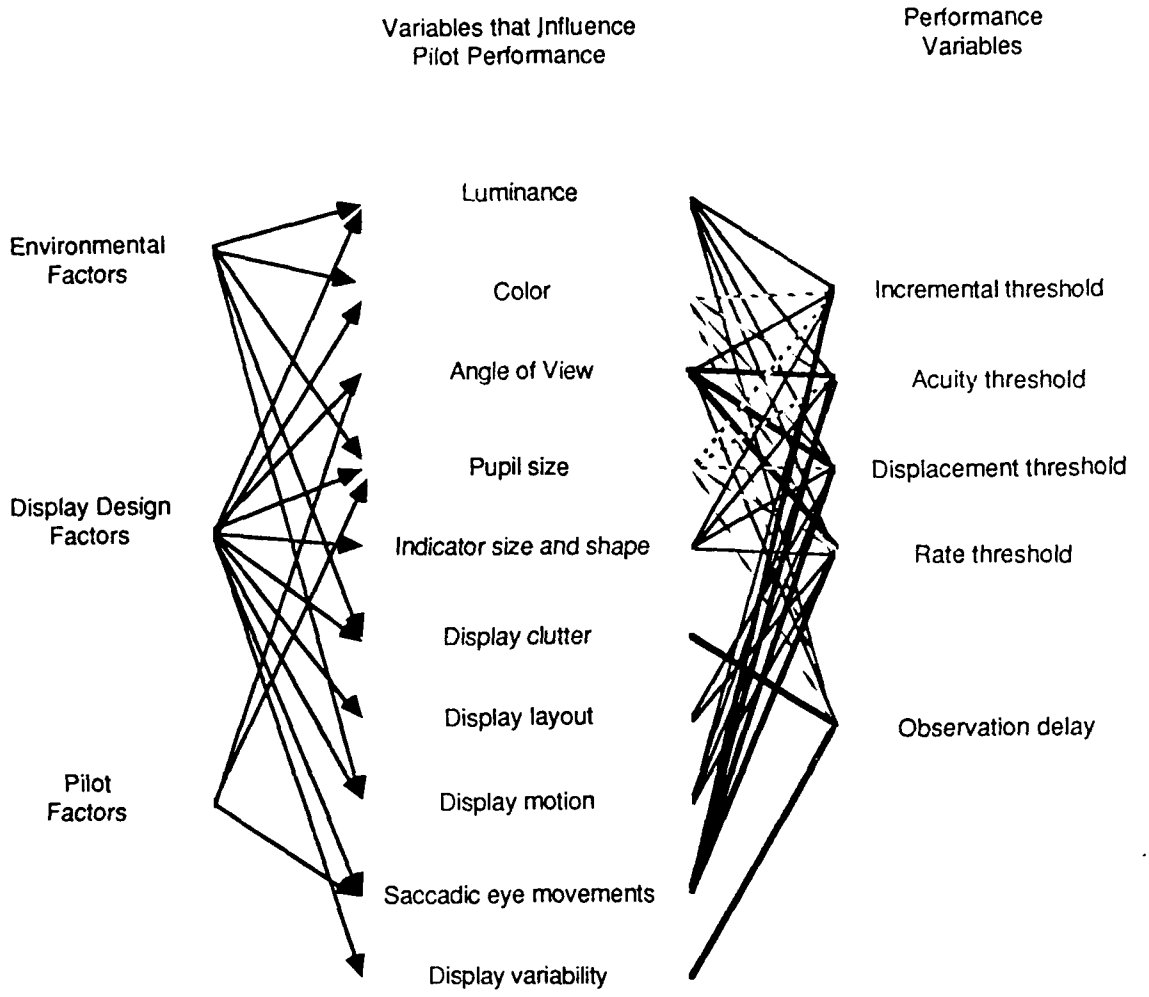

Figure A-23. **Effects of Stimulus (environmental and display design) and Pilot Variables on Pilot Observation Thresholds and Observations Delay (Line width between influencing and performance variables indicates strength of relationship; variables that have a greater effect on pilot performance are connected with heavier lines**

of this variable. If there is no significant compensation, then visual performance may be assumed to be a function of the single limiting variable. If there is significant compensation, then visual performance may be assumed to be limited by the second-most detrimental variable,

and so on. If variables are independent, then modeling may be made easier by the assumption that there is no compensation in the form of improved conditions in some variables when conditions deteriorate in other variables.

As a final point, although examples of nonadditivity between variables abound in near-threshold conditions, they are rare in suprathreshold conditions, i.e., in conditions in which the critical portion of the display can be seen with ease. Therefore, it is reasonable to assume the effects of the above variables on suprathreshold performance, such as reflected by variations in observation delay, are additive.

References

Alpern, M. (1971). Effector mechanisms in vision. In J. A. Kling & L. A. Riggs (Eds.), *Experimental Psychology*. New York: Holt, Rinehart, and Winston.

Atkinson, R. C., Holmgren, J. E., & Juola, J. F. (1969). Processing time as influenced by the number of elements in a visual display. *Perception & Psychophysics, 6*, 321-326.

Attneave, F. (1954). Some informational aspects of visual perception. *Psychological Review, 61*, 183-193.

Aubert, H. (1886). Die Bewegungsempfindung. *Arch. ges. Physiol., 39*, 347-370.

Baron, S., & Levison, W. H. (1973). *A manual control theory analysis of vertical situation displays for STOL aircraft*. NASA-CR-114620.

Basler, A. (1906). Uber des Sehen von Bewegungen. I. Die Wehrnehmung kleinster Bewegungen. *Arch. ges. Physiol., 115*, 582-601.

Blackwell, H. R. (1946). Contrast thresholds of the human eye. *Journal of the Optical Society of America, 36*, 642-643.

Brown, J. L., & Mueller, C. G. (1965). Brightness discrimination and brightness contrast. In C. H. Graham (Ed.), *Vision and visual perception*. New York: John Wiley & Sons.

Corcoran, D. W. J. (1971). *Pattern recognition*. Baltimore: Penguin Press.

Crozier, W. J., & Holway, A. H. (1939). Theory and measurement of visual mechanisms. I. A visual discriminometer. II. Threshold stimulus intensity and retinal position. *Journal of General Physiology, 22*, 341-364.

Donders, F. C. (1868). Over de snelheid van psychische processen. Onderzoekingen gedaan in het Psyiologish Laboratorium der Utrechtsche Hoogeschool: 1868-1869. Tweede Reeks, II, 92-120. Translated by W. G. Koster in W. G. Koster (Ed.), Attention and Performance II. *Acta Psychologica*, 1969, *30*, 412-431.

Estes, W. K. (1972). Interactions of signal and background variables in visual processing. *Perception & Psychophysics, 12*, 278-286.

Farmer, E. W., & Taylor, R. M. (1980). Visual search through color displays: Effects of target-background similarity and background uniformity. *Perception & Psychophysics, 27*, 267-272.

Fitts, P. M., & Seeger, C. M. (1953). SR compatibility: Spatial characteristics of stimulus and response codes. *Journal of Experimental Psychology, 46*, 199-210.

Gordon, D. A. (1947). The relation between the thresholds of form, motion, and displacement in parafoveal and peripheral vision at a scotopic level of illumination. *American Journal of Psychology, 60*, 202-225.

Graham, C. H., & Bartlett, N. R. (1940). The relation of size of stimulus and intensity in the human eye: III. *Journal of Experimental Psychology, 27*, 149-159.

Graham, C. H., & Kemp, E. H. (1938). Brightness discrimination as a function of the duration of the increment in intensity. *Journal of General Physiology, 21*, 635-650.

Hansteen, R. W. (1971). Visual latency as a function of stimulus onset, offset, and background luminance. *Journal of the Optical Society of America, 61*, 1190-1195.

Harwerth, R. S., & Levi, D. M. (1978). Reaction time as a measure of suprathreshold grating detection. *Vision Research, 18*, 1579-1586.

Hecht S. (1934). Vision: II. The nature of the photoreceptor process. In C. Murchison (Ed.), *A handbook of general experimental psychology*. Worchester, Mass: Clark University Press.

Hecht, S. (1937). Rods, cones, and the chemical basis of vision. *Physiological Review, 717*, 239-290.

Hecht, S., Peskin, J. C., ,& Patt, M. (1938). Intensity discrimination in the human eye: II. Relation between the Weber ratio and intensity for different parts of the spectrum. *Journal of General Physiology. 19*, 7-19.

Hick, W. E. (1950). The threshold for sudden changes in the velocity of a seen object. *Quarterly Journal of Experimental Psychology, 2*, 33-41.

Holway, A. H., & Hurvich, L. M. (1938). Visual differential sensitivity and retinal area. *American Journal of Psychology, 51*, 687-695.

Hyman, R. (1953). Stimulus information as a determinant of reaction time. *Journal of Experimental Psychology, 45*, 188-196.

Jones, L. A, & Higgins, G. C. (1947). Photographic granularity and graininess. III. Some characteristics of the visual system of importance in the evaluation of graininess and granularity. *Journal of the Optical Society of America, 37*, 217-263.

Kaplan, I. T., & Carvellas, T. (1965). Scanning for multiple targets. *Perception and Motor Skills, 21*, 239-243.

Keele, S. W. (1973). *Attention and human performance.* Pacific Palisades, CA: Goodyear.

Klein, G. S. (1942). The relation between motion and form acuity in parafoveal and peripheral vision and related phenomena. *Archives of Psychology, 39*, 1-70.

Kleinman, D. L., & Baron, S. (1971). *Analytic evaluation of display requirements for approach to landing*, NASA CR-1952, November 1971.

Kleinman, D. L., Baron, S., & Levison, W. H. (1970). An optimal-control model of human response, Part I: Theory and validation. *Automatica, 6*, 357-369.

Lamar, E., Hecht, S., Hendley, C. D., & Shlaer, S. (1948). Size, shape, and contrast in detection of targets by daylight vision. II. *Journal of the Optical Society of America, 38*, 741-755.

Lamar, E., Hecht, S., Shlaer, S., & Hendley, C. D. (1947). Size, shape, and contrast in detection of targets by daylight vision. I. *Journal of the Optical Society of America, 37*, 531-545.

Latour, P. L. (1962). Visual threshold during eye movement. *Vision Research, 2*, 261-262.

Levison, W. H., Baron, S, & Kleinman, D. L. (1969). A model for human controller remnant. *IEEE Transactions on Man-Machine Systems, MMS-10*, 101-108.

Liebowtiz, H. W. (1955a). The relation between the rate threshold for the perception of movement and luminance for various durations of exposure. *Journal of Experimental Psychology, 49* , 209-214.

Liebowitz, H. W. (1955b). Effect of reference lines on the discrimination of movement. *Journal of the Optical Society of America, 45*, 829-830.

Ludvigh, E. (1948). The visibility of moving objects. *Science, 108*, 63-64.

Ludvigh, E. (1949). Visual acuity while one is viewing a moving object. *Archives Opthalmology,* Chicago, *42*, 14-22.

Mackworth, N. H., & Kaplan, I. T. (1962). Visual acuity when eyes are pursuing moving targets. *Science, 136*, 387-388.

McColgin, F. H. (1960). Movement thresholds in peripheral vision. *Journal of the Optical Society of America, 50*, 774-778.

McRuer, D., Graham, D., Krendel, E., & Reisener, W. (1965). *Human pilot dynamics in compensatory systems: Theory, models and experiments with controlled-element and forcing function variations.* ARRDL-TR-65-15.

Moon, P., & Spencer, D. E. (1944). Visual data applied to lighting design. *Journal of the Optical Society of America, 34*, 605-617.

Mueller, C. G. (1951). Frequency of seeing functions for intensity discrimination at various levels of adapting intensity. *Journal of General Physiology, 34*, 463-474.

Notterman, J. M., & Page, D. E. (1957). Weber's law and the difference threshold for the velocity of a seen object. *Science, 126*, 652.

Pease, V. P., & Sticht, T. G. (1965). Reaction time as a function of onset and offset stimulation of the fovea and periphery. *Perceptual and Motor Skills, 20*, 549-554.

Riggs, L. A. (1965). Visual acuity. In C. H. Graham (Ed.), *Vision and visual perception*. New York: John Wiley & Sons.

Roufs, J. A. J. (1963). Perception lag as a function of stimulus luminance. *Vision Research, 3*, 81-91.

Saslow, M. G. (1967). Latency for saccadic eye movement. *Journal of the Optical Society of America, 57*, 1030-1033.

Shlaer, S. (1937). The relation between visual acuity and illumination. *Journal of General Physiology, 21*, 165-188.

Sloan, L. L. (1961). Area and luminance of test object as variables in examination of the visual field by projection perimetry. *Vision Research, 1*, 121-128.

Sloan, L. L. (1968). The photopic acuity luminance function with special reference to parafoveal vision. *Vision Research, 8*, 901-911.

Volkmann, F. C. (1962). Vision during voluntary saccadic eye movements. *Journal of the Optical Society of America, 52*, 571-578.

Volkmann, F. C., Schick, A. M. L., & Riggs, L. A. (1968). Time course of visual inhibition during voluntary saccades. *Journal of the Optical Society of America, 58*, 362-369.

Wald, G. (1945). Human vision and the spectrum. *Science, 101*, 653-658.

Wagner, G., & Boynton, R. M. (1972). Comparison of four methods of heterochromatic photometry. *Journal of the Optical Society of America, 62*, 1508-1515.

Westheimer, G. H. (1954). Eye movement responses to a horizontally moving visual stimulus. *Archives of Ophthalmology, 52*, 932-943.

Wilson, A. J., & Lit, A. (1981). Effects of photopic annulus luminance level on reaction time and on the latency of evoked cortical potential responses to target flashes. *Journal of the Optical Society of America, 71*, 1481-1486.

Wurtz, R. H. (1976). Extraretinal influences of the primate visual system. In R. A. Monty & J. W. Senders (Eds.), *Eye movements and psychological process*. Hillsdale, NJ: Lawrence Erlbaum Associates, 231-244.

APPENDIX B

TRANSFER FUNCTIONS OF STOL VEHICLE CASES

APPENDIX B
TRANSFER FUNCTIONS OF STOL VEHICLE CASES

This appendix documents the key transfer functions of the STOL vehicle for the four cases considered in Section IV. In all cases, the following notational shorthand is used:

$$\left\{K(1/\tau)\ [\zeta;\ \omega_N] = K(s + 1/\tau)(s^2 + 2\zeta\,\omega_N s + \omega_N^2)\right\}$$

Case 1: Unaugmented Vehicle (see Section IV, subsection 1):

$$D(s) = [0.62;\ 0.25]\,(-0.853)\,(1.535)$$

$$N_{\delta_H}^{q} = -1.763\ (0)\,(-0.040)\,(0.493)$$

$$N_{\delta_{TV}}^{q} = -1.432\ (0)\,(-0.075)\,(0.492)$$

$$N_{\delta_F}^{\alpha} = -0.101\ (-1.706)\ [0.51;\ 0.33]$$

$$N_{K_{TR}}^{u_f} = -0.294\ (0.069)\ (-1.27)\ (1.73)$$

Case 2: Baseline (Augmented) Vehicle (see Section IV, subsection 1):

$$D(s) = \left[\ \omega_{ph};\ \zeta_{ph}\right]\left[\ \omega_{sp};\ \zeta_{sp}\right]$$

$$= \left[0.54;\ 0.11\right]\left[0.64;\ 2.50\right]$$

$$N_u^{u_f} = -0.118\ (0.192)\,(3.452)\,(87.82)$$

$$N_u^{\alpha} = 0.826\ [\,0.65;\ 0.197]\,(25.68)$$

$$N_u^q = 21.21\ (0)\ (0.096)\ (0.74)$$

$$N_u^\gamma = -0.826\ (0.055)\ (-3.75)\ (3.96)$$

Case 3: Vehicle-Only Augmentation Using Cooperative Approach (see Section IV, subsection 3.b.2):

$$D(s) = (0.114)\ (1.159)\ [0.57;\ 1.48]$$

$$N_u^{u_f} = 0.260\ (0.125)\ (2.774)\ (-44.0)$$

$$N_u^\alpha = 0.338\ [0.82;\ 0.167]\ (77.37)$$

$$N_u^q = 27.63\ (0)\ (0.093)\ (0.542)$$

$$N_u^\gamma = -0.338\ (0.064)\ (3.82)\ (-7.93)$$

Case 4: Simultaneous Vehicle Control/Flight Director Synthesis (see Section IV, subsection 3.b.3):

$$D(s) = (0.147)\ (0.905)\ [0.40;\ 1.54]$$

$$N_u^{u_f} = -0.690\ (0.126)\ (2.782)\ (11.751)$$

$$N_u^\alpha = 0.233\ (0.048)\ (0.344)\ (76.46)$$

$$N_u^q = 18.35\ (0)\ (0.175)\ (0.606)$$

$$N_u^\gamma = -0.233\ (0.229)\ (4.645)\ (-6.674)$$

$$N_u^{FD} = -0.058\ (0.229)\ (4.02)\ (4.645)\ (-6.674)$$

☆ U.S. GOVERNMENT PRINTING OFFICE 1988 548-054-80977